UNIVERSITY
OF TRENTO - Italy
DEPARTMENT OF INDUSTRIAL ENGINEERING

XXVIII cycle

Doctoral School in Materials Science and Engineering

Ceramic aerogels of the Si-C-N-O system from pre-ceramic polymer

Emanuele Zera

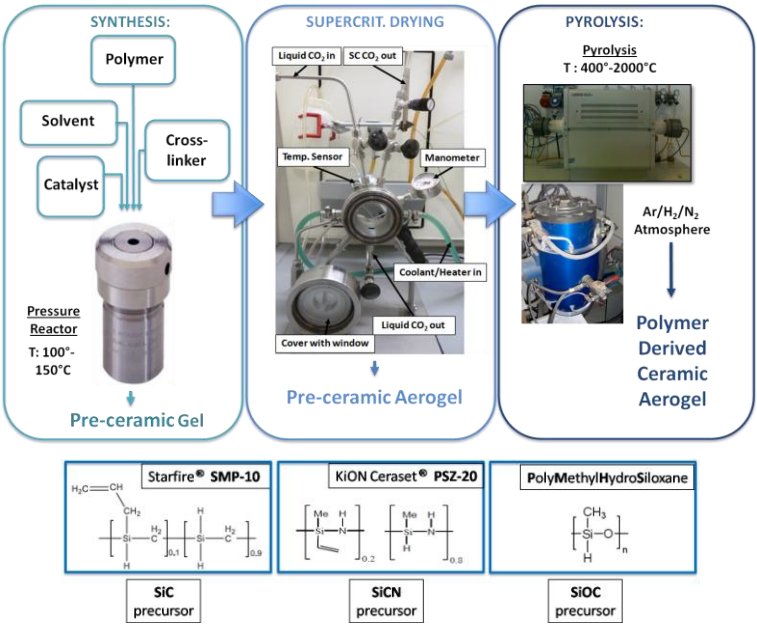

June 2016

CERAMIC AEROGELS OF THE SI-C-N-O SYSTEM FROM PRE-CERAMIC POLYMERS

Emanuele Zera
E-mail: emanuele.zera@unitn.it

Approved by:

Prof. Gian D. Sorarù, Advisor
Department of Industrial Engineering
University of Trento, Italy.

Ph.D. Commission:

Prof. Vincenzo M. Sglavo,
Department of Industrial Engineering
University of Trento, Italy.

Prof. Nuno M. Neves,
Department of Polymer Engineering
University of Minho, Portugal.

Prof. Cekdar Vakifahmetoglu,
Department of Mechanical Engineering
University of Istanbul Kemerburgaz, Turkey.

University of Trento,
Department of Industrial Engineering

June 2016

University of Trento - Department of Industrial Engineering

Doctoral Thesis

Emanuele Zera - 2016
Published in Trento (Italy) – by University of Trento

ISBN: - - - - - - - - -

To you!

Abstract

Research in materials science field is often driven by the necessity to overcome problems in fast, reliable and possibly cost effective ways. Many times the starting point to find a solution is a literature survey, to understand if someone already encountered a similar problem and proposed an answer, or if some authors developed a material that can be used to solve the issue. The work performed within this thesis however fits in another type of approach, i.e. research for the research's sake.

In this kind of approach the efforts are not dedicated directly to solve a given, precise and detailed problem, but to invent and develop new types of materials, characterizing them so that other researchers can take benefits from both the synthetic way and the measured properties of the new material produced.

In particular, this PhD thesis deals with the combination of two "exotic" class of materials, which are aerogels and polymer derived ceramics.

Aerogel is actually a shape, more than a material, from the proper chemical point of view. This kind of shape, anyway, is so peculiar that many of the properties are common to all the aerogels' products, similarly to what happen for other class of materials like conductivity for metals, hardness for ceramics and high specific strength for polymers. These common properties are: low density, high specific surface and predominantly mesoporous microstructure.

Polymer derived ceramic (PDC) denotes a family of ceramic materials that can be obtained by a controlled thermolysis of a polymeric precursor. These polymers are usually Si based and contain functional groups that allow to control the final chemistry of the ceramic produced, along with the great advantage that the shape can be set already in the polymeric state.

Successfully combining the two techniques, i.e. to produce polymer derived ceramic aerogel, is the core of this thesis.

Preference was given to the use of commercially available pre-ceramic polymers so ceramic aerogels belonging to the SiOCN system were produced, starting from polycarbosilane (SMP-10), polysilazane (PSZ-20) and polysiloxane (PMHS).

A reliable procedure was set up to produce aerogels with different composition and microstructure, leading to a wide range of properties in terms of density, specific surface, high temperature stability, electrochemical functionality etc., as will be better depicted through the thesis.

Additionally, some application of the materials produced were tested, in which the aerogel shape, combined with the proper chemistry, was expected to give interesting results.

Table of contents

Chapter I

Introduction

1.1 Aerogels

Aerogels are highly porous materials, in which the volume is occupied for the most part by small, open and highly interconnected pores. These pores are sub-micrometric and therefore cannot be seen at naked eye, the material appears indeed very homogenous and *solid*, even though it's usually made of air by more than 90% in volume. The first, and most known, aerogel type is the silica one; produced in 1931 by S. S. Kistler [1] and made of pure amorphous silica. These types of aerogels are transparent with a typical blue nuance when observed on dark background, due to Rayleigh scattering of the light, as can be appreciated in figure 1-1.

Figure 1-1: Silica aerogel disk produced as a reference

Many other types of aerogels were produced after the pioneer work of Kistler, with research devoted to both changing the chemistry of the solid part and to modify the drying route. Up to now, metal oxides, carbides, nitrides and chalcogenides, along with organic and carbonaceous aerogels were produced and studied. An interesting handbook reassuming most of the aerogel synthetic ways, properties and applications was edited in 2011 [2]; it should be noted that at that time, no polymer derived ceramics aerogels were mentioned, since they had not yet been produced.

1.1.1 Production

Many different ways are proposed in literature to produce aerogel materials, with some efforts devoted to study the gel formation pathway and many others focused on modifying the drying procedure. Indeed, two main steps can be defined in the production of an aerogel, the gel formation and its drying.

1.1.1.1 Gel formation

To produce metal oxides gels at least three routes are well studied, all of them taking advantage of the *soft chemistry* process, that enables the processing of solid materials at room temperature from a liquid phase.
The oldest technique is using a solution of sodium metasilicate, Na_2SiO_3, in water. The water is acidified with HCl, and the sodium metasilicate reacts producing NaCl and SiO_2 trough the reaction:

$$Na_2SiO_3 + 2\,HCl + x\,H_2O \rightarrow 2NaCl + SiO_2 + (x+1)H_2O.$$

The water produced, and the one already present in the starting solution, is used to control the porosity of the gel, while the silica builds the solid skeleton creating the gel structure. This route is very cheap since all the chemicals are widely available but needs long processing time, due to the necessity of removing first the NaCl ions through multiple washing with deionized water, followed by a substitution of the water with alcohol or acetone to perform the supercritical drying. It has mostly an historical importance since it was the process used by Kistler to produce the first aerogels.
A more widely applied route is the sol-gel one, that takes advantage of metal alkoxides as metal oxides precursors. The synthesis starts with the hydrolysis of the metal alkoxide as in:

$$M - OR + H_2O \rightarrow M - OH + ROH$$

that is usually promoted by acids and performed in diluted condition using the same alcohol that will be produced by the hydrolysis reaction. Further, the metal hydroxide can condense:

$$M - OH + OH - M \rightarrow M - O - M + H_2O$$

producing the metal oxide solid phase, that usually is in form of colloidal particles suspended in the liquid phase. When the concentration of the colloidal particles is sufficiently high a continuous solid skeleton is built, producing the typical colloidal gel structure.

The last method, named epoxide-initiated (or -assisted) gelation, uses a solution of metal salts, like chloride or nitrate, and initiate the formation of the metal oxide with a proton scavenger, commonly an organic epoxide. The pH increase leads to the subsequent formation of the metal hydroxide and, later on, to the metal oxide, very similarly to what happens in the classical sol-gel route. The main difference from the classical sol-gel technique is the starting precursor, that being a simple metal salt open the possibility to produce gels of many metal oxides, whose alkoxides may be hardly available.

Some other routes to metal sulphides and nitrides gels are actually present, see for example the thio or hydrazide sol–gel processes reviewed by A. L. Hector [3], but much less applied or applied only for very special synthesis.

Another very wide field of aerogel materials is represented by the organic ones, in which polymeric carbon-based precursors are used to produce the gel. The preliminary work was done by R. W. Pekala and his coworkers and published for the first time in 1989 [4]. These gels were produced reacting resorcinol and formaldehyde, producing a network formed by the aromatic rings of the resorcinol bonded by ether bridges, as summarized in figure 1-2. This type of aerogels, along with other similar system like melamine-formaldehyde [5] and polyacrylonitrile [6], can be heat treated in inert atmosphere to convert them into conductive carbonaceous aerogel and graphitic aerogel.

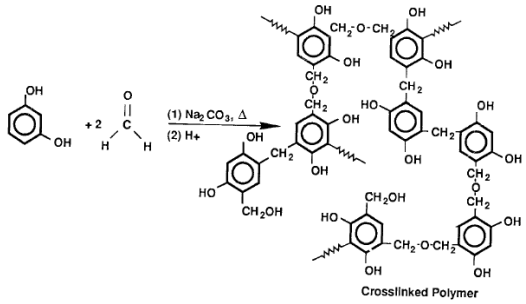

Figure 1-2: Resorcinol formaldehyde gel chemistry [4]

Up to date, many other polymeric aerogels were produced using both natural and synthetic polymers, like cellulose [7], lignin [8], agar [1] and polysaccharides in general [9], polyurethane [10], polystyrene [11] and polypyrrole [12], among many others.

N. Leventis and coworkers opened the way to produce metallic aerogels by carbothermal reduction of metal oxides, using precursors for both carbon and metal oxides and heat treating the intimately mixed system [13]. With the same technique it was possible also to produce metal carbides for those oxides that cannot be reduced

to pure metallic material by carbothermal reduction. In the case of noble metals, it's possible to produce directly the metallic gel and supercritically dry it, as proposed in [14].

1.1.1.2 Drying

The peculiarity of the aerogel production route consists in the distinct drying procedure, which is performed bringing the liquid present in the pores to supercritical conditions and removing it as a supercritical fluid. This "trick" allows to remove the liquid without crossing the equilibrium line of liquid and vapor phase, so no meniscus is formed inside the pores. The presence of the meniscus is indeed accompanied by the development of stresses; for the liquid these are related to the dimension of the pore, the surface tension and the contact angle, through the Young–Laplace equation:

$$p_c = \frac{2\gamma Cos(\theta)}{R}$$

in which γ is the surface tension of the liquid, θ is the contact angle between solid and liquid, R is the radius of the pore (assumed to be cylindrical, as in figure 1-3) and p_c is the capillarity pressure experienced by the liquid, the direction of this pressure is parallel to the cylinder axis.

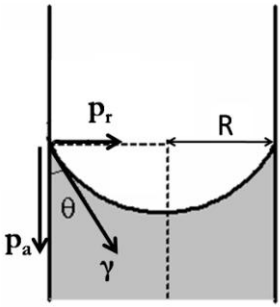

Figure 1-3: p_r and p_a acting on the pore walls

The walls of the pore on the other side experience both a radial pressure, that can be expressed as:

$$p_r = \gamma Sen(\theta)$$

and an axial pressure, expressed as:

$$p_a = \gamma Cos(\theta).$$

This pressure, applied to the surface of the pore walls, may lead to a closure of the pores during a conventional drying. Indeed, it must be considered that the specific surface area (SSA) of these gels is in the order of hundreds of m^2/g, with a total porosity around 90 %vol and density usually about 0.1-0.2 g/cm^2 ; meaning an average pore size in the range 10 - 200 nm. High values of specific surface means high total resulting pressure, that can be hardly tolerated by the low amount of solid material present. In other words, small pores give rise to high SSA values, increasing the total force applied to the skeleton which builds up the pore walls. During a common evaporative drying the surface tension leads to cracks and/or densification, a gel dried with this route is often called *xerogel*.
The path followed during a supercritical drying procedure, summarized in figure 1-4, avoids the formation of the meniscus, therefore no capillary stresses arise and crack-free dry gels can be obtained, in which the solid skeleton of the gel is preserved along with the small pores present among the particles.

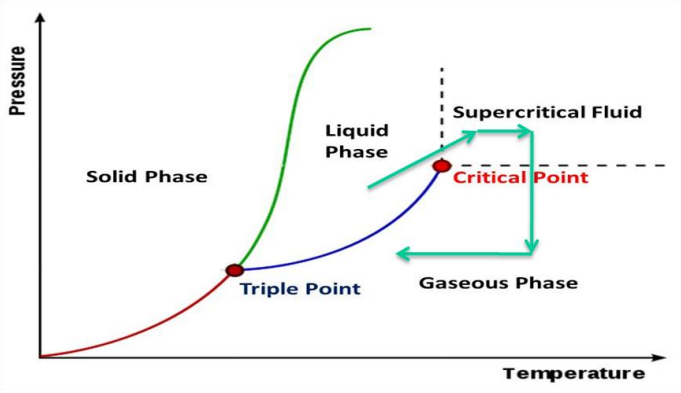

Figure 1-4: Supercritical drying path

In principle, most of the liquids used for gelation and present in the pores after the gel formation can be brought to supercritical condition. Unfortunately, these conditions are usually reached at high temperature and high pressure, that can be prohibitive in a practical reactor, mostly for safety reasons (solvents are typically flammable or toxic). In addition, sometimes the supercritical phase can react with the solid phase as in the case of supercritical water, that is able to readily dissolve some metal oxides. To overcome these problems, a widely used liquid for supercritical drying of gels is CO_2, that possess a practical critical temperature of 31 °C and a critical pressure of 74 bars in addition to be non flammable and non toxic. Accordingly, the liquid of the gel is first exchanged with liquid CO_2 in an autoclave through some washing steps; once CO_2 fully substituted the starting liquid it's

brought above the critical conditions and removed as supercritical phase with a controlled pressure release rate. If the starting liquid in the gel is not miscible with liquid CO_2, for example in the case of water, an intermediate liquid exchange step is introduced with a liquid miscible with both the starting one and the carbon dioxide.
Research efforts are dedicated to speed up the overall process, that on laboratory scale can last more than one week, by using a constant stream of already supercritical CO_2 and proper reactor design.
Other research works try to obtain the same aerogel microstructure avoiding the supercritical fluid approach, by acting on the surface tension of the liquid in order to minimize the stresses due to the meniscus presence. This technique uses drying control chemical additives (DCCA) that allow to produce aerogel-like materials with a much simpler evaporative drying. These additives reduce the surface tension of the liquid and diminish the forces experienced by the solid skeleton during the evaporative drying. With this route the microstructure of the gel shows typically smaller pores and higher density compared to material obtained with the supercritical way, due to the interaction of the DCCA with the gelling solution [15] and to the rising of some stresses related to the meniscus formation. Anyway, mesopores are preserved and the gel is able to sustain the drying and survive as a monolith, being called *ambigel*. Some authors also modify the surface of the solid skeleton, so that part of the shrinkage experienced during controlled evaporative drying can be recovered with a "spring back" phenomenon, triggered by a moderate temperature treatment (100-200°C) and made possible by the absence of chemical bond formation on the pore walls [16] [17].

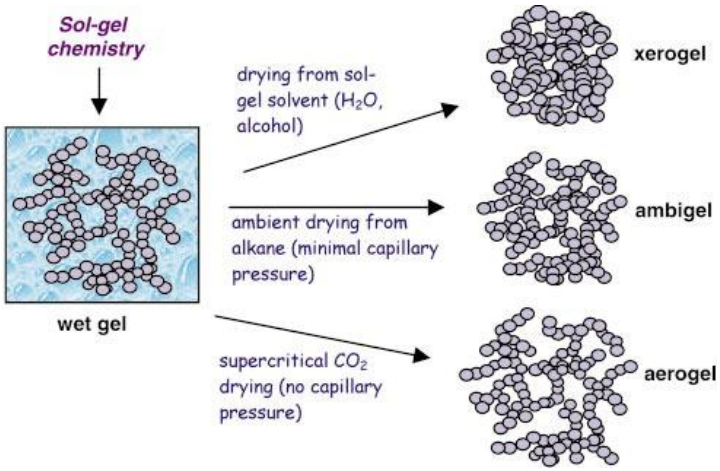

Figure 1-5: Xerogel, ambigel and aerogel route difference [18].

These three types of dried gel structures, aerogel, ambigel and xerogels are summarized in figure 1-5.
To be precise, also freeze-drying is sometimes considered a way to produce aerogels. The technique consists in removing the liquid phase first solidifying it and then sublimating the solid. This kind of drying may allow the production of monolithic materials called *cryogels*, even though most of the times just porous powders are obtained. Additionally, the formation of crystals while freezing the liquid modify the gel structure, introducing anisotropy and much bigger pores compared to those originally present in the gel, making the products very different from the more general aerogel structure.

1.1.2 Properties

Aerogels are composed by two phases, the solid skeleton and gas/pore system. The properties of an aerogel are given by the ratio between these two phases, their connectivity, their morphology and the chemistry of the backbone. As well depicted by G. Reichenauer in [2], "a first visual and manual inspection of an aerogel usually already provides quite a bit of information: is the material transparent or translucent, is it brittle or ductile, how easily can the sample be deformed, how does it sound when you drop a piece of the aerogel under investigation on your table?"
All these first eye properties are the result of the interaction between the density, the pore size distribution and the properties of the solid part. To produce a transparent aerogel it is not enough to have a transparent solid phase, the second condition to be fulfilled is the absence of large pores, precisely pores whose size is comparable with the wavelength of the visible light. The sound produced when dropped is affected, as a first approximation, by the bulk density and the elastic modulus of the solid. Though silica aerogel are fragile, robust aerogels are obtained if the silica backbone is covered with a cross-linked polymer as in [19], pointing out the importance of the bridges between the solid particle to increase the mechanical strength.
More detailed information about the properties can be retrieved by structural and chemical characterization. The most popular characterization techniques applied to aerogels are devoted to understand the microstructure (SEM, N_2 physisorption), the mechanical properties (flexure and compression test) and the chemistry (FT-IR, NMR, XPS). Other characterization methods are applied when a particular application is investigated.
Some typical properties, related to the highly porous nature of aerogel materials are:

- low density (0.01-0.5 g/cm^3),
- high specific surface area (SSA, 100-1000 m^2/g),
- low thermal conductivity (0.015-0.050 W/mK),
- small pores (10-500 nm).

While some other important properties depend on the solid part:

electrically conductive aerogels can be produced by carbonization of various carbon precursors [4],

mechanically strong aerogels (2-8 MPa) are produced if polyimides are used to build the backbone [20],

silica aerogels possess very low dielectric constant (k<2) [21] and high acoustic impedance (10^{-4} - 10^{-5} kg m^2 /s).

transparent aerogels with high transmittance can be produced, for example with SiO_2 (Tr > 90% for 1 cm thick sample [22]) and cellulose (Tr>85% for 0.5 cm thick sample [23]).

These features are not only rare for other types of solids, but can also be tuned changing the chemical precursors, their ratio and the processing route (time, temperature, amount of solvent) used to produce the aerogel.

1.1.3 Applications

Aerogels are used, or their use was proposed, in a very wide number of fields, all of which take advantage of the combination of the porous microstructure and the versatile composition of the solid part.

As major fields, catalysis, thermal insulation, electrochemistry and gas storage can be defined, while other niches like Cherenkov detectors, acoustic coupling, thickening agents, nontoxic pesticides, hypervelocity particle capture, special electronic parts, artistic samples, special molds for aluminum, drug delivery systems, personal care products, optical and electrical sensors, special filters, nuclear waste confinement, nano-thermites and water purification find benefits from the particular aerogel properties as collected in many review articles [24] [25] [2] [26] [27].

Regarding commercial products anyway, mainly thermal insulation is exploited and applied to architectural, petrochemical and clothing fields, with two companies that produce mostly SiO_2 based aerogel blankets, specifically for low (-200°C) and high (650°C) temperature: Cabot Corporation [28] and Aspen Aerogels [29]. Another company, Oros apparel [30], sells an aerogel insulated jacket (of composition not better defined than "SolarCore aerogel") after a Kickstarter campaign to raise funds to start the production. A fourth company, named Aerogel Technologies LLC [31], sells products of the first three and additional polyurea and polyimide aerogels possessing much better mechanical properties (MPa range), but lower maximum temperature (80-300°C) and slightly higher thermal conductivity than SiO_2 aerogels. Aerogel Technologies sells also monoliths of silica, resorcinol-formaldehyde and carbon aerogels, along with art pieces like those produced by Ioannis Michalous [32]. Further commercialization of aerogels is hindered by the relatively high price of these materials with respect to competitors, that often show worse properties but are much cheaper. In those cases in which the properties cannot be matched by other

existing materials (usually due to limitations in space and weight) the aerogels are applied, funding the R&D that allows to compete on a wider playground.

1.2 Polymer derived ceramics (PDC)

The use of a polymer as a precursor for a non-oxide ceramic material was for the first time reported more than 50 years ago from Chantrell and Popper [33]. Some years later a patent was deposited by W. Verbeek [34] to produce ceramic fibers (and other "shaped articles") made of homogeneous mixture of silicon carbide and silicon nitride through the pyrolysis of a polysilazane precursor. About in the same years, Yajima published a procedure to produce a polycarbosilane that could be melt-spun to produce SiC fibers after pyrolysis [35]. The PDC route is somehow similar to the sol-gel route, i.e. the object is shaped at low temperature and the final chemistry is controlled by the precursors chemistry, with a main difference that carbide and boride ceramics can be produced (sol-gel is developed for mainly oxides, nitrides and chalcogenides) and that a thermal treatment (pyrolysis) is needed to convert the polymer into the ceramic material.
Some review papers and books were published, trying to summarize the vast field of PDC materials in terms of chemistry, properties and applications. [36] [37] [38] [39] [40] [41] [42] [43] [44] [45] [46] [47].

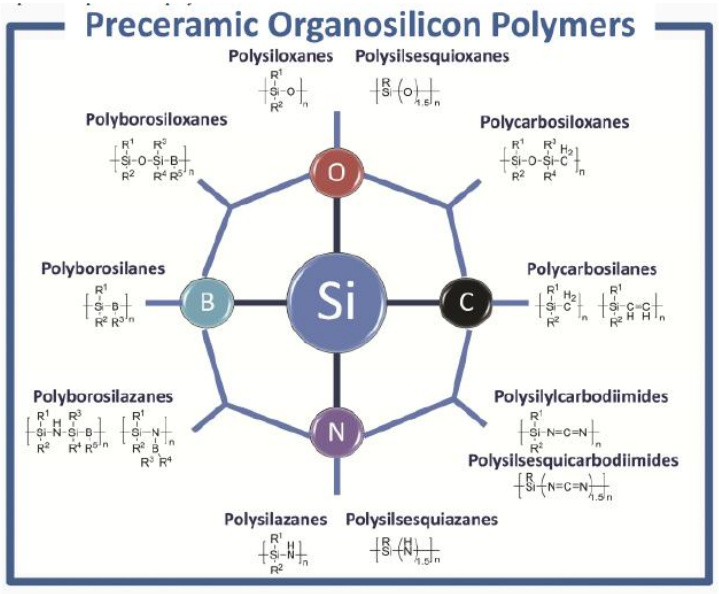

Figure 1-6: General composition of organosilicon polymers [32]

Typically, pre-ceramic polymers are Si based polymers, with composition and relative general name summarized in figure 1-6.
Polymers based on boron and aluminum, precursor for BCN and AlCN, can also be produced but are much less common, and used mostly for research purpose and in limited amounts.

1.2.1 Production

The production of organosilicon polymers starts from silicon chlorides, that are obtained by reaction of silicon with Cl_2 or HCl at high temperature. The silicon source can be either metallic silicon, ferrosilicon alloys, silicon carbide or mixtures of silica and carbon. The Si-Cl and Si-H bonds are fairly reactive and can be used to introduce different functionalities, expressed in figure 1-7 as Si-R.

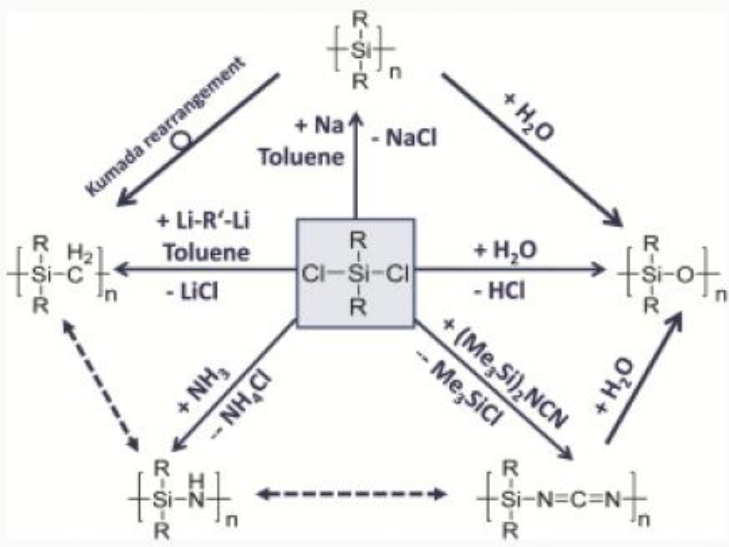

Figure 1-7: Typical routes to different organosilicon polymers [32]

The chlorosilane monomers can be polymerized with different compounds to obtain polysiloxanes, polysilazanes, polysilanes, polycarbosilanes and polysilylcarbodiimides and further functionalized to introduce extra elements like boron, hafnium etc., as reviewed in [38].
Apart from the chemistry, which is controlling (together with the pyrolysis atmosphere) the composition of the final ceramic, an important feature of a pre-ceramic polymer is the pyrolysis yield, i.e. the %mass of ceramic material obtained

after the thermolysis in inert environment. To reach high yield values (typically 70-80%), the polymer should be of sufficiently high molecular weight to avoid volatilization during shaping and cross-linking; cages, rings and branched structure also help to reduce the production of volatile fragments during pyrolysis [48]. Regarding the possibility to shape the component, the polymer should be either liquid, meltable or soluble in a solvent; the presence of latent reactivity is useful to cross-link the polymer in order to set the shape.
The ceramic is obtained, as previously introduced, by a thermal treatment in inert atmosphere called pyrolysis, typically, after a treatment above 1000°C an amorphous ceramic material is produced. During this treatment the polymer experiences a mass loss, due to the production of volatile molecules like small silanes, hydrogen, methane and other hydrocarbons, and a shrinkage related to the change from a polymer, with a typical density of ~ 1 g/cm^3, to a silicon-based ceramic having a density of ~ 2-3 g/cm^3. During the pyrolysis treatment many factors can play a role on the properties of the ceramic material obtained. Among them, the type of gas used (inert, reactive, vacuum) [49] [50], the heating rate, maximum temperature reached and dwelling time, the presence of fillers and their composition, shape and dimensions [51] [52] can modify the chemistry and the microstructure of the PDC produced.

1.2.2 Properties

Si-based PDCs are a wide family of ceramic materials; changing the starting organosilicon polymers is possible to produce amorphous Si-C, Si-C-N, Si-O-C along with nanocomposites of the previous ceramics and amorphous carbon. It's also possible to introduce boron [53], hafnium [54], zirconium [55] and aluminum [56] , creating a lot of different materials with tunable properties. This is to point out that, as previously seen with aerogels properties, a proper discussion on PDC properties can be very long as one should consider all the specific compositions and features. For the readers' sake just a brief summary of the general properties of the most studied PDC system, will be presented.
Typically, the dispersion of the elements in the ceramics obtained by PDC route is so good that after pyrolysis the material is an amorphous ceramic, showing high resistance to crystallization and to creep, good hardness, high resistance to chemical attack and toward oxidation. In some cases, PDCs start to crystallize around 1200-1300°C (Si-C, Si-O-C) [57], [58], [59] while in others the crystallization temperature can reach very high values, as in the case of Si-B-C-N which crystallize above 1700°C [53]. Aside the remarkable high temperature properties, Si based PDCs also possess various functional features like piezoelectricity [60], electrical conductivity and semiconductivity [61] [62], ferromagnetism [63], transparency [64] [65], lithium host capacity [66] and photoluminescence [67].

1.2.3 Applications

A key advantage of using the PDC process to produce ceramic materials is the versatility of shaping technologies that can be used. Indeed, nearly all the techniques developed for conventional polymeric materials were applied to pre-ceramic polymers. Among these, thin layer technologies like tape casting [68], dip- and spin-coating [69] [67], spraying [70], ink jetting [ref], UV lithography [71] allow to produce high tech coatings and microcomponents. Ceramic matrix composites (CMC) can be produced by impregnation of a fiber fabric with the ceramic precursor and subsequent pyrolysis (PIP process, polymer impregnation and pyrolysis), multiple PIP cycle allow obtaining a dense CMC [72]. In addition, the fibers can even be produced by PDC route so fully ceramic CMC are obtained. Ceramic nanopowders can be obtained by emulsion process [73] while dense components are produced by warm pressing [74]; direct blowing of pre-ceramic polymers allows producing ceramic foams [75] and layers of pre-ceramic polymer with proper filler materials can be used to join ceramic monoliths [76]. The polymer to ceramic transformation can be stopped at intermediate temperature (450-800°C) to take advantage of the microporosity formed during the ceramization reactions for gas sorption or separation application [77]. Micro- and meso- porous materials can also be obtained by etching the PDC with HF to remove silica nanodomains [78] or with Cl_2 to selectively remove Si atoms [79].

Thanks to such a versatile shaping approach, PDC are applied as structural and thermo-structural components in harsh/high temperature environment, as in the case of CMCs and fibers [80], and micro mechanical system (MEMS) [44]. Additionally, functional application like optical and electrical sensors [81], catalyst support [82], gas separation membranes [77] and gas storage [83], lithium batteries anodes [84], anti-graffiti coatings [85], high temperature sealant [86], heating elements [87] and brake pads binder [88].

On the market is present a wide range of siloxanes, also called silicones, that can be used as precursors for SiOC ceramics. (Note that not all the silicones can be used since, as previously stated, apart from the chemistry the polymeric precursor should have reactive moieties that can be used to cross-link the polymeric chains and decrease their volatilization during pyrolysis). Polycarbosilanes are also on market, with widely known SMP-10 product from Starfire Systems Inc. and polysilazanes from KiON Defense Technologies. Other ceramic precursors were commercialized in the past, like Nippon Carbon or Sigma Aldrich polycarbosilanes, or are produced by specialized companies to be directly used to manufacture fibers as in the case of Nicalon, Sylramic and Tyranno Si(O)C fibers.

1.3 Motivation of the work

We are interested in producing silicon carbide, oxycarbide and carbonitride aerogels. In literature, metal carbides aerogels are produced only by carbothermal reduction, heat treating at high temperature in inert atmosphere aerogels composed by a mixture of oxides and carbon; if nitrogen and/or ammonia atmosphere is used, carbonitrides aerogels can be obtained. Taking advantage of the PDC process to produce these kinds of aerogels is believed to greatly enhance the versatility and simplify the production route. Silicon oxycarbides areogels on the other side can be produced by classical sol-gel technique and the PDC route in this case could be beneficial to expand the chemical composition range of this kind of materials.
In this thesis the objective was to produce gels made of pre-ceramic polymers, like polysiloxane, polycarbosilane and polysilazane, to dry them with supercritical CO_2 method, and heat treat them in controlled atmosphere to obtain the relative silicon carbide, carbonitride or oxycarbide. This method started to be developed in the Ceramic and Glass Laboratory of the University of Trento right before the beginning of this PhD thesis work [89].

Chapter II

Experimental

In this chapter, a brief description of the experimental part will be given, starting with some details about the equipments used to obtain the PDC aerogels, the reagents and the characterization methods; to move in the end to the synthesis procedure.

2.1 Equipments

2.1.1 Parr digestion vessel

As will be illustrated in the last paragraph of this chapter, the synthesis route requires a mild temperature (150°C) to increase the cross-linking rate of the polymers. Unfortunately, the solvents used to produce the gels possess a boiling point at ambient pressure well below that temperature (56-81°C) so a way has to be found to keep the solvent liquid during the cross-linking and formation of the gel. The solution adopted is to perform the gelation in a closed vessel, in this manner during heating part of the solvent will evaporate and the pressure will rise to match the vapor pressure of the solvent, maintaining it liquid. The vessel should be able to stand the pressure, the temperature and be non-reactive with any of the chemicals used. Parr digestion vessels (Parr Instrument Company) are widely used for this kind of tasks, as shown in figure 2-1 they consist of a chrome plated bronze jacket that provide the mechanical strength required, an inner chemically inert PTFE (polytetrafluoroethylene) liner and a sealing cap provided with a spring, able to release unpredicted high pressure build up.
The used model is a Parr Digestion Vessel 4749, with an inner cup capacity of 23 mL, a maximum temperature allowed of 250°C and a maximum pressure of 125 bar.

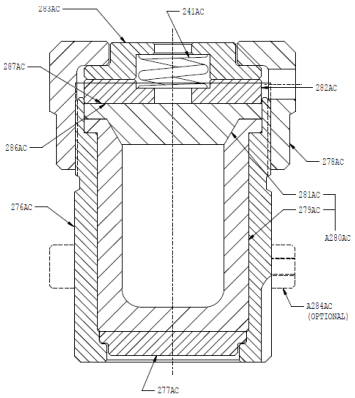

Parts List	
Part No.	Description
241AC	Spring
264AC2	Hook Spanner
276AC	Vessel Body (23 mL)
276AC2	Vessel Body (45 mL)
277AC	Bottom Disc
278AC	Screw Cap
A280AC	PTFE Cup with cover (23 mL)
A280AC2	PTFE Cup with cover (45 mL)
282AC	Pressure Plate, lower
283AC	Pressure Plate, upper
A284AC	Tumbling Ring
A285AC	Holding Fixture
286AC	Corrosion Disc, .002"
287AC	Rupture Disc, .003"

Figure 2-1: Parr digestion vessel schematics and spare part list

2.1.2 CO_2 autoclave and thermo bath

Once the gels are obtained, the starting solvent must be substituted with liquid CO_2, through multiple washing, before bringing the CO_2 above the critical point to remove it as supercritical fluid. To perform these washing steps and supercritical drying (SCD) it's needed an autoclave that can withstand the high pressure (100 bar) involved and whose temperature can be precisely controlled, at least within 1°C, and changed at will. Some commercial autoclaves specifically designed for CO_2 SCD exist on the market, for example automatic critical point drier provided by Tousimis®, manual autoclave from Structure Probe Inc. and reactor systems for industrial volumes provided by Parr Instruments Company and Amar Equipments Pvt Ltd. Unfortunately, all the commercial devices are pretty expensive (>10000 €) and designed for drying well know samples with less devotion to research custom features.

For these reasons, a custom autoclave was built by the UniTN department of physics machine shop, using schematics, ideas and solutions from the web [29], from professors R.Campostrini, G.D.Sorarù, V.M.Sglavo and V.Fontanari along with work experience of technician P.Gennara.

The autoclave, shown in figure 2-2, has the great advantage of possessing two glass windows, that allow to see through to evaluate the liquid level and, most importantly, to follow samples behavior during all the liquid exchange steps and drying (figure 2-3). Valves, pipings and joints were purchased from Swagelok® while the CO_2 tank (figure 2-4) was provided with a deep drain tube to extract directly the liquid CO_2.

The design of the autoclave provided the possibility to change the temperature of the device connecting it to a thermostated water bath (figure 2-4).
The thermobath was not only used to bring the whole system above the critical temperature of CO_2 to perform the SCD, but also to fill the autoclave with liquid CO_2. Indeed, there's no reason for the liquid CO_2 to fill the autoclave since no pump is connected to the system and, in absence of other external factors, the equilibrium pressure would be quickly reached on both the branches of the system. However, by using the thermobath to cool the autoclave below room temperature it's possible to create a stable difference in pressure between the CO_2 tank (which is at room temperature) and the autoclave, allowing the draining of liquid from the tank for the exchange steps.

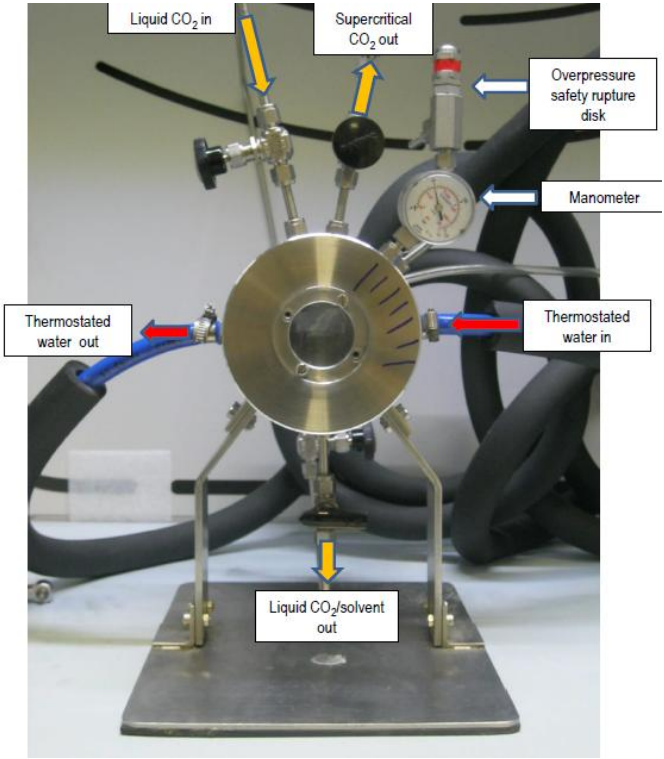

Figure 2-2: CO_2 supercritical autoclave

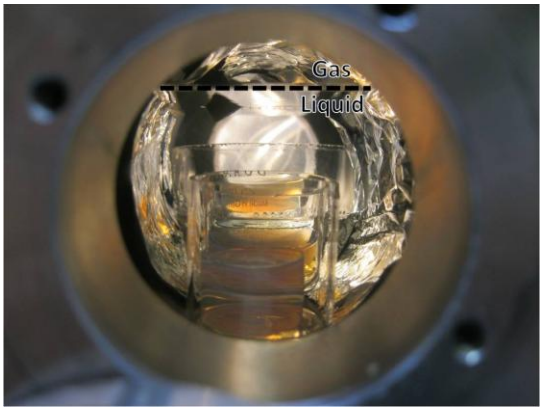

Figure 2-3: Three fully visible samples immersed in liquid CO_2

Figure 2-4 : Thermostated water bath and liquid CO_2 tank

2.1.3 Tubular furnaces

To convert the pre-ceramic aerogels into silicon carbide, oxycarbide and carbonitride aerogels a thermal treatment in inert environment (pyrolysis) is needed. Tubular furnaces allow to control the atmosphere inside the tube and are often applied for this kind of treatments. Within this work, two types of tubular furnaces were used, the most used one is a Lindbergh Blue high temperature furnace with an alumina tube, shown in figure 2-5, capable of reaching 1600°C as a maximum temperature and connected to argon, nitrogen and synthetic air lines. The second one is a Gero tubular furnace limited to 1100°C and equipped with a silica tube, that was used for special treatments with Cl_2 and H_2 gas flow in the Technical University of Dresden (TUD).

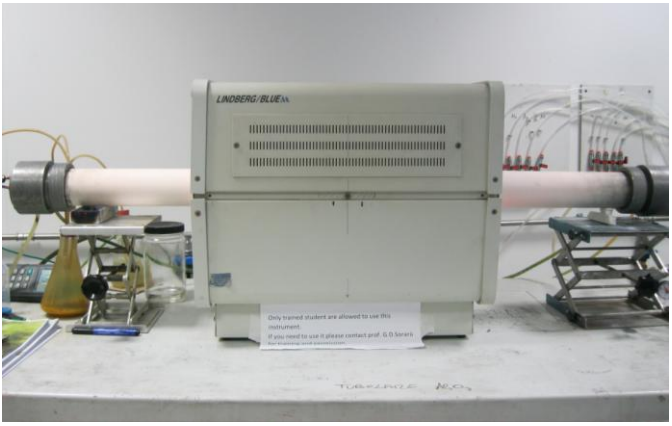

Figure 2-5: High temperature tubular furnace Lindbergh Blue

2.1.4 Graphite furnace

For high temperature stability test a high temperature graphite furnace (Astro model 1000-4560-FP30, Thermal Technology LLC, figure 2-6) was used, connected to argon line and to flowing water cooling. The original graphite/boron carbide thermocouple was calibrated with a C type thermocouple and a Ircon Ultimax® pyrometer.

Figure 2-6: Astro high temperature graphite furnace

2.2 Reagents

Three commercially available liquid pre-ceramic polymers were chosen to produce ceramic aerogels belonging to the Si-C-N-O system, all of them bearing Si-H moieties in order to be cross-linked by the hydrosilylation reaction.

2.2.1 Polycarbosilane SMP-10

Starfire's SMP-10 allylhydropolycarbosilane (also known as AHPCS) imposed itself as the world's most used polycarbosilane thanks to some key features that allow good processability and final properties of the ceramic. First of all it's a low viscosity liquid that can be used in PIP (polymer infiltration and pyrolysis) process, filling all the voids and pores without the need to be melted. Second, as can be seen in the

structural formula drawn by L.Interrante in [90] and reported in figure 2-7, it possesses allyl moieties that can be used to thermally cross-link it at a moderate temperature, that can be also lowered with the addition of a peroxide radical initiator. Third, the presence of abundant Si-H groups makes possible to keep the Si/C molar ratio close to 1. The combination of branched structure, high presence of reactive group and low amount of carbon allow to obtain, after pyrolysis, a nearly stoichiometric SiC with high mass yield of ~80%.

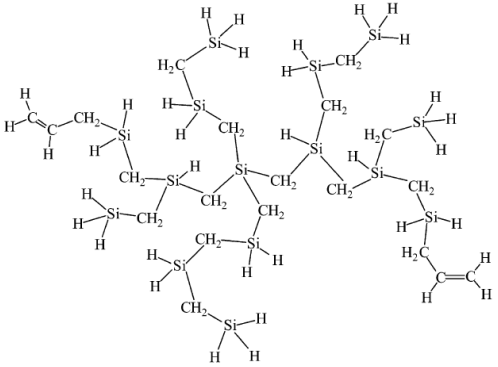

Figure 2-7: Structural formula of AHPCS as resulted from GPC and NMR studies [90]

Some properties of the polymer are reported in table 2-1 as specified in Starfire's datasheet.

	Properties of StarPCS™ SMP-10
Density	0.998 g/cm^3
Appearance	Clear, Amber liquid
Viscosity	40 to 100 cPs at 25°C
Compatible Solvents	Hexanes, Tetrahydrofuran, Toluene, Insoluble in water
Flash Point	89°C
Moisture Absorption	<0.1% in 24 hours at room temperature, moisture sensitive
Surface Tension	30 dynes/cm^2
Storage	Vacuum container or inert environment; Refrigerated
Cross-linking	180-400°C

Table 2-1: SMP-10 general properties

The polymer was characterized with NMR and FT-IR analysis, the results are reported in figures 2-8, 2-9 and 2-10. Assignments of the peaks in the NMR and FT-IR spectra were done based on literature [91] [92] [93].

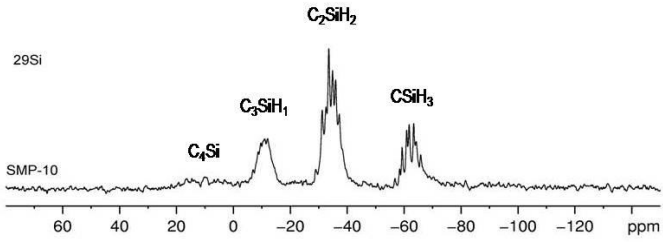

Figure 2-8: 29Si NMR spectrum of virgin SMP-10

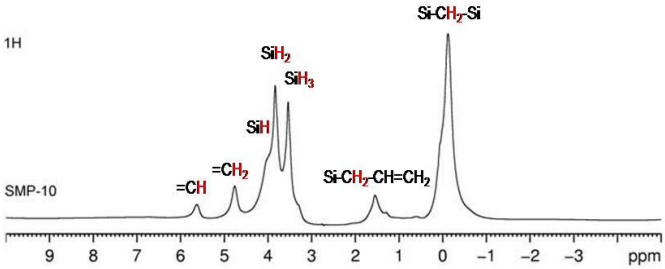

Figure 2-9: 1H NMR spectrum of virgin SMP-10

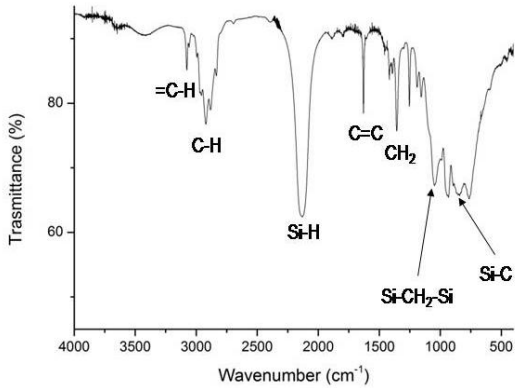

Figure 2-10: FT-IR transmission spectrum of virgin SMP-10

The spectra reveals a structure very similar to the one reported in figure 2-7 which is also close, in Si-H and C=C moieties ratio, to the average composition reported by Starfire's vendor and presented in figure 2-11.

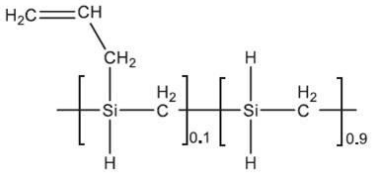

Figure 2-11: Average composition of SMP-10 as declared by Starfire's vendor

Thermogravimetry was performed on the neat SMP-10, cross-linked at 150°C with the addition of 10 ppm of Pt catalyst (Karstedt's catalyst), in Argon flow with a heating rate of 10°/min (figure 2-12). The Pt catalyst promotes the hydrosilylation cross-linking as will be shown later on. It can be seen that most of the weight loss is experienced below 1000°C, reaching a total value slightly above 20%. This mass loss is attributed to evolution of H_2, CH_4, SiH_4 and CH_3SiH_3 produced by dehydrocoupling and redistribution reactions among Si-C, C-H and Si-H bonds. [93]

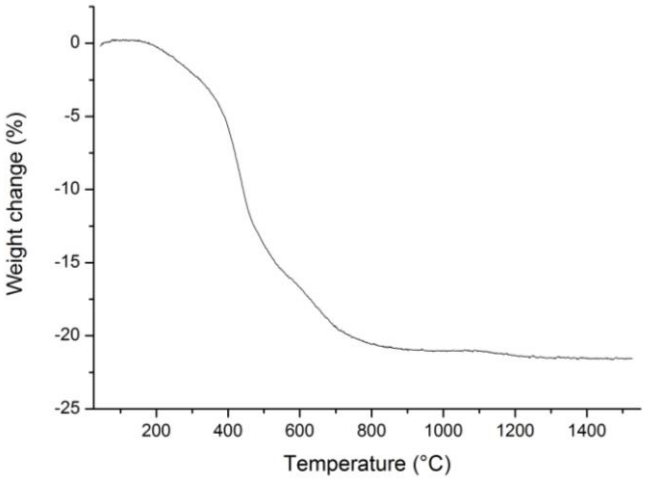

Figure 2-12 :TG curve measured on cross-linked SMP-10

2.2.2 Polysilazane PSZ-20

Ceraset® PSZ-20 is a liquid polymeric precursor for Si-C-N ceramics sold by Clariant GmbH and originally developed by KiON Defense Technology. Some properties extracted from the Clariant's datasheet are reported in table 2-2.

Properties of Ceraset® PSZ 20	
Density	1.0-1.1 g/cm^3
Appearance	Pale yellow liquid
Viscosity	180 to 750 cPs at 20°C
Compatible Solvents	Dry aprotic solvents (alkanes, ethers, esters)
Flash Point	63°C
Moisture Absorption	Moisture sensitive, quick processing in air possible
Storage	Refrigerated (4°C), 6 months shelf life
Cross-linking	100-250°C

Table 2-2: General properties of PSZ-20

The structure of this polymer, similarly to SMP-10 polycarbosilane, contains both C=C and Si-H groups, as can be seen from the figure 2-13 reported in the technical bulletin provided by KiON [94], that allow a the cross-linking of the polymer.

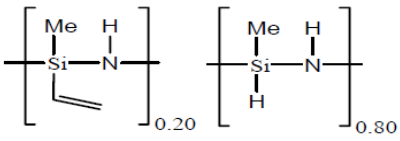

Figure 2-13: Average composition of PSZ-20

The characterization with NMR and FT-IR (spectra in figure 2-14, 2-15, 2-16) confirmed the average structure provided by the company.

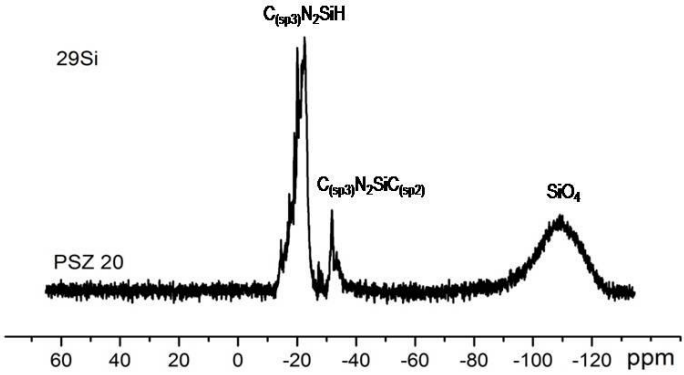

Figure 2-14: 29Si NMR spectrum of PSZ-20

The SiO_4 units presence evidenced by the peak at -110 ppm in the ^{29}Si spectrum indicates the reactivity of the polymer towards atmospheric moisture. It should be noted that the acquisition of ^{29}Si spectrum took more than one day while the open air use for the synthesis was maintained in seconds-to-minutes range, indeed, no silica traces were observed in the FT-IR spectrum. Assignments of the peaks in the NMR and FT-IR spectra were done accordingly to literature [95] [96] [97].

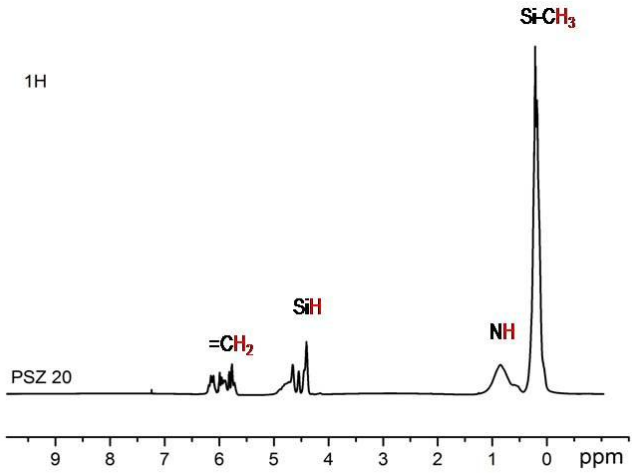

Figure 2-15: 1H NMR spectrum of PSZ-20

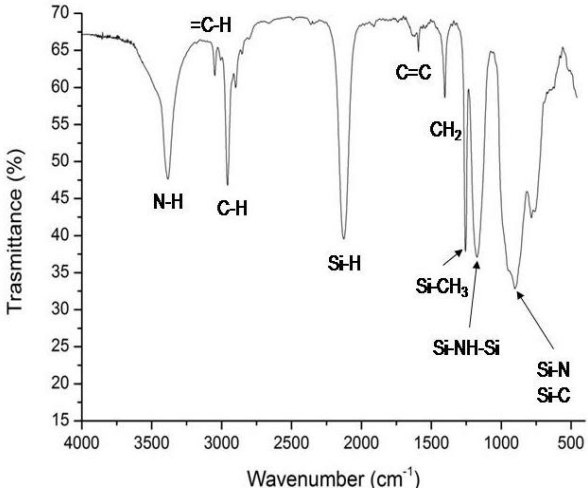

Figure 2-16: FT-IR spectrum of PSZ-20

Thermogravimetry (figure 2-17) was performed, as for the SMP-10 polymers, after cross-linking the PSZ-20 at 150°C with the addition Karstedt's catalyst. Argon flow was used. PSZ-20 experiences a mass loss due to evolution of oligomers (low temperature, first step) higher than SMP-10, but a final mass loss lower than the polycarbosilane. Additionally, at temperature higher than 1400°C the TG curve shows a new mass loss step related to the decomposition of silicon nitride, with production of silicon carbide and nitrogen gas as depicted by the equation:

$$Si_3N_4 + 3C \rightarrow 3SiC + 2N_2$$

as in reference [98]. The decomposition at 1400°C is visible if argon is used as a inert gas, while is hindered/delayed in nitrogen flow [99]. From literature, the evolved products in the case of silazanes pyrolysis are similar to those found for polycarbosilanes, with the addition of N containing molecules like ammonia or small organic amines deriving from transamination reactions and N_2 at high temperature [100].

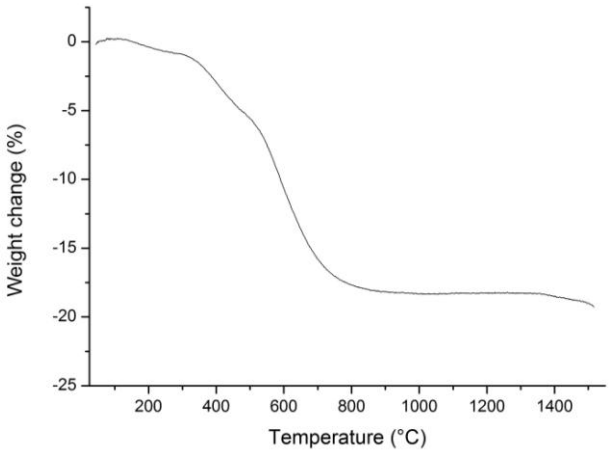

Figure 2-17: TG in argon flow of Pt cross-linked PSZ-20

2.2.3 Polysiloxane PMHS

PolyMethylHydroSiloxane (PMHS), is a transparent liquid silicone oil possessing low viscosity and widely used as mild reducing agent in organic chemistry. Differently from SMP-10 and PSZ-20, it's not a proprietary silicon based polymer, it possesses a linear structure and does not bear C=C moieties. Some properties are reported in table 2-3, collected from various datasheet (Sigma-Aldrich, Alfa Aesar) and from reference literature. The polymer used in this thesis work was purchased from Alfa Aesar and possessed a viscosity of 25 cPs and a purity of 97%. To be used as a pre-ceramic polymer it must be modified to be properly cross-linked prior to pyrolysis. A first method was used by Lu [101] who converted part of the Si-H in Si-OH, the Si-OH groups can then condense and produce oxygen bridges that render the polymer infusible. A pyrolysis in nitrogen at 700°C of this condensation cross-linked PMHS gives a yield of 73%. Another method, developed by Blum [102] is to use the Si-H bonds to cross-link and functionalize the polymer with a vinyl bearing siloxane or with divinylbenzene (DVB). Depending on the amount of DVB used, SiOC ceramic are obtained after pyrolysis with different yield and free carbon content [103].
NMR characterization was not performed since the structure, reported in figure 2-18, is well established in siloxane field.

Properties of PMHS	
Density	1.0 g/cm^3
Appearance	Transparent liquid
Viscosity	10 to 50 cPs at 20°C
Compatible Solvents	Hydrocarbons, ethers, acetone, alcohols but MeOH
Flash Point	204°C
Moisture Absorption	Slightly moisture sensitive
Storage	Cool, dry storage, no special requirements
Cross-linking	Oxidation, Hydrosilylation

Table 2-3 : General properties of PMHS

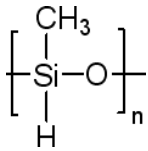

Figure 2-18:Average structural formula of PMHS

A control FT-IR spectrum (figure 2-19) was acquired which confirms very well the structure proposed above.

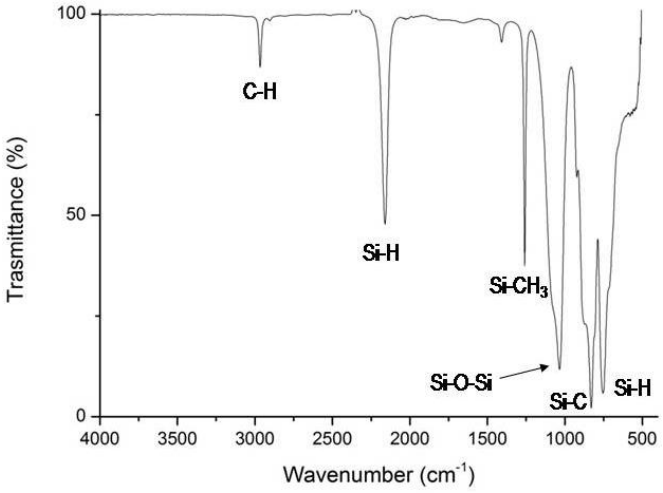

Figure 2-19: FT-IR spectrum of PMHS polymer

2.2.4 Cross-linkers, DVB and TVS

As was presented before, all the used ceramic precursors bear Si-H functional groups that can be used to cross-link them by means of hydrosilylation reaction. This type of addition reaction, as shown in the equation below, is free of by-products and can be efficiently catalyzed by Pt compounds, allowing the curing of the pre-ceramic resins at low-to-mild temperature (RT to 200°C)

$$Si - H + C = C \rightarrow Si - C - C$$

The first cross-linker investigated was divinylbenzene (DVB), being an aromatic ring with two vinyl groups in ortho or meta positions as shown in figure 2-20. It was bought from Sigma Aldrich, technical grade, 80% mixture of isomers with ethylvinylbenzene and diethylbenzene. Even though it contains 1% of polymerization inhibitor it must be stored in a cold place (2-8°C), indeed after some days at room temperature it turns from a clear liquid into a transparent solid resin.

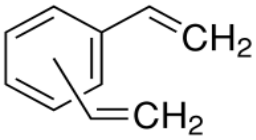

Figure 2-20: Structural formula of DVB

The FT-IR spectrum of DVB is reported in figure 2-22 and confirms the structure, evidences of the mixture of o- and m- disubstituted benzene are noted, the assignment of the peaks was done from reference literature [104].
The second cross-linker used was tetravinylsilane (TVS), a tetrafunctional Si-based molecule which structure is reported in figure 2-21.

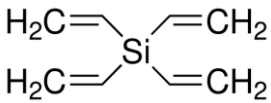

Figure 2-21: Structural formula of TVS

It was purchased from Fluorochem ltd. with a declared purity of 97% and stored in the same conditions as DVB, even though its reactivity was noticed to be lower (no solid formation if left out from the fridge for some days). The corresponding FT-IR

spectrum is reported in figure 2-23, the assignments were done based on literature [105] and confirm the structure of figure 2-21.

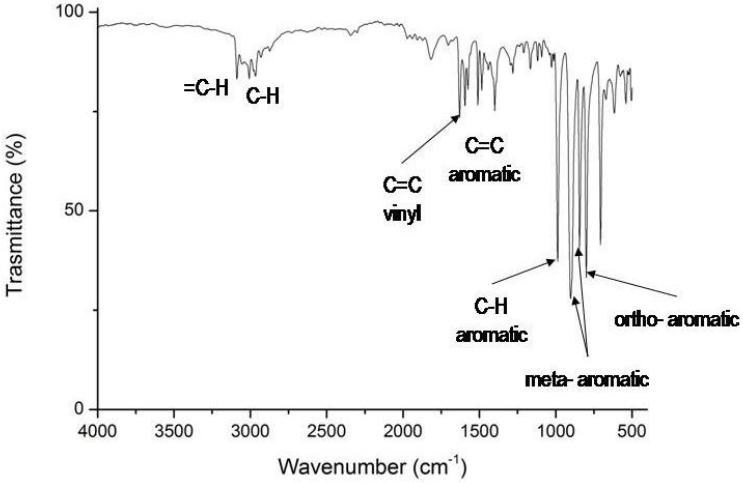

Figure 2-22: FT-IR spectrum of DVB

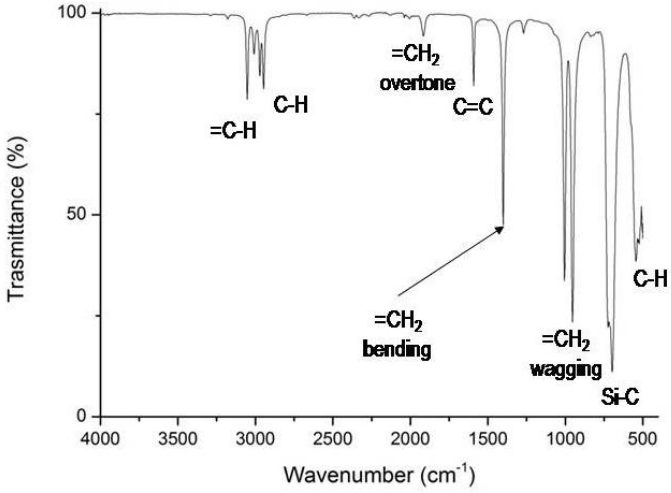

Figure 2-23 FT-IR spectrum of TVS

2.2.5 Solvents and catalyst

The solvents requirements in this works were: ability to dissolve all the reagents, inertness with regard to the reagents, in particular to Si-H groups, and possibly mixable with liquid CO_2. Cyclohexane is a very low polarity aprotic solvent that perfectly matches all these requirements so it was used in high quantities and from different sources, i.e. Sigma Aldrich, Exacta-Optech and Alfa Aesar, the purity being always higher than 99.5%. Acetone is an aprotic highly polar solvent and was used only to produce some PMHS/DVB gels to investigate the role of the solvent in the gelation and drying processes. Similarly, tetrahydrofuran (THF) was used to produce some SMP-10 gels with a polar solvent since the polycarbosilane could not be easily dissolved in acetone.

	Acetone	Cyclohexane	THF
Boiling point (°C)	56	81	66
Density (g/cm^3)	0.79	0.77	0.88
Dipole moment (D)	2.7	0	1.8
Dielectric constant (ε_r)	20.7	2.0	7.6
Surface tension (mJ/m^2)	25.2	25.0	26.4
Vapor pressure 150°C (bar)	10.7	6.7	8.0

Table 2-4 : General properties of the solvents used

Both THF and acetone were purchased from Sigma Aldrich with a purity >99.5%; THF contained 250 ppm of BHT as peroxide inhibitor. Some properties of these three liquids are reported in table 2-4. The hydrosilylation reaction, even though thermodynamically favored, do not proceed in absence of catalyst at low temperature, indeed the exploit of this reaction started after the discovery of the very efficient hexachloroplatinic acid catalyst by J.L.Speier [106] [107] [108]. Another very powerful Pt catalyst is the so called "Karstedt's catalyst" that consist of a Pt(0) organometallic compound in which the platinum atoms are coordinated with the vinyl groups of 1,3-divinyl-1,1,3,3-tetramethyldisiloxane as shown in figure 2-24.

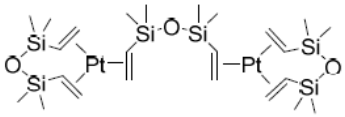

Figure 2-24: Structural formula of Karstedt's catalyst complex

This catalyst is even more active than the hexachloroplatinic acid and can be dissolved in organic non polar solvent, making it the most used hydrosilylation catalyst in the silicone industry [109] [110]**.** It was purchased from Sigma-Aldrich in a xylene solution containing 2% of Pt. For practical dosing this solution was further diluted 1:19 in xylene to obtain a practical 0.1% Pt catalyst solution.

2.3 Characterization methods

Here will be presented some details of the characterization techniques used.

2.3.1 Density measurements

To characterize highly porous materials like aerogels, the first, important and (usually) simple method is to measure the "bulk" density (also called geometrical density), defined as the ratio between the weight and the geometrical volume occupied. This is not an intrinsic property of a material but depends on the amount of porosity and the true density (also, skeleton density) of the solid material, as depicted in figure 2-25**.**

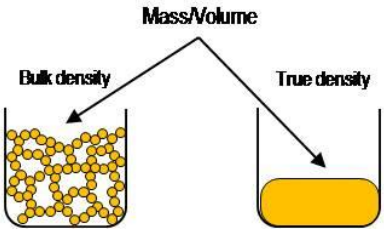

Figure 2-25: Concept definition of bulk and true density

If the sample is a monolith with a regular shape like a cylinder or a parallelepiped, the task is easily accomplished with a caliper and an analytical scale. For this reason, care was taken to produce regular cylindrical aerogels sample of appropriate volume (>1-2 cm^3) to minimize the errors done by caliper measuring.
The true density was measured by helium picnometry with a Micromeritics instrument (model 1035). Helium picnometry allows indeed to measure the real volume occupied by the solid part of the sample, if closed porosity is absent. The general scheme of a picnometer is shown in figure 2-26 in which Vs is the volume of the sample, Vc is the volume of the chamber without the sample, Vr is a reference volume and M represents the manometer.

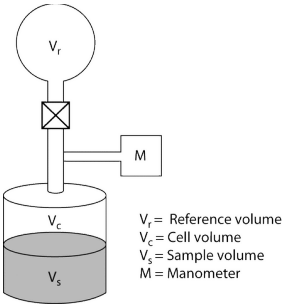

Figure 2-26: General scheme of a picnometer

The working principle is the following:

in isothermal state, the chamber containing the sample is pressurized with helium, which amount is given by the volume occupied (Vc-Vs) and the pressure reached (P_1) by the well know gas equation PV=nRT;

the helium is expanded in a reference volume (Vr) and the equilibrium pressure is measured (P_2);

being known Vr and Vc, and P_1 and P_2 is possible to calculate Vs through the equation:

$$Vs = Vc - \frac{Vr}{(\frac{P1}{P2} - 1)}.$$

The calculated Vs represents the volume that cannot be occupied by helium gas, so the real volume of the solid part of the sample, plus the volume occupied by closed porosity, if present. If this value is used to calculate the density, the true density of the solid is computed.

2.3.2 Porosity measurements

Measuring the porosity means to quantify the amount of pores present in the sample. The quantity is usually expressed in volumetrical percent (%vol) or in a kind of "inverted" density expressed as cm^3 of pores per gram of material (cm^3/g or cc/g).
The total amount of pore volume can be quickly computed from bulk (ρ_b) and skeleton (ρ_s) density values, by applying the equation:

$$\%vol_{pores} = 1 - \frac{\rho_b}{\rho_s}.$$

This value accounts just the total pore volume, giving no information about the size of the pores present in the material. To estimate the pore size distribution (PSD), nitrogen physisorption and mercury porosimetry methods can be used.
Mercury is non-wetting liquid (contact angle between 135° and 142° with most solids) that can be pushed (intruded) inside the pores of a material by applying an external pressure. The volume of liquid intruded *vs* applied pressure (P_{ext}) is used to compute the volume of pores with a certain size (D_p), through the equation:

$$D_p = \frac{1470\ kPa \cdot \mu m}{P_{ext}}.$$

With mercury porosimetry the distribution of the size of the pores in a range from hundreds of micron to 2-3 nm can in principle be measured; it should be noted anyway that mercury necessitate high pressure to fill the smallest pores, this can modify the actual size of the pores or even cause the breaking of the sample.
Nitrogen physisorption on the other side, instead of pushing a liquid inside the pores, take advantage of the adsorption of gas on the surface and of the thermodynamically favored condensation of it in small pores. A general scheme of a physisorption instrument is reported in figure 2-27.

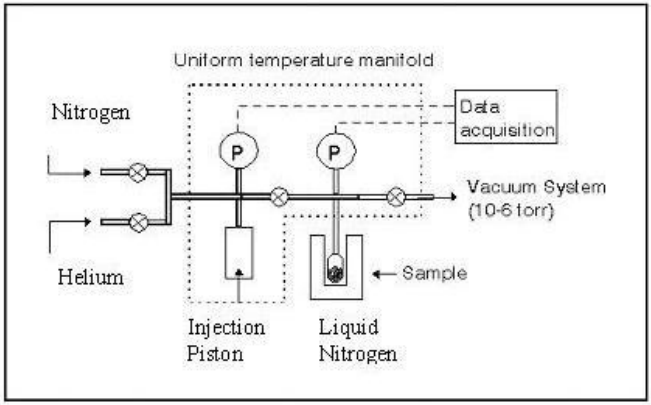

Figure 2-27: General schematics of a physisorption measurement instrument [111]

The measurement is carried out by first evacuating the sample to low pressure, then the sample chamber is brought to liquid nitrogen temperature and a known amount of nitrogen gas is inserted in the sample chamber. Once the equilibrium pressure is reached, the amount of nitrogen (moles or cm^3 at STP) *vs* pressure is measured.

Then, another *dose* of nitrogen is inserted and so on, measuring a series of points that build a nitrogen physisorption isotherm curve, as those reported in figure 2-28 representing the possible types of isotherms as from IUPAC definition [112]. The type of hysteresis (difference between adsorption and desorption curve) is also important, and for this reason four types of hysteresis loops are specifically defined by IUPAC and reported in figure 2-29.

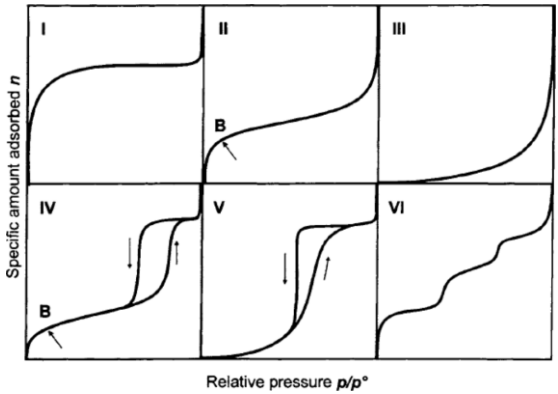

Figure 2-28: Types of physisorption isotherms as from IUPAC specification [112].

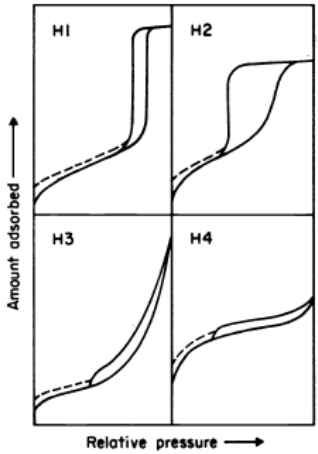

Figure 2-29: Types of hysteresis loop as from IUPAC specification [73].

By interpolation of the points in the p/p_0 range 0.05-0.30 with the BET equation (Brunauer, Emmett, Teller) it's possible to calculate the specific surface area (SSA). The BET equation is:

$$\frac{p}{v(p_0 - p)} = \frac{1}{v_m c} + \frac{(c-1)}{v_m c}\frac{p}{p_0}$$

where p and p_0 are the equilibrium and saturation pressure of the gas, *v* is the volume adsorbed, c is the so called BET constant and v_m is the monolayer adsorbed gas quantity; v_m is estimated by the interpolation and used to calculate the surface of the sample, being known the molar volume of the gas and the adsorption cross-section of the gas molecules. The value of surface so calculated is divided by the mass of sample to obtain the SSA value.

Additionally, by applying the BJH (Barrett-Joyner-Halenda) method to the nitrogen isotherms, the distribution of the pores (PSD) in the range 3-200 nm can be computed using the Kelvin equation, that predicts the anticipated condensation of nitrogen in the pores within this range. The PSD can also be calculated by applying more complex computational procedure called density functional theory; in particular, quenched solid density functional theory (QSDFT) was also applied in some cases to obtain information about distribution of pore size by using the dedicated kernel of the program AsiQwin of Quantachrome Instruments.

Physisorption was extensively applied to characterize the porosity of the aerogels produced within this thesis, while mercury porosimetry resulted in unreliable results so only data calculated from nitrogen isotherms will be presented in the manuscript.

The used gas porosimeters were an ASAP 2010 system (Micromeritics), a Quadrasorb SI surface area analyzer (Quantachrome Instruments) and an Autosorb analyzer (Quantachrome Instrument). Autosorb was also used to measure the CO_2 absorption capacity at 0°C of N-doped carbide derived carbon aerogels.

2.3.3 Chemical composition and phase analysis

To evaluate the chemical composition and the chemical bonds present in the produced aerogels, Fourier-Transform Infrared (FT-IR), Nuclear Magnetic Resonance (NMR) and X-ray Photoelectron (XPS) spectroscopies were used. NMR was mainly used to characterize the starting polymers and an unexpected reaction between the PSZ-20 and CO_2 while FT-IR was more extensively applied to investigate the chemical bonds. The spectrometer used for NMR was an AVANCE400 (Bruker Instruments) with 4 mm probe-head operating at a proton frequency of 400.13 MHz. XPS was used only to characterize the chemistry of N-

doped carbide derived carbons, using a Kratos Axis Ultra DLD instrument equipped with a hemispherical analyzer and a monochromatic Al Kα (1486.6 eV) x-ray source. FT-IR spectra were acquired in transmission mode with KBr pellet with a FT-IR Nicolet Avatar 330 (Thermo Electron) spectrometer and in diffused reflectance mode (DRIFT) with a VERTEX 70/70v FT-IR instrument (Bruker). NMR spectra were acquired by Dr. Emanuela Callone and XPS spectra by Dr. Lia Vanzetti.
Phase analysis was performed with X-ray Diffraction (XRD) on powders of ceramic aerogels with a Rigaku D/Max diffractometer (Rigaku, Tokyo, Japan) in the Bragg–Brentano configuration, using Cu Kα radiation and a monochromator in the diffracted beam, in the range 20° - 80° (2θ) with a 0.05°step and 5 s acquisition time. For smaller samples, an EQUINOX 3500, (Inel, France) equipped with a curved real-time detector was used, using Cu Kα radiation and 15 min acquisition time.

2.3.4 Thermal analysis

The thermal evolution of the pre-ceramic aerogels to Si-C-N-O aerogels was followed also by thermogravimetry (TG) and differential thermal analysis (DTA) with a Netzsch STA 409 instrument. When inert gas was required, the whole instrument chamber was evacuated to 0.1 bar and refilled with argon three times before starting the measurements. The amount of sample for every run was around 20 mg for aerogels and 80 mg for dense samples.

2.3.5 Microstructure

The peculiar microstructure of an aerogel is visible only at high magnification, indeed if an optical microscope is used the sample would appear homogeneously dense even at the maximum magnification. This points out the need of using a Scanning Electron Microscope (SEM) to resolve the small pores from the solid part that builds the aerogel skeleton. Among the various SEM available, field emission gun (FE-) SEMs are able to reach very good values of resolution thanks to the smaller spot size that can be focused to probe the sample. The instrument used to investigate the microstructural features of the aerogels produced was a FE-SEM Zeiss Supra-60 equipped with secondary, backscattered and in-lens electron detectors. The samples were prepared depositing coarse aerogel powders on silver paste and sputtering them with Au-Pd alloy to assure sufficient conductivity.

2.3.6 Electrochemistry

SiOC aerogels and N-doped Carbide Derived Carbon (CDC) aerogels were characterized for electrochemical applications. In particular, SiOCs were tested as anode for Li-ion batteries and N-doped CDCs as electric double layer capacitor

(EDLC) electrodes. For Li-ion a Swagelok® type cell was assembled in a glove box using metallic lithium as counter electrode and $LiPF_6$, 1M in ethylene-diethyl carbonate mixture (1:1 ratio) was used as electrolyte. Galvanostatic charge-discharge measurements at different current densities were performed with a multipotentiostat (BioLogic Science instruments) by Dr. Vallachira Sasikumar Pradeep. For EDLC characterization, two symmetrical electrodes were prepared with the aerogel samples, soaked with 1M aqueous H_2SO_4 and separated by a glass fiber filter. Cyclic voltammetry and galvanostatic charge-discharge experiments were performed with an Ivium Stat electrochemical interface & impedance analyzer (Ivium Technologies) by Dr. Guang-Ping Hao. In both the cases the load of active material was around 2-4 mg/cm^2.

2.4 Synthesis procedure

The developed procedure to produce PDC aerogels is general and can be applied not only to the pre-ceramic polymers shown in this thesis; indeed BCN and AlCN aerogels were also prepared using the very same technique with the additional care of using a glove box for the preparation of the gels [113].

2.4.1 Gels preparation

The first step to prepare a gel is to decide the recipe that will be used, in terms of the ratios: solvent/polymer, polymer/cross-linker, catalyst/polymer, time and temperature for cross-linking along with the chemistry of the single components. All these parameters affect the final properties of the ceramic aerogel produced and can be used to control the microstructure and the chemistry of the solid part.
The production route started with weighting on an analytical scale (precision 0.01 g) the desired amounts of solvent and polymer directly in the PTFE liner of the Parr digestion vessel. The two liquids were then mixed with a stirring plate until a homogenoeus solution was obtained and the desired quantity of cross-linker was then added by putting again the liner on the analitical scale. Again, the solution was stirred until homogenization and the proper amount of catalyst solution was added, using a micropipette and keeping the solution stirred under a gentle flow of argon, to protect the catalyst bottle and the gelling solution from excessive contamination from atmospheric moisture. The stirrer plate and the analitical scale were placed under the fume hood to avoid the breathing of the vapors of the substances used.
At the addition of the catalyst solution, some bubbling started, especially in the case PMHS composition and when acetone was used as solvent. The solution was mixed for 10 minutes, then the stir bar was removed and the PTFE cup was sealed in the

digestion vessel. The vessel was put in a oven pre-heated at the desired temperature for the time selected for the cross-linking. After extraction from the oven, the vessel was allowed to cool freely to room temperature. The gels were extracted as cylindrical monoliths and placed in a glass vase with a screw cap and filled with fresh solvent in a quantity equal to 8-10 times the gel volume. With some recipes the gels were already cracked or it was necessary to cut them to remove them from the cup. In these cases, coarse and irregularly shaped pieces were obtained. The typical appearance of the gels is shown in the pictures in figure 2-30.
The bath of fresh solvent was renewed once a day for three days to remove unreacted polymer, cross-linker and catalyst, so that in the pores of the gel only solvent mixable with liquid CO_2 was present before the insertions in the SCD autoclave.

Figure 2-30: Typical appearance of the as-produced gels

2.4.2 Solvent exchange and drying

For drying the gels, and obtain the relative pre-ceramic aerogels, the starting solvent must be replaced by liquid CO_2 before removing it as a supercritical fluid. To do this, the gel samples were put in a glass sample holder, always kept soaked (figure 2-31) with the solvent, and loaded in the chamber of the autoclave (figure 2-32) priorly cooled to 15°C by the thermostated water bath.

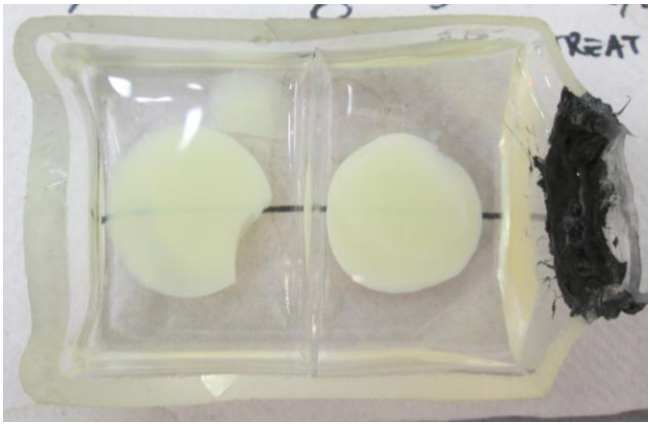

Figure 2-31: Gels soaked with solvent and sample holder for SCD

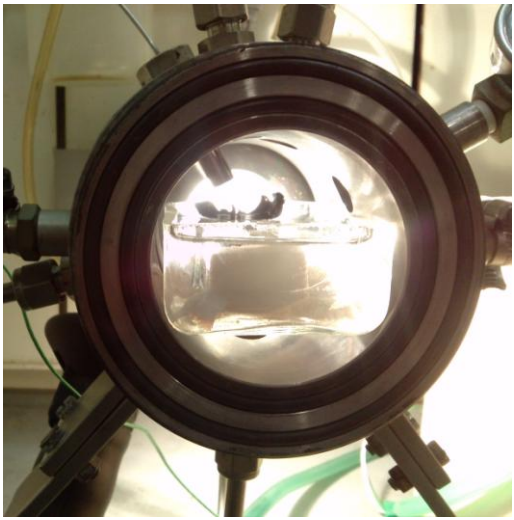

Figure 2-32: Loading of the samples in the SCD autoclave

The autoclave was then pressurized by opening the valve between the chamber and the CO_2 tank, paying attention of increasing the pressure slowly, to avoid possible damages to the samples due to sudden pressure rise. The pressure was increased by steps of 5 bars, with 5-10 minutes of homogenization between each step until the condensation pressure for CO_2 at 15°C was reached (~50 bar). At this point, liquid

CO_2 came directly from the tank or dew drops of liquid CO_2 started to form on the inner walls of the autoclave chamber. The liquid level was let rise slowly up the limit of the sample carrier (also called boat), stopping it at a height above the boat to assure the constant soaking of the gels (figure 2-33).
At least 10 hours of homogenization time was given before proceeding to the first solvent exchange step. This procedure allows to enrich step after step the liquid present in the autoclave with CO_2 and wash away the original solvent. It is performed by removing the liquid in the autoclave from the bottom, keeping just that present in the boat to maintain the gels soaked. To do this, first the inlet valve is slightly open, in order to maintain the pressure inside the autoclave high enough to avoid the boiling of the liquid, (an effect that would be caused by the pressure drop subsequent to the removal of the liquid). Then the bottom on-off valve is opened, limiting the flow with the metering valve, and the excess liquid is removed from the bottom. At last, the outlet valve is closed and the inlet one is widely opened to allow the liquid CO_2 inside the autoclave, reaching again the desired level before closing the inlet valve. These washings were repeated at least twice a day for 5 days in order to substitute all the starting solvent with liquid CO_2.

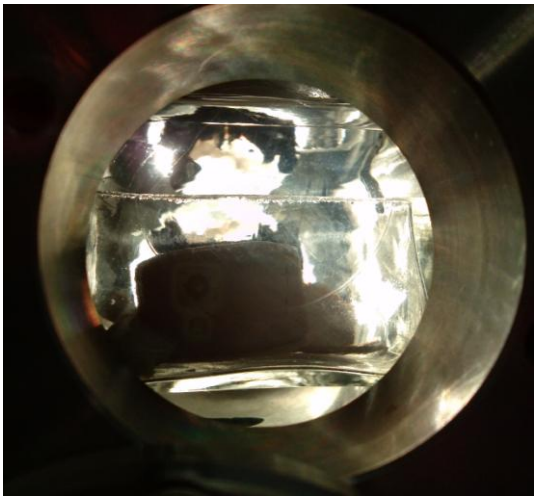

Figure 2-33: Detail of the samples in the autoclave filled with solvent and liquid CO_2

The amount of residual solvent was evaluated by collecting all the removed liquid for every step by condensing it through a polyethylene bottle, which got very cold due to CO_2 evaporation/sublimation, and observing the liquid left after CO_2 sublimation. When no traces of residual solvent were observed, and in any case not before 8

washing cycles, the autoclave was brought for one hour to 29 °C, by means of the thermostated bath, and then to 45°C. The supercritical transition was observed around 31°C and the pressure rose up to 100 bar at 45°C. After one hour the outlet metering and bleeding valves, put on top right of the autoclave, were opened and the gas flow was set around 2-300 mL/min by a bubbler connected to the bleeding valve. It usually took roughly 10 hours to reach room pressure, and multiple setting of the bleeding valve to maintain the constant flow required. Once the pressure was lower than 10 bar also the temperature was lowered in order to remove the samples at room temperature. An example picture of the samples before and after SCD is shown in figure 2-34.
The gels were weighted, measured with a caliper and kept in plastic vials in a desiccator before further characterization or treatments.

Figure 2-34: Picture of gels before (top) and after (bottom) SCD

2.4.3 Pyrolysis and post treatments

To obtain the ceramic aerogels, a pyrolysis is needed to convert the pre-ceramic network into the corresponding ceramic one. The polymeric aerogels were then put in a sample holder, made of the same material as the tube of the tubular furnace, and loaded in the middle of the selected furnace. The importance of careful purging of the furnace with inert gas was noted, due to the high reactivity of the pre-ceramic aerogels with oxygen and moisture already at mild temperature (120-150°C) as will be explained in section 3.1.2. Alumina tubular furnace possesses a inner volume of the tube equal to 9 liter, so very long purging (>10 hours with flow of 200 mL/min) was needed to assure the removal of starting atmospheric air before starting the heating. In the case of fused quartz furnace, the tube was much smaller (volume <1L) and 90 minutes with a flow of 150 mL/min were considered to be enough. For graphite furnace, vacuum could be applied so 3 cycles of vacuum to argon were performed before heating. The schedule for the pyrolysis treatment consisted in a ramp with a fixed heating rate up to the maximum temperature, a soaking time at the desired temperature, and a free cooling of the furnace. The actual temperature inside the furnace was checked from time to time with an external S type thermocouple and the controller of the furnace was set in order to reach a correct temperature with an error within 10°C from the desired actual value. The exhaust gases were bubbled in a silicone oil bubbler and directed to the fume hood to be filtered and disposed. A trap to avoid the risk of bubbler oil sucking inside the furnace in case of shortage of the inlet gas was added after an episode of gas cut during the cooling branch of the thermal schedule.

Post treatment with Cl_2 gas was performed to produce N-doped CDC aerogel, using a fused quartz tubular furnace connected to Ar, Cl_2 and H_2 gas. The whole furnace was kept under a fume hood together with the chlorine bottle used for the chlorination. Additional details for this treatment will be given in the section 3.4.2.

Chapter III

Results and discussion

3.1 Si-C system

Part of this section was published in " Zera, E., Campostrini, R., Aravind, P. R., Blum, Y., & Sorarù, G. D. (2014). Novel SiC/C aerogels through pyrolysis of polycarbosilane precursors. Advanced Engineering Materials, 16(6), 814-819"

Silicon carbide is probably the most widely used non-oxide ceramic material, possessing very high values of elastic modulus, hardness, specific strength, thermal stability, oxidation resistance, chemical inertness and thermal conductivity; it possesses low thermal expansion and it is a semiconductor with wide band-gap. Thanks to these properties, it is used in high temperature and harsh environments like components for gas turbines, kilns, heat exchangers, bearings, nuclear fuel cladding etc. Its natural occurrence is extremely rare and most the SiC used in the industry is artificially made by the Acheson process. This process consists of reacting SiO_2 and C in a high temperature electric furnace, the carbothermal reduction of silica produces carbon monoxide and silicon carbide, whose purity and crystalline size depends on the position inside the furnace. Objects made by silicon carbide are usually sintered at high temperature (~2000°C) with addition of sintering aids, or produced by infiltrating liquid silicon in a green object made by a mixture of carbon and SiC powders. These techniques strongly limit the shaping possibility and great advantages were introduced with the use of polycarbosilanes.
Often SiC derived by polymers is produced with an excess of carbon, making the ceramic black, electrically conductive and lowering the resistance to oxidation.
The Si-C system was extensively studied since ceramic aerogels made by silicon carbide could benefit of its outstanding thermal and mechanical properties. Efforts were dedicated to understand how to tune the chemistry and the microstructure of these aerogels and to measure some properties related to possible application.

3.1.1 Production details

As previously mentioned, to produce aerogels belonging to the silicon-carbon system SMP-10 polycarbosilane was used as pre-ceramic polymer. The recipe to produce the pre-ceramic gels took care of setting:

- the starting dilution (as %vol of solvent),
- cross-linker type
- the ratio between Si-H and C=C moieties,
- the cross-linking temperature,
- the cross-linking time,
- the amount of catalyst (as weight ratio between Pt and SMP-10).

The amount of solvent is easily computed once the volume of SMP-10 and that of the cross-linker are known, by assuming no ΔV of the components upon mixing. The solvent used for SMP-10 was mainly cyclohexane.

Taking as reference the average composition of figure 2-11**,** a mean amount of 41 mmol of Si-H groups per gram of SMP-10 can be calculated. In the same way, 15 mmol of C=C groups are contained in 1 gram of DVB, while 29 mmol of C=C come from 1 gram of TVS. These quantities allowed to calculate the weight ratio between SMP-10 and cross-linker once the ratio between Si-H and C=C was set. The allyl groups of the SMP-10 and the impurities in DVB were not considered for the computation.

The influence of the above mentioned parameters was investigated, and some of them were fixed in order to study the free carbon amount in the ceramic material, the bulk density, the SSA and the microstructural stability at high temperature.

As a result of the optimization, devoted to diminish the shrinkage during SCD, to increase the SSA and the total porosity of the gels; the time, temperature and catalyst amount for the gel production were fixed and in particular:

- the cross-linking time was set for DVB (5 hours) and for TVS (7 days),
- the Pt/SMP-10 weight ratio was $8*10^{-5}$ (for DVB) to $80*10^{-5}$ (for TVS),
- the cross-linking temperature was set at 150°C.

3.1.2 TVS and DVB cross-linkers (and purging time)

The role of cross-linker was studied since this could allow to modify the carbon amount in the ceramic aerogel, along with the microstructure, without modifying so much the starting synthesis parameter. Additionally, cross-linking SMP-10 with TVS was never reported in literature so this study could also have led to interesting side results. For the following discussion, TVS refers to TVS cross-linked SMP-10 aerogels, and similarly DVB will refer to DVB cross-linked SMP-10 aerogels.

Accordingly, TVS and DVB cross-linked SMP-10 aerogels were produced by gelling a solution of polymer and cross-linker with 90%vol of cyclohexane, Si-H/C=C ratio of 1 and following the parameters depicted above. The white, monolithic polymeric aerogels showed similar appearance even though pretty different density and shrinkage values were measured, as reported in table 3-1.

	TVS	DVB
SCD Linear shrinkage (%)	14 ± 8	5 ± 1
Density (mg/cc)	129 ± 33	69 ± 6
Skeleton density (g/cc)	1.04	1.09
Gel yield (%)	87 ± 14	69 ± 7
SSA (m^2/g)	960	447
N_2 Pore Volume (cc/g)	4.41	1.19
Total Pore Volume (cc/g)	6.79	15.76

Table 3-1: Shrinkage, density and gel yield values of SMP-10 gels obtained with TVS and DVB cross-linker

The higher gel yield, calculated with respect to the sum of SMP-10 and cross-linker, and the higher shrinkage during SCD led to a nearly doubled density in the case of TVS with respect to DVB.

From the FT-IR spectra obtained on the as-produced aerogels (figure 3-1), is possible to notice that despite of the gel formation, and of the very long time for cross-linking in the case of TVS, still a very intense peak related to Si-H bonds is present. The DVB and TVS aerogels spectra are very similar, differing mostly by the presence of aromatic ring peaks in the case of DVB (refer to figure 2-22), with an indication of unreacted C=C visible from the small but distinct peaks relative to =C-H around 3050 cm^{-1}.

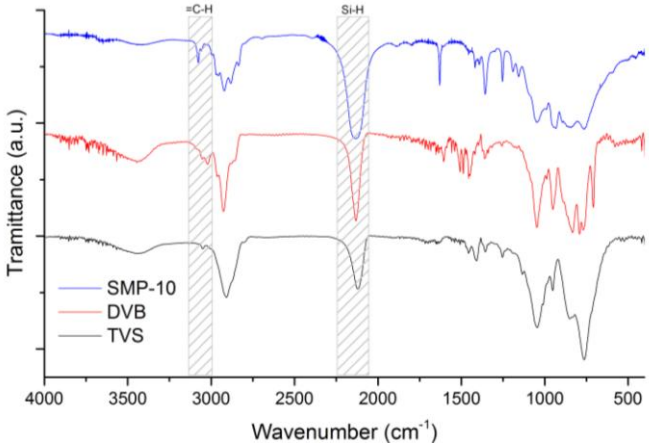

Figure 3-1 : FT-IR spectra of DVB and TVS aerogels with liquid SMP-10 as reference

Both this observations point out an incomplete cross-linking reaction that leaves unreacted Si-H and C=C groups, which will react during the subsequent thermal

treatment but could also be used to modify the surface of the gel in the wet state to functionalize the surface of the final aerogel.

The microstructure of the polymeric aerogels and the amount of the porosity was studied by means of, N_2 physisorption and density measurements, some data are reported in table 3-1. The N_2 pore volume was calculated from the adsorption isotherm at 0.99 relative pressure while total pore volume was computed from bulk and skeleton density by applying the equation:

$$Total\ Pore\ Volume = \frac{1}{\rho_b} - \frac{1}{\rho_{sk}}.$$

Nitrogen isotherms reveal a much higher SSA and pore volume for the TVS aerogel, despite its higher density compared to the DVB one. This can be rationalized reminding that nitrogen physisorption allows to study the pores up 50-200 nanometers, so the pores within the size range 200 nm - 1 µm, which presence is confirmed by FE-SEM micrographs (reported here just for the pyrolized DVB and TVS aerogels), cannot be probed and do not contribute to the total pore volume measured with this technique. Therefore, from the total pore volume and the N_2 physisorption results it clearly appears that, for DVB aerogel, most of the pores are bigger than 200 nm while for TVS more than half of them are below 100 nm in size. The isotherms measured on the two aerogels are reported in figure 3-2, along with the pore size distribution obtained both from BJH (desorption branch, figure 3-4) and QSDFT (N_2 on carbon cylindrical/spherical pores, adsorption branch, figure 3-3) methods.

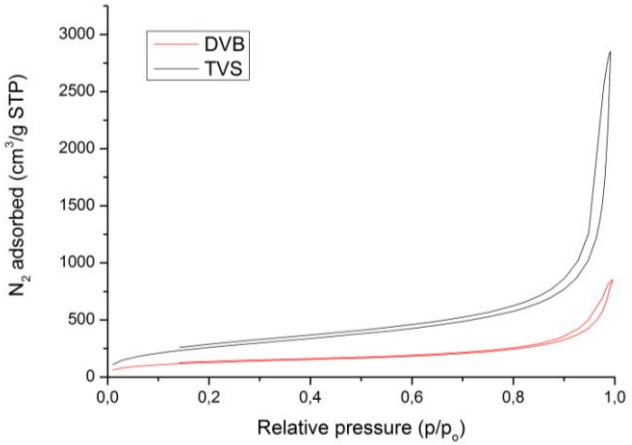

Figure 3-2: N_2 physisorption isotherms of TVS and DVB aerogels

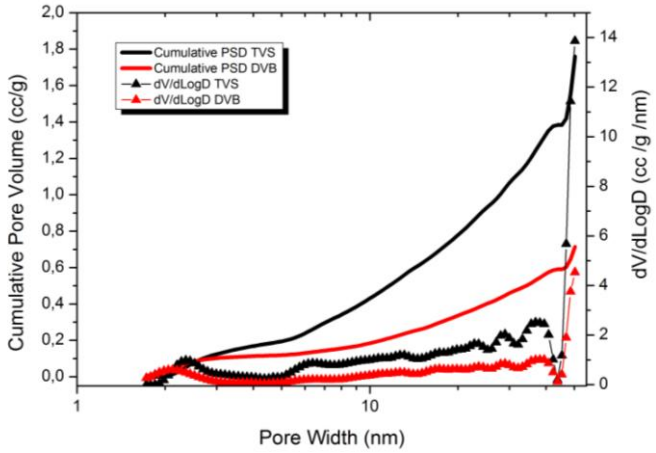

Figure 3-3: QSDFT PSD calculated for TVS and DVB aerogel

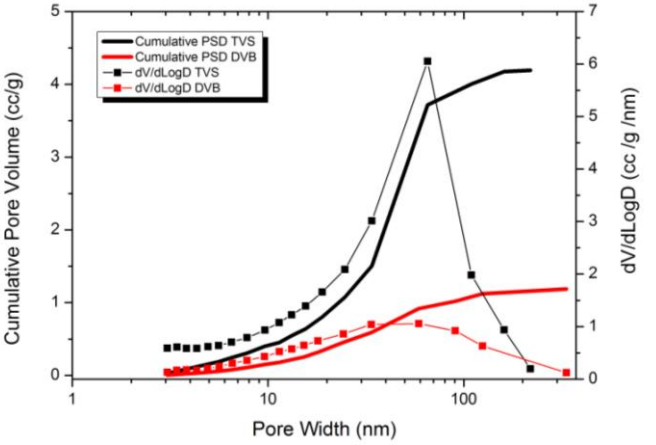

Figure 3-4 : BJH PSD calculated for TVS and DVB aerogel

As can be seen from figures 3-3 and 3-4, different methods to compute the PSD can give different results, mostly arising from the model used in the case of small pores, and from the hysteresis loop for the bigger dimension range. Anyway, for both the TVS and DVB aerogels a broad, hierarchical distribution of pores in the whole measured range can be appreciated, with a relative maximum centered around 50 nm.

The two aerogels were pyrolized at different maximum temperature to evaluate the ceramic aerogel properties and the stability at increasing temperature. Maximum values were chosen to understand: the changes upon polymer to ceramic transformation (1000°C), potential carbothermal reduction effects (1500°C, important if oxygen impurities are present), and the resistance to crystallization/sintering (2000°C). The first data collected, reported in table 3-2 and consisting of mass loss, shrinkage, SSA and pore volume, were indicating a high oxygen content in the aerogels produced at 1000°C, visible as a strong evolution of mass loss from 1000°C to 1500°C due to carbothermal reduction of SiO_2 by means of free C.

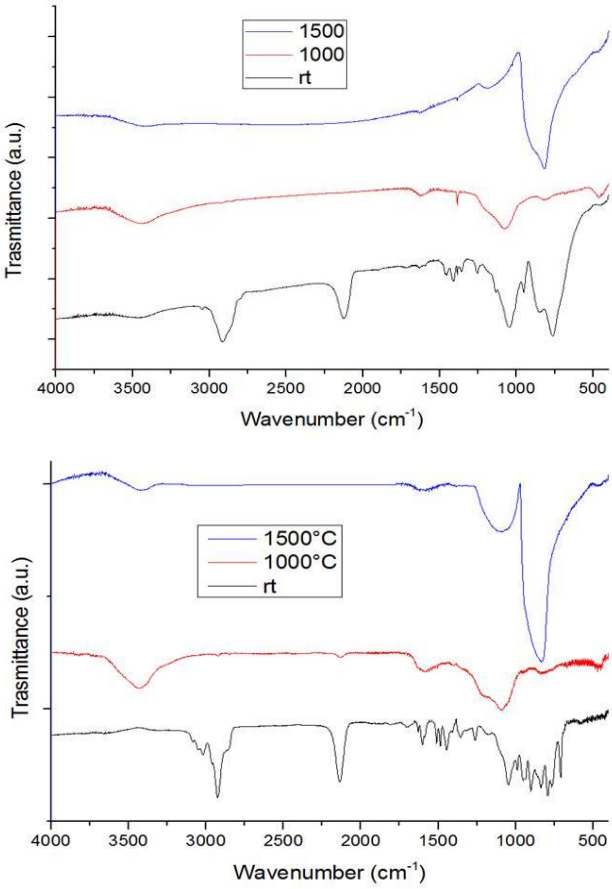

Figure 3-5 : FT-IR spectra of TVS (top) and DVB (bottom) aerogels

	TVS 1000°C	TVS 1500°C	DVB 1000°C	DVB 1500°C
Linear shrinkage (%)	32	Debris	46	55
Mass loss (%)	22	58	52	79
SSA (m^2/g)	313	160	96	400
N_2 Pore Volume (cc/g)	0.82	1.29	0.31	0.69

Table 3-2: First data collected on pyrolized TVS and DVB aerogels at 1000°C and 1500°C, mass loss and shrinkage are relative to the polymeric aerogel.

Also the FT-IR spectra (figure 3-5) clearly show Si-O related peaks (1100 and 450 cm^{-1}) in the samples obtained at 1000°C.
The carbothermal reduction is a two step reaction that proceed as the equations:

$$SiO_{2_s} + C_s \rightarrow SiO_g + CO_g$$
$$SiO_g + 2C_s \rightarrow SiC_s + CO_g.$$

The reaction leads to a mass loss due to the evolution of CO gas and eventually unreacted SiO gas. If over-stoichiometric C/SiO_2 ratio is assumed, it can be calculated that every gram of SiO_2 leads to a weight loss of 0.58 g, explaining the mass loss measured. Additionally, the loss of solid material creates new porosity as it is measured by N_2 physisorption (table 3-2). The new porosity formed in the case of TVS leads to a lowering of the SSA value while for DVB material an increase in SSA value is measured. The reason for the high content of oxygen in the material obtained at 1000°C was deeply investigated, and for DVB pre-ceramic aerogel elemental analysis was performed by Mikroanalytisches Labor Pascher (An der Pulvermühle 1, D-53424 Remagen), revealing an oxygen content of 1.3 %wt, with 7.3 %wt of Si, 7.9 %wt H and C to 100%. At 1000°C the composition changes to: Si 22.4 %wt, C 60.4 %wt and O 17.2 %wt, pointing to a strong enrichment of O during pyrolysis treatment. After some trials and errors the reason was found in the insufficient purging time for the relatively big alumina tube of Lindbergh furnace, as anticipated in section 2.4.3. Indeed, as shown from the TG curves reported in figure 3-6, the aerogels can easily react with O_2 already at low temperature (150-200°C), creating Si-OH and Si-O-Si moieties that enrich dramatically the precursor with oxygen, also thanks to the high SSA values of the polymeric aerogels and to the high presence of unreacted Si-H groups.

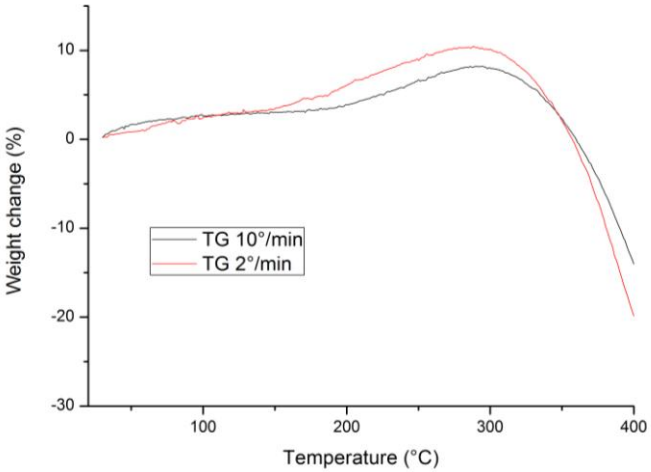

Figure 3-6 : TG curves of DVB aerogel heated in air

From this point on, care was taken to purge for sufficient time all the tubular furnaces used for the pyrolysis treatments. The features of the ceramic aerogels obtained from SMP-10 cross-linked with TVS and DVB, and properly pyrolized at increasing temperature, are then reported in table 3-3, isotherms and PSD are reported in figures 3-7, 3-8, 3-9 and 3-10.

	TVS 1000°C	TVS 1500°C	TVS 2000°C	DVB 1000°C	DVB 1500°C	DVB 2000°C
Linear shrinkage (%)	32	37	52	54	56	59
Mass loss (%)	18	23	35	65	68	70
SSA (m^2/g)	276	271	135	111	146	130
N_2 Pore Volume (cc/g)	1.13	1.03	0.81	0.41	0.44	0.53
Density (g/cc)	0.45	0.46	0.92	0.25	0.28	0.33

Table 3-3 : Features of TVS and DVB aerogels pyrolyzed at increasing temperature mass loss and shrinkage are relative to the polymeric aerogel.

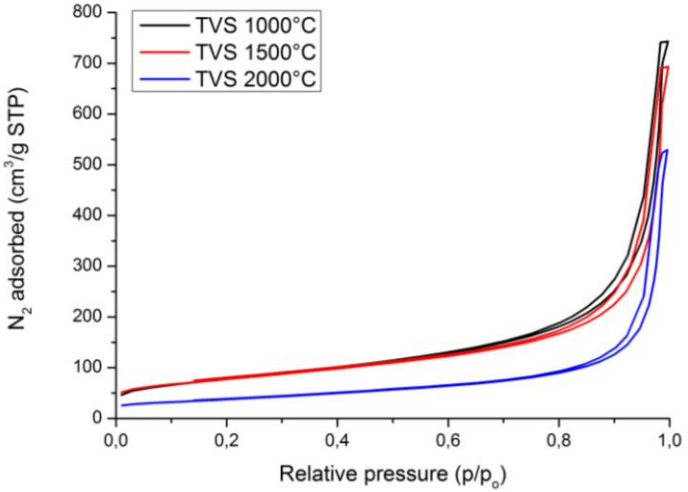

Figure 3-7 : N_2 physisorption isotherms of TVS ceramic aerogels

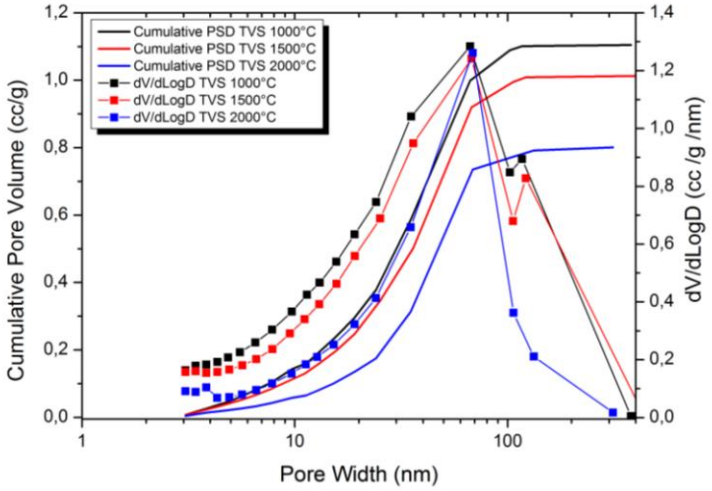

Figure 3-8 : BJH PSD calculated for TVS ceramic aerogels

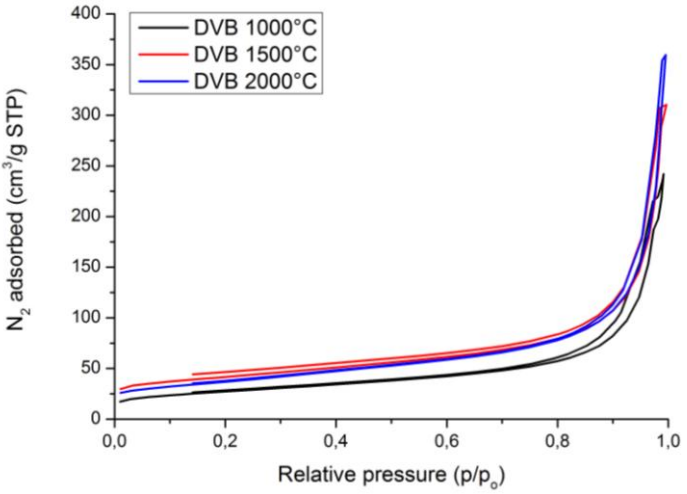

Figure 3-9 : N_2 physisorption isotherms of DVB ceramic aerogels

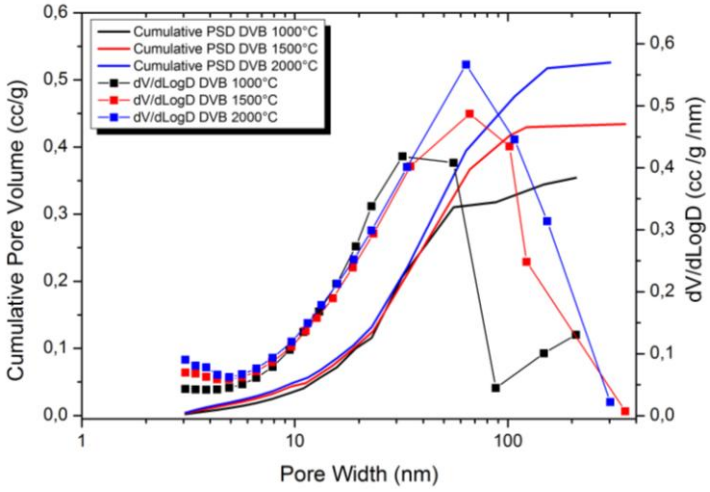

Figure 3-10 : BJH PSD calculated for DVB ceramic aerogels

The first striking result is that, despite the very high temperature reached, high SSA values and low density of the ceramic aerogels are maintained. Such a stability of an aerogel was measured before only for pure, non graphitizable, carbon aerogels [114]. This is thought to be due to the peculiar properties of SiC that resist to sintering even at temperature as high as 2000°C. Another clear result is the higher stability of the DVB aerogels compared to the TVS ones in the range 1500-2000°C. Indeed, hints of densification are noted as an increase in shrinkage and density, accompanied by a not well understood increase in mass loss. The FE-SEM pictures, figure 3-11, confirm the densification, showing the sintering of some particles for the TVS aerogels treated at 2000°C while DVB aerogel exhibits a still microstructure. The reason for this different behavior could probably be found in the higher SSA and bulk density shown by the TVS 1500°C aerogel, that lead to an increased driving force (SSA) and kinetic (ρ_b) for sintering.

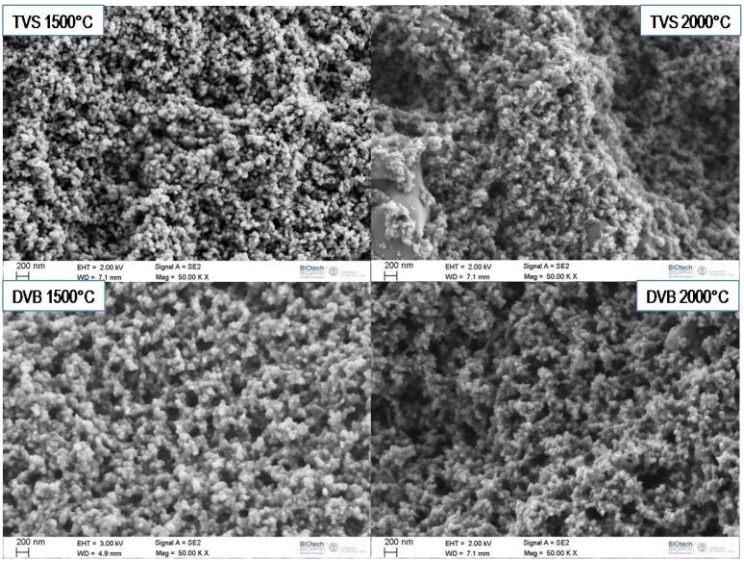

Figure 3-11 : FE-SEM micrographs of pyrolized DVB and TVS aerogels

The x-ray diffraction patterns (figure 3-13, 3-14**)** and the FT-IR spectra (Figure 3-12**)** confirmed the composition of the skeleton to be a mixture of silicon carbide, amorphous at low temperature and β-phase at high temperature, and free carbon. A higher content of carbon in the DVB aerogel is readily visible at 1000°C in the XRD pattern, while become less apparent when silicon carbide starts to crystallize. In FT-

IR spectra, the free carbon presence is revealed by a small broad peak around 1600 cm^{-1} while Si-C bonds resonance give rise to the main peak centered at 830 cm^{-1}.

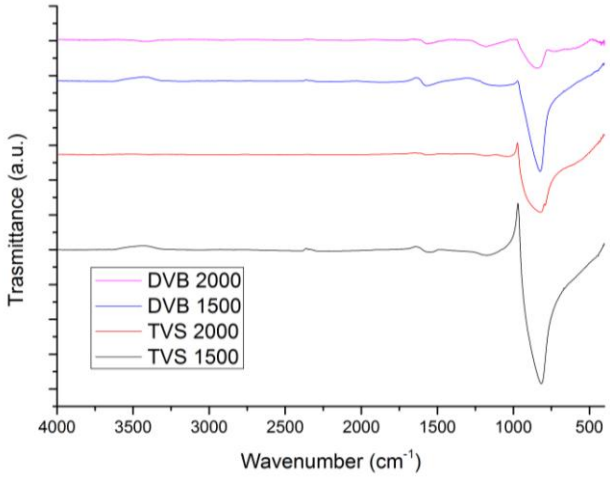

Figure 3-12: FT-IR spectra of pyrolized TVS and DVB aerogels

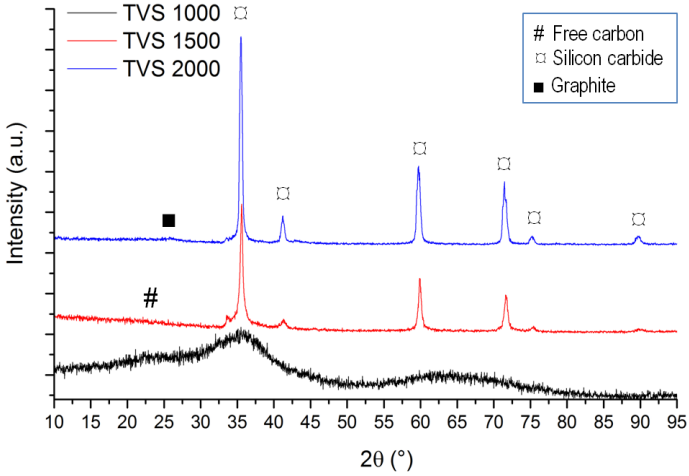

Figure 3-13: XRD pattern of TVS aerogels

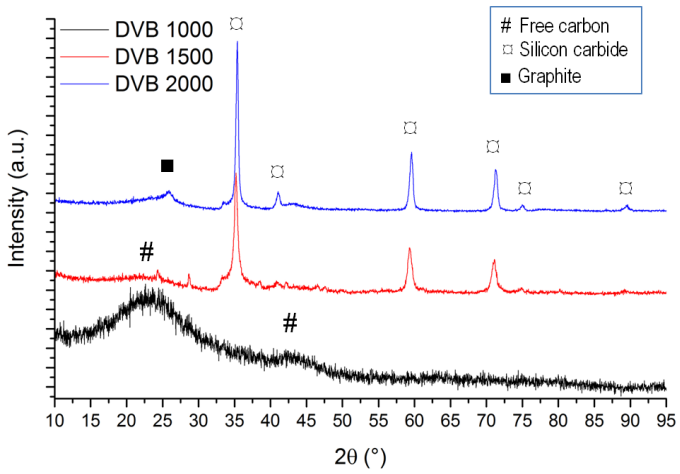

Figure 3-14: XRD patterns of DVB aerogels

The amount of free carbon was evaluated by a TG in air on the aerogels obtained at 1500°C and presented in figure 3-15. As visible, in air flow the SiC/C aerogels show a first weight loss, starting around 600°C and due to the combustion of the free carbon, followed by a weight gain due to the oxidation of the remaining SiC. It should be noted that, being the size of the particles building the skeleton in the nano range, the mass gain due to SiC oxidation is reaching a nearly theoretical value (50% mass increase from SiC to SiO_2) already below 1400°C. The oxidation in tubular furnace with air flow at 600°C for 1 h of bulk samples of aerogels treated at 2000°C showed very similar weight losses, being 34% for TVS and 55% for DVB. After oxidation both the aerogels are broken in debris suggesting that the high carbon content is limiting the possible application of these aerogels at high temperature in oxidizing environment.

It is therefore demonstrated the possibility to produce SiC/C aerogels that, even after a thermal treatment at 2000°C (in inert environment), still possess high porosity (up to 89%), high specific surface area (130 m^2/g) and hierarchical pore structure from µm to nm scale. The free carbon amount can be changed, along with the microstructure and the thermal stability, with the use of TVS rather than DVB as cross-linker.

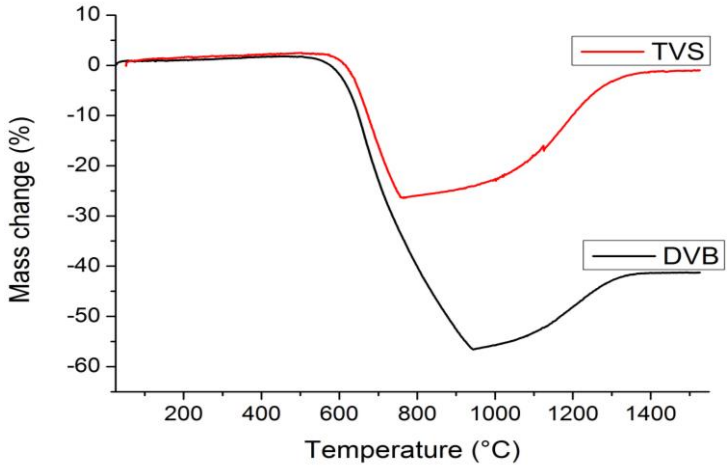

Figure 3-15 : TG curves in air flow of TVS and DVB aerogels previously pyrolized at 1500°C in argon

3.1.3 Ratio between DVB and SMP-10

In the previous section the ratio between Si-H and C=C moieties was kept equal to one, in order to promote a fast cross-linking and to evaluate differences given by the use of different cross-linkers. In this section on the contrary, the cross-linker used was DVB and the ratio between the reactive groups was varied. To mitigate the effect of a slower cross-linking, the dilution was decreased to 70%vol while the solvent (cyclohexane), the amount of catalyst ($8x10^{-5}$ Pt/SMP-10 weight ratio), time and temperature for cross-linking (6h at 150°C) were similar to those used in the previous section. The reason for this study was to investigate if it's possible to decrease the amount of carbon in the final ceramic by lowering the quantity of cross-linker, and how this affects the microstructural features of the aerogels produced. Six samples were produced with increasing ratio between Si-H and C=C, the starting compositions of the gelling solution are summarized in table 3-4.
As shown in table 3-5, the shrinkage and consequently the density of the pre-ceramic aerogels varied with the ratios investigated.

Si-H/C=C	SMP-10 (g)	DVB (g)	Cyclohexane (g)	0.1% Karstedt (uL)
32	3.00	0.25	5.94	279
16	2.75	0.46	5.88	256
8	2.35	0.79	5.78	218
4	1.90	1.27	5.88	177
2	1.35	1.81	5.90	126
1	0.85	2.28	5.88	80

Table 3-4: Starting composition of the gelling solution for the Si-H/C=C ratio investigation

The shrinkage increased as the amount of DVB was decreased, pointing out that a lower cross-linking degree was detrimental to the preservation of the gel structure during the SCD procedure. Additionally, thanks to the glass windows present in the autoclave, it was possible to identify the source of shrinkage in the first enrichment of the cyclohexane with liquid CO_2, so even before the first complete "washing". The effect is shown in figure 3-16, where two pieces of the wet gels produced with ratios of 4 and 8 are followed during the SCD procedure. It's visible the higher shrinkage for the sample 8 during the first CO_2 enrichment; after the first step the sample's dimensions are constant.

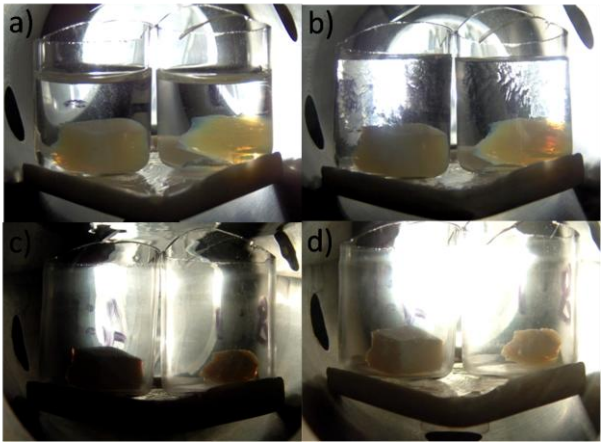

Figure 3-16: Evolution of 4 (left) and 8 (right) gels during the first liquid CO_2 insertion. a) liquid phase is pure cyclohexane. b) CO_2 enriched cyclohexane (30 bar). c) cyclohexane - liquid CO_2 mixture. d) supercritical CO_2.

Si-H/C=C	ρ_{Poly} (g/cm^3)	ΔL_{SCD} (%)	$P_{SiC/C}$ (g/cm^3)	ΔL_{Pyro} (%)	Δm_{Pyro} (%)	free C (wt%)
32	0.40	43	0.86	30	32	5
16	0.50	37	1.02	30	32	11
8	0.39	28	0.80	32	39	31
4	0.28	17	0.58	37	46	44
2	0.22	8	0.51	44	62	54
1	0.21	4	0.56	55	74	62

Table 3-5 : Some properties measured on the aerogels produced at different Si-H/C=C ratios. ρ_{Poly}: bulk density of polymeric aerogels; ΔL_{SCD}: linear shrinkage after SCD; $\rho_{SiC/C}$, Δl_{Pyro},, Δm_{Pyro}: bulk density, linear shrinkage and mass loss after pyrolysis

This demonstrate that the shrinkage, in this case, is not due to an incorrect SCD procedure, as it could be concluded if no glass windows were present, but to some stresses that arise during the cyclohexane to CO_2 liquid exchange procedure.

Non negligible shrinkage values due to solvent exchange and SCD with CO_2 are already reported in literature for lignin [115] [116], tin oxide [117], APTES/RF [118], RF [119], and SiO_2 aerogels [120]. The shrinkage is ascribed to a series of reasons, some of which are intrinsic of the system, like surface potential of the particles [117], difference in the solid-liquid interfacial energy [117] and hydrogen bonding capabilities of the solid [115], while others are connected to the experimental procedure like depressurization rate of SC CO_2 [119] or the presence of an interface between the two liquids [120]. These last reasons can be avoided with a proper drying procedure (slow depressurization and slow liquid exchange). In our case we observed a shrinking of the samples only during the first liquid exchange, in which the cyclohexane was diluted approximately to 50% with liquid CO_2 within 1 day. This was already observed in [89] where acetone was exchanged with CO_2 in PMHS/DVB gels and ascribed to the impossibility for CO_2 to swell the polymer network at the same extent as acetone. This explanation fits well with the experimental results: it's known that the swelling degree of a polymer is inversely proportional to the cross-links density, and it can be expected that higher initial content of DVB leads to a more cross-linked final gel. In addition, a more cross-linked network can withstand higher stresses without being damaged or deformed, contributing to lower the observed shrinkage.

The bulk density of the polymeric aerogels, on the other side, is affected by two kind of effects: the first one is the shrinkage, higher values of ΔL lead to density higher than the target one (being around 0.30 g/cc in this case); the second one is the incomplete reaction between DVB and SMP-10 that tends to lower the final density. In this way it's possible to explain the measured densities of samples 1-2-4, which

are even below the expected value. Unfortunately, the measurement of the gel yield, that would clarify this interpretation, was not possible due to the loss of some fragments of the gels before the SCD procedure.

The pre-ceramic aerogels were subsequently pyrolized at 1500°C in flowing argon for 1h to get the SiC/C ceramic aerogels; the measured mass loss, shrinkage and bulk density are reported in table 3-5. It can be seen that the trend for the density is very similar to the polymeric aerogels, while the shrinkage trend is now inverted compared to that measured during SCD. During pyrolysis, high quantity of DVB leads to increased mass loss, due to the easier loss of aromatic compounds, that also enhances the shrinkage due to ceramization. Eventually, high quantity of DVB enrich also the SiC aerogel with free carbon, which content was measured as the weight loss upon oxidation in synthetic air flow at 600°C for 1h (reported in table 3-5). Additionally, from figure 3-20 it can be seen that if the amount of carbon is higher that 31% (sample 8) the oxidation leads to a complete fragmentation of the ceramic aerogel. The appearance of the aerogels before and after the pyrolysis treatment and the oxidation of free carbon are shown in figure 3-17, 3-18, 3-19 and 3-20.

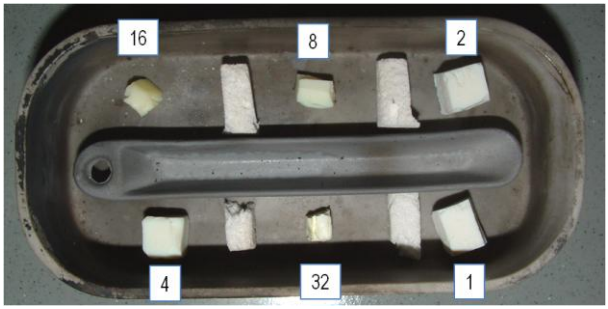

Figure 3-17 : Appearance of the polymeric aerogels before the pyrolysis treatment

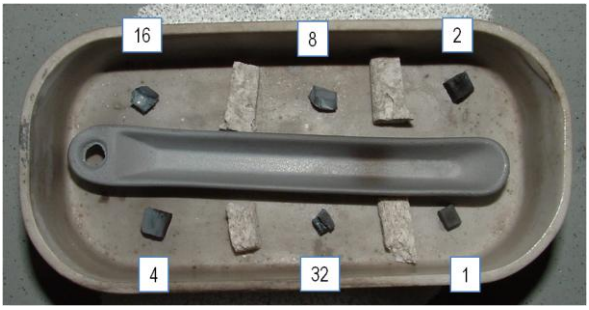

Figure 3-18 : Appearance of the polymeric aerogels after the pyrolysis treatment

Figure 3-19 : Appearance of the ceramic aerogels before the oxidation treatment

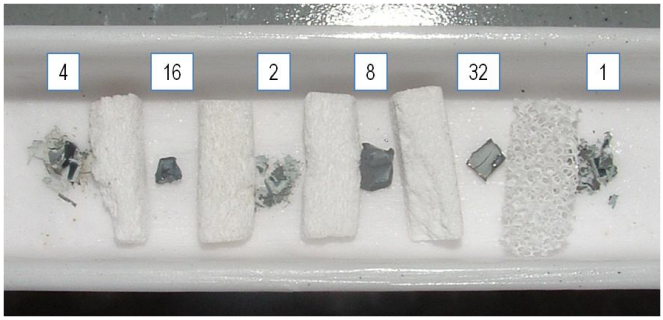

Figure 3-20: Appearance of the ceramic aerogels after the oxidation treatment

The microstructure of the aerogels, studied by N_2 physisorption, is also strongly affected by the moiety ratio used in the synthesis, as can be seen from the isotherms and the PSD curves (reported in figures 3-21 to 3-26) and from the calculated SSA and pore volume (table 3-6).

Concerning the pre-ceramic aerogels, a decrease in the DVB amount leads to a monotonic decrease of the SSA value and to a general decrease of the pore volume. This is consistent with a better preservation of the gel structure for the aerogels produced with nearly stoichiometric ratio between the active cross-linking moieties, as already commented for the shrinkage and density values. PSDs show generally higher amount of small mesopores for the aerogels produced with high DVB content.

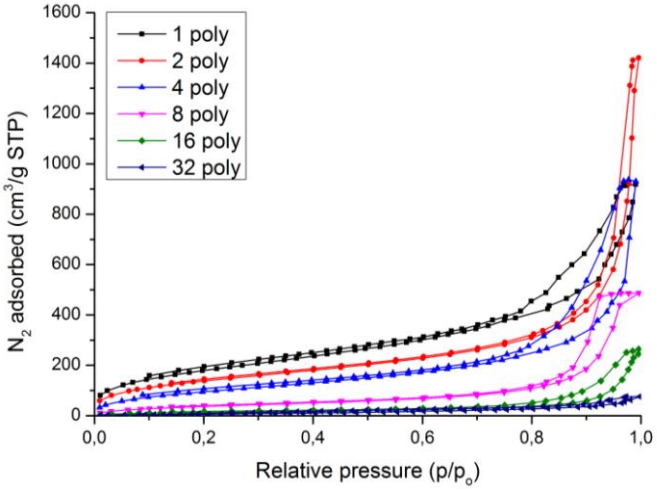

Figure 3-21 : N_2 isotherms measured on the polymeric aerogels produced with different Si-H/C=C ratios.

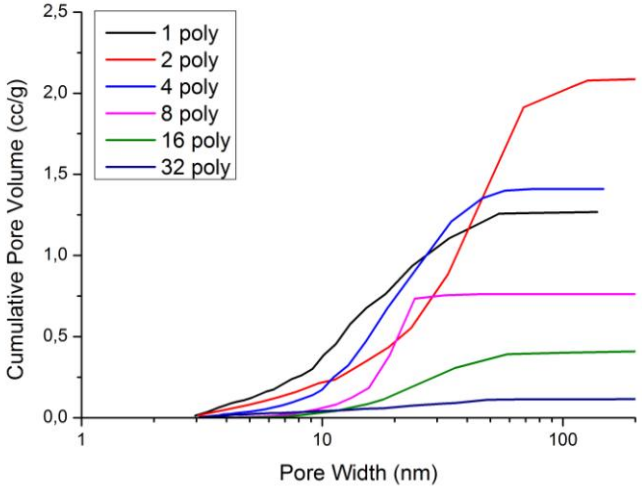

Figure 3-22 : BJH cumulative PSD curves for the polymeric aerogels produced with different Si-H/C=C ratios.

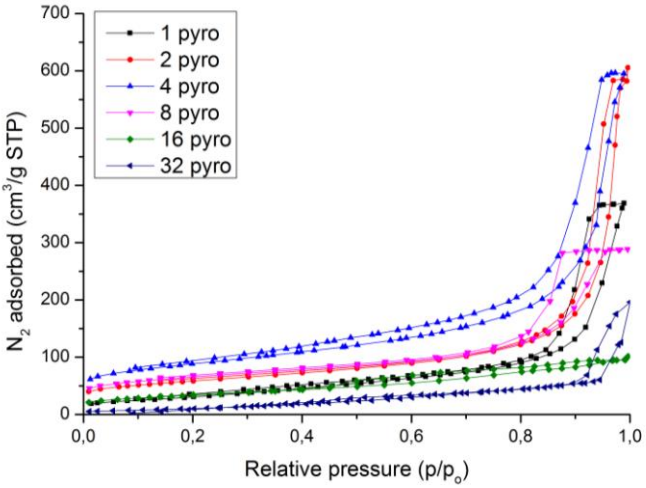

Figure 3-23 : N_2 isotherms measured on the aerogels produced with different Si-H/C=C ratios and pyrolyzed at 1500°C.

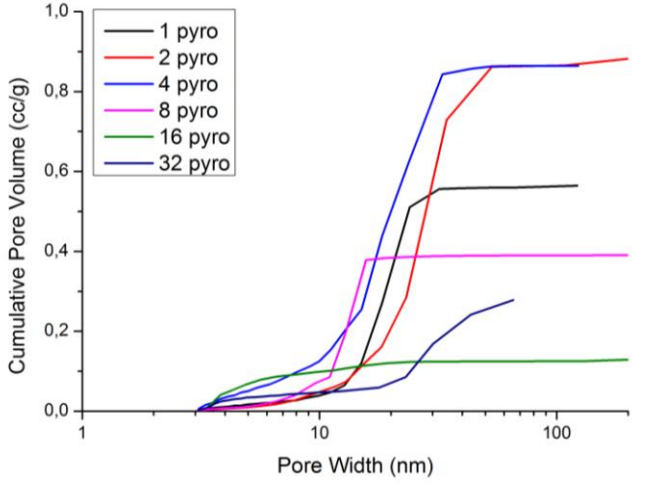

Figure 3-24 : BJH cumulative PSD curves for the aerogels produced with different Si-H/C=C ratios and pyrolyzed at 1500°C.

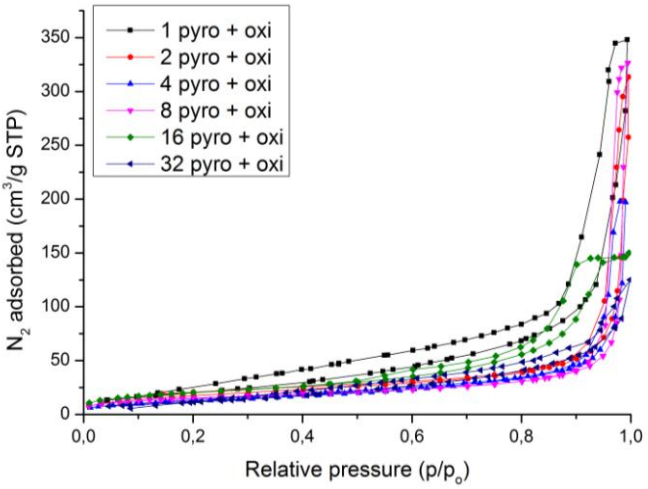

Figure 3-25 : N_2 isotherms measured on the aerogels produced with different Si-H/C=C ratios, pyrolyzed at 1500°C and oxidized at 600°C in synthetic air flow for 1 h.

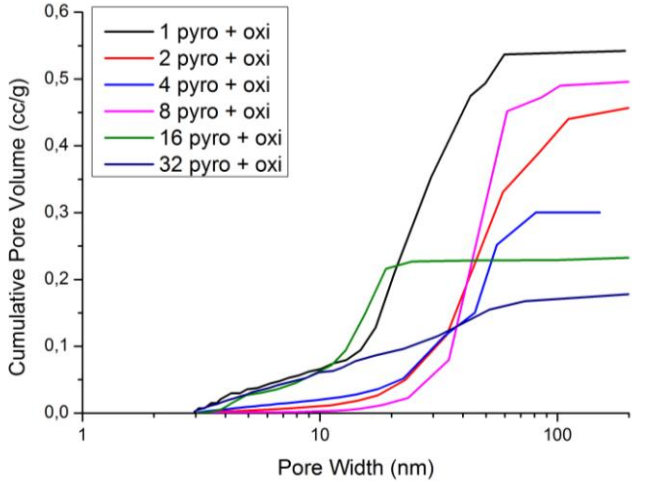

Figure 3-26 : BJH cumulative PSD curves for the aerogels produced with different Si-H/C=C ratios, pyrolyzed at 1500°C and oxidized at 600°C in synthetic air flow for 1 h.

Si-H/C=C	SSA_{Poly} (m^2/g)	$V_{Pore\ Poly}$ (cm^3/g)	$SSA_{SiC/C}$ (m^2/g)	$V_{Pore\ SiC/C}$ (cm^3/g)	SSA_{SiC} (m^2/g)	$V_{Pore\ SiC}$ (cm^3/g)
32	33	0.12	49	0.19	46	0.19
16	55	0.40	120	0.14	72	0.23
8	147	0.75	222	0.40	53	0.49
4	371	1.43	313	0.92	46	0.30
2	512	2.16	201	0.87	66	0.45
1	671	1.42	111	0.57	77	0.46

Table 3-6: SSA and pore volume measured with N2 physisorption on the aerogels produced with different Si-H/C=C ratios. Poly refers to pre-ceramic aerogels, SiC/C refers to aerogels pyrolized at 1500°C and SiC refers to aerogels pyrolized at 1500°C and oxidized in air at 600°C.

After pyrolysis the trend of the porosity features changes, showing a maximum in SSA and pore volume for sample 4, thanks to the combination of starting pre-ceramic microstructure, mass loss and shrinkage during ceramization. Interestingly, the pore size distributions reveal the formation of small pores for the samples produced with high amount of SMP-10, that contribute to increase the SSA for the sample 32, 16 and 8. Finally, after carbon removal the values are generally decreased, showing no clear trend, with SSA values scattered around 60 m^2/g and additional pore formation for the aerogels 16 and 8, which sustained the oxidation without breaking in debris. Sample 32 shows nearly no effects upon oxidation at 600°C thanks to the very low amount of free carbon present.
Therefore, depending on the possible application needs and concerns, the features of the SiC/C aerogels can be tuned also by changing the starting SMP-10/DVB ratio. It was revealed that, increasing the DVB amount a better preservation of the original gel structure could be granted during the SCD procedure, leading to lower shrinkage and density of the polymeric aerogel. Upon pyrolysis, on the other side, high contents of DVB lead to increased mass loss and shrinkage, modifying the starting aerogel microstructure and causing a loss of SSA and mesoporosity, even though the low density values are maintained. Additionally, the SMP-10/DVB ratio can be used to tune the free carbon amount in the SiC/C aerogel, with very low content of 5 %wt for sample 32 and high content of 62%wt for sample 1.

3.1.4 Pure SMP-10 aerogels

The task of producing pure SMP-10 was undertaken in the last part of the PhD research work, even if only limited efforts could be dedicated to the study. Anyway, the question spontaneously arise: "is it possible to produce pure SiC aerogels?".

The first problem was to obtain a wet gel using no additional cross-linker for the stoichiometric SiC precursor, SMP-10. The possibility was investigated and some pure SMP-10 wet gels were obtained by using a high amount of catalyst ($4x10^{-4}$ Pt/SMP-10 weight ratio), 90%vol cyclohexane and cross-linking for 1 week at 150°C. These gels were yellow/opaque and the mechanical properties were barely sufficient to maintain the shape and to allow the manipulation of the gel to load it in the SCD autoclave. A very strong shrinkage was noted as soon as the cyclohexane started to be substituted with liquid CO_2 and a nearly complete densification was observed by measuring a density of the SCD gel close to 1 g/cc. Later, an attempt to strengthen the network of the pure SMP-10 gel was tried, by treating a fragment of the gel in a solution of cyclohexane and DVB (1-1 weight ratio of SMP-10 gel to DVB, 90%vol of cyclohexane, Pt/SMP-10 $8x10^{-4}$, 3 days at 100°C).

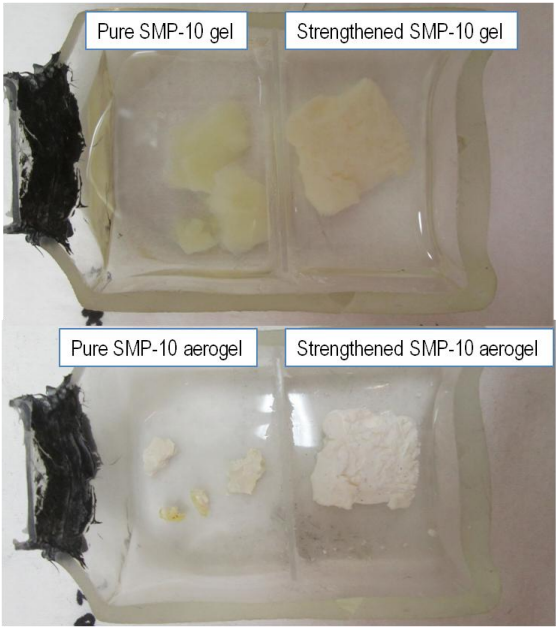

Figure 3-27 : Appearance of SMP-10 gels before and after SCD

The gel changed appearance to white and no extra gel was formed in the solution around the original fragment. The strengthened SMP-10 gel was then SC dried, showing negligible shrinkage during the procedure. The very different behavior of the virgin and the strengthened SMP-10 gels during SCD is illustrated by figure 3-27.

The pyrolysis treatment was simulated in the thermobalance and the measured curves are reported in figure 3-28. As can be seen, the pure SMP-10 (aero)gel shows the same behavior as dense cross-linked SMP-10, which TG is shown in figure 2-12, while the DVB treated aerogel shows and increased mass loss and some evidences of an extra mass loss, probably due to oxygen contamination present in the aerogel.

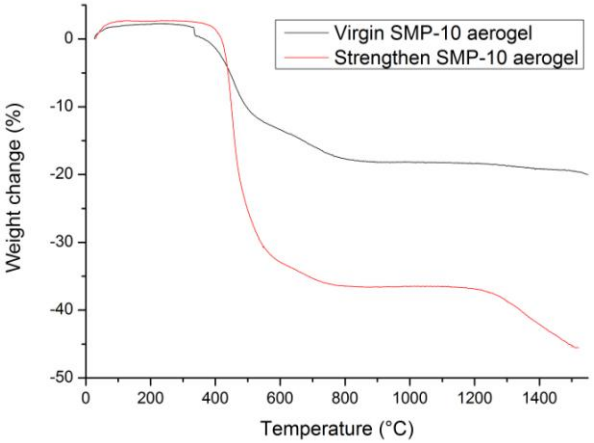

Figure 3-28 : TG curves in flowing argon of the pure and DVB treated SMP-10 aerogels

The microstructure of the two aerogels pyrolized at 1500°C are shown in figure 3-29. It appears that the pure SMP-10 aerogel, despite the high density, still possess some porosity, being composed by particles in the size range 100-500 nm. The DVB treated aerogels on the other side, shows a microstructure much closer to that already observed for the aerogels investigated in the previous sections, formed by particles smaller than 100 nm and with a much higher porosity. Unfortunately, the use of DVB again strongly increased the amount of free carbon, as was measured by a TG in air flow on the aerogels pyrolyzed at 1500°C in flowing argon (figure 3-30). Interestingly the oxidation of the pure SMP-10 aerogel led to a weight gain of nearly 20%, meaning that even if the microstructure is coarse, the building of the SiO_2 passivation layer on the small SiC particle consumes approximately 1/3 of the original SiC, similarly to what already commented in section 3.1.2.

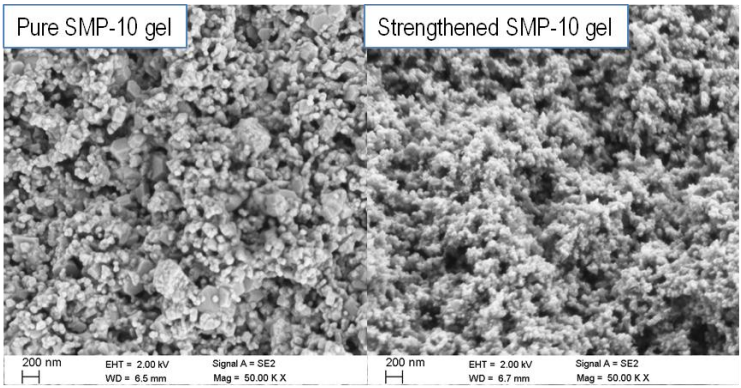

Figure 3-29 : Microstructure of pure and DVB treated SMP-10 aerogels pyrolized at 1500°C

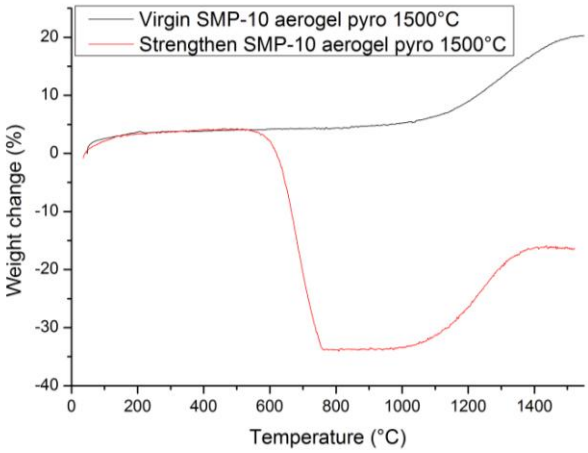

Figure 3-30 : TG curves in air flow of the aerogels pyrolized at 1500°C

Another approach to try to reduce the shrinkage of the pure SMP-10 gel during SCD, and obtain a proper, low density SMP-10 aerogel, was to use a different solvent to reduce the swelling effect that is believed to be responsible for the shrinkage.

To do so, tetrahydrofuran (THF) was used as a gelling solvent, thanks to the ability to readily dissolve SMP-10 with the difference of being a highly polar molecule, that could interact differently with the SMP-10 with respect to cyclohexane. It must be noted that, by this time, the SMP-10 was already out of the shelf-life (even if was properly kept in an argon filled flask stored at low temperature) and the viscosity was

greatly increased up to "honey-like" values. A gel was obtained using 1 gram of aged SMP-10, 8 grams of THF (90%vol), 105 µL of catalyst 0.1%Pt (Pt/SMP-10 $9x10^{-5}$), 100°C overnight and 1 day at 150°C. (The experiment was recently repeated with fresh SMP-10 and the gel was obtained after 2 days at 200°C.)

The SCD of this gel showed a linear shrinkage of 40%, still high but much lower compared to the gel produced with cyclohexane. In spite of the relatively high shrinkage, a bulk density of 0.25 g/cc was measured and was considered acceptably low compared to the previous results. The aerogels were pyrolized at 1200°C and 1500°C, bulk density, mass loss and shrinkage are reported in Table 3-7.

From the evolution from 1200°C to 1500°C of the mass loss, it was suspected a contamination with oxygen of the pre-ceramic polymer. Another unexpected result is the change in color from black (1200°C) to grey (1500°C) shown in figure 3-32. Both Lindbergh and Astro furnaces were used to pyrolyze the aerogels at 1500°C showing identical results and excluding an effect of the pyrolysis atmosphere.

The grey color can be an evidence of high purity crystalline SiC with no free C present, supporting the carbothermal reduction interpretation of the mass loss since the free carbon present at 1200°C could be completely consumed by the reaction. FT-IR analysis was performed (figure 3-31) and confirms the presence of a very small amount of Si-O (shoulder at 1050 cm^{-1}) and C=C (broad feature at 1600 cm^{-1}) bonds in the aerogel obtained at 1200°C.

The FE-SEM images (figure 3-33) reveal a highly porous microstructure, still aerogel-like but with a shift of pores and particles toward bigger size compared to the microstructure of the previously seen SiC/C aerogels. The SSA is indeed much reduced compared to the previous Si/C aerogels, consistent with particles size in the range 100 (RT) to 80 nm (1200-1500°C), which are the dimensions that can be estimated also from the FE-SEM micrographs. The pores are for the vast majority out of the range measurable from N_2 physisorption, so the N_2 pore volume appears highly underestimating the total pore volume that can be expected by the relatively low bulk density measured and from the FE-SEM images.

Temperature	P_{bulk} (g/cm^3)	ΔL (%)	Δm_P (%)	SSA (m^2/g)	N_2 pore volume (cc/g)
RT	0.25	40[a]	-	32	0.11
1200°C	0.60	26[b]	32[b]	20	0.06
1500°C	0.56	38[b]	37[b]	14	0.03

Table 3-7: Bulk Density, linear shrinkage and mass loss of the pure SMP-10 aerogels produced using THF as solvent. a)with respect to wet gel, b) with respect to pre-ceramic aerogel.

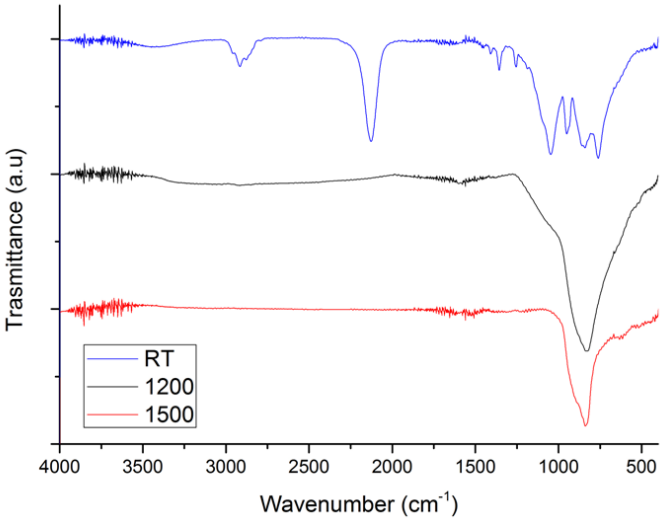

Figure 3-31: FT-IR spectra of pure SMP-10 aerogels obtained using THF as solvent and pyrolized at 1200° and 1500°C

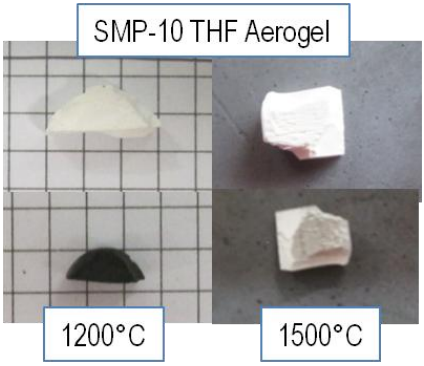

Figure 3-32 : Appearance of cm size SMP-10 aerogels produce using THF as solvent (top) and pyrolized at 1200°C (bottom left) and 1500°C (bottom right)

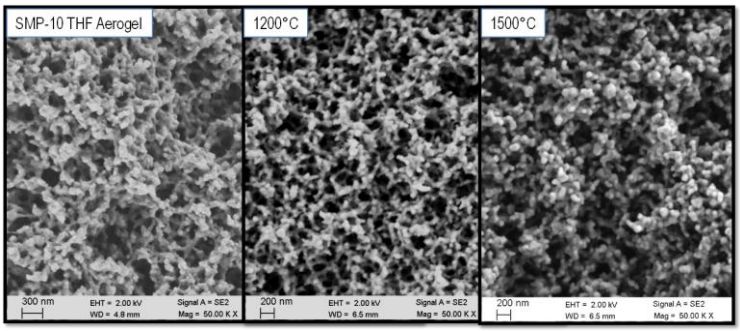

Figure 3-33 : FE-SEM images of the microstructure of pure SMP-10 aerogels at rt, 1200°C and 1500°C.

It is then demonstrated the possibility to produce gels of pure SMP-10 polycarbosilane. When THF is used as solvent the wet gels can be SC dried with low shrinkage producing low density SMP-10 aerogels. These can be converted to pure SiC aerogels upon pyrolysis at 1500°C. The SiC aerogels produced show lower SSA compared to SiC/C ones and reduced mesoporosity but can offer a much higher resistance in oxidative environment (up to 1000°C) and possibility of electronic/optical application thanks to the absence of free carbon. It is also expected that with more research devoted to the optimization of the recipe, SiC aerogel with higher meso pore volume and SSA can be produced, that would be very interesting as catalyst support.

3.2 Si-O-C system

Part of this section will be published in " Sasikumar, P. V., Zera, E., Graczyk-Zajac, M., Riedel, R., & Sorarù, G.D., (2016) Structural Design of Polymer Derived SiOC Ceramic Aerogels for High-rate Li-ion Storage Applications. Journal of the American Ceramic Society, Manuscript accepted for publication"

Silicon oxycarbide is a complex material in which the silicon atoms are bonded at the same time to oxygen and carbon. It can be represented as an amorphous silica network in which some oxygen atoms are substituted with carbon. The stoichiometric composition of oxycarbide is $SiC_xO_{2(1-x)}$ with $x<1$, but very often additional carbon is present and constitutes a free-carbon additional phase. A broad range of compositions can be produced varying x and the free carbon amount, affecting the mechanical and chemical properties of the material.

Additionally, depending on the pyrolysis temperature, the oxycarbide can be either amorphous (up to 1250 °C) or phase separated in nanodomains of SiO_2, SiC and C. Intriguingly, the structure of these glasses is still an open debate, and efforts are dedicated to understand how Si, O, and C are arranged, especially in the ceramics synthesized at low temperature.
The interest for this kind of materials is driven by the fact that the mixed bonds confer to the material interesting functional properties, like the possibility to intercalate lithium ions [84], piezoresistivity [121], gas sensing [122], luminescence [123] and bioactivity [124], in addition to increased mechanical and chemical strength compared to the parent amorphous silica [57] [125]. SiOC aerogels were produced to combine the porous features of the aerogel structure with the high lithium uptake of the SiOC phase, in order to enhance the capacity at high charge/discharge rate.
The effects of the porosity was studied by using two different solvents, i.e. cyclohexane and acetone, that, as will be shown, give rise to very different microstructure. Additionally, two different atmosphere were used, Ar or Ar/H_2, since a slightly reducing pyrolysis atmosphere was demonstrated to increase the performance of the SiOC anode.

3.2.1 Production details

The composition of the SiOC aerogels was aimed to be the one already studied in a previous PhD thesis in the group of Prof. Sorarù by V.S.Pradeep [66]. The recipe was then tuned to have 200 %wt of DVB compared to PMHS as precursor for the solid part of the aerogel, while the amount of solvent was set at 80 %vol, to give rise to a high amount of porosity. To obtain the gels, 15µL of 2%Pt catalyst per gram of PMHS were used and the solution was cross-linked at 150°C for 6 hours.

3.2.2 Solvent effects on the microstructure

The appearance of the gels obtained using acetone and cyclohexane is shown in figure 3-34. Wet cyclohexane gels are translucent while acetone gels are opaque white.
During SCD procedure both the gels show a non negligible shrinkage, higher in the case of cyclohexane (33%) than for acetone sample (13%); similarly to the SMP-10 gels, this shrinkage is experienced in the first part of the liquid exchange procedure. Both the gels were white after SCD, the acetone aerogel presented a density equal to 0.29 g/cc while in the case of cyclohexane the value was measured to be 0.67 g/cc.

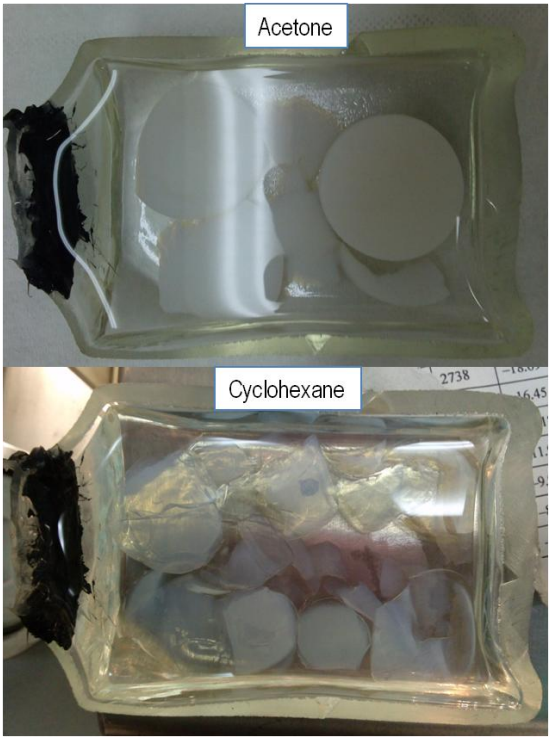

Figure 3-34: Appearance of PMHS/DVB gels synthesized with acetone (top) and cyclohexane (bottom)

The obtained siloxane aerogels were divided into two batches and pyrolized, one in pure argon and one in a H_2/argon mix (3% H_2), with a heating rate of 5°C/min up to 900°C, for 1h of dwell time for pure Ar and 7h for H_2/Ar mixture. The time, temperature and atmosphere of pyrolysis were chosen accordingly to those already optimized (for dense samples) by V.S.Pradeep [66] for increasing the lithium capacity of high carbon SiOC material. The samples were labeled as AcAr, AcH_2, CyAr and CyH_2 depending on the solvent, (Ac for acetone, Cy for cyclohexane) and the pyrolysis atmosphere.

Some features of the 4 samples after pyrolysis are reported in table 3-8; the shrinkage and the bulk density during pyrolysis are reported only for the samples obtained in Ar flow since the aerogels pyrolyzed in H_2/Ar consisted of irregular fragments. FE-SEM images showing the microstructure are presented in figure 3-35 while N_2 isotherms and BJH PSD curves are reported in figure 3-36 and 3-37.

	Linear shrinkage (%)	Mass loss (%)	Bulk density (g/cc)	BET SSA (m^2/g)	N_2 pore volume (cc/g)
AcAr	35	45	0.65	186	0.76
AcH_2	-	50	-	162	0.58
CyAr	32	44	0.98	95	0.18
CyH_2	-	50	-	77	0.13

Table 3-8: Features of cyclohexane and acetone SiOC/C aerogels produced in different pyrolysis atmosphere

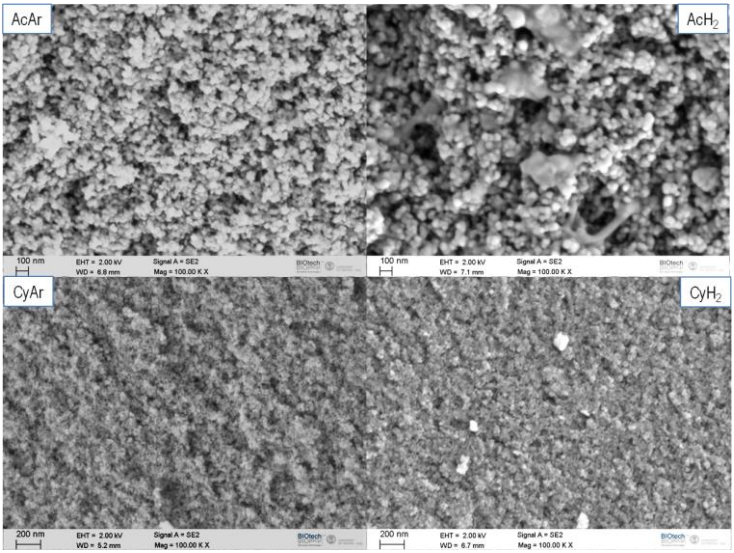

Figure 3-35: Microstructure of cyclohexane and acetone SiOC/C aerogels produced in different pyrolysis atmosphere

By using different solvents for the gel production, very different microstructures can be obtained as concerning particles dimension and pore size. This is thought to be due to two concurrent effects. The first is, as already commented for SMP-10 aerogel obtained using THF and cyclohexane as solvents (section 3.1.4), the different swelling ability of polar/apolar liquids, that lead to different shrinkage during the solvent to CO_2 exchange, as measured also in this case. The second is that the type of solvent can also modify the path for the formation of the gel, and in particular the dimension of the nanoparticles that build up the skeleton of the gel.

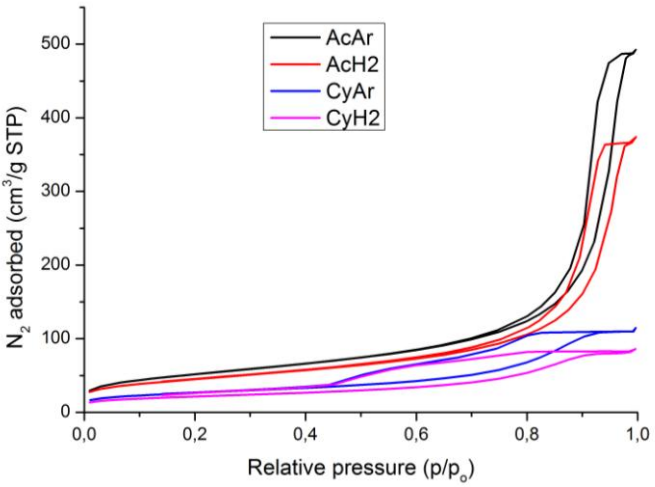

Figure 3-36 : N_2 physisorption isotherms of cyclohexane and acetone SiOC/C aerogels produced in different pyrolysis atmosphere

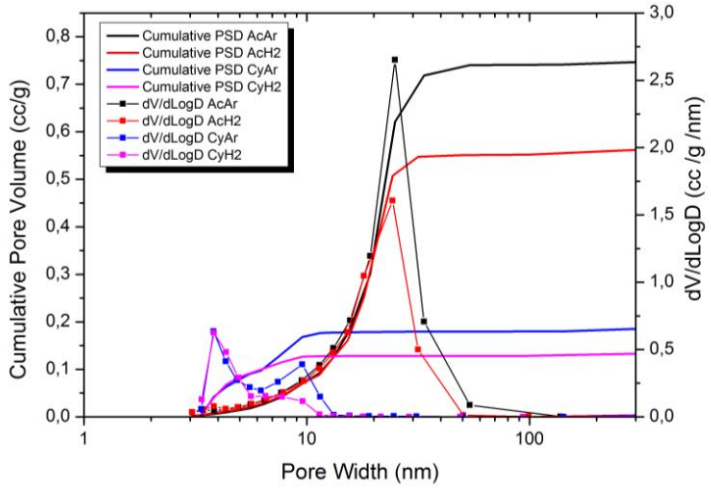

Figure 3-37 : BJH PSD of cyclohexane and acetone SiOC/C aerogels produced in different pyrolysis atmosphere

When a "better" solvent is used, the cross-linked polymeric nuclei can phase separate later, so the growth step is delayed and the particles are smaller compared

to those produced with a "worse" solvent. In this case, cyclohexane is considered to be a better solvent from the fact that it swells much more the PMHS/DVB network, causing a higher shrinkage during SCD. The better swelling ability was confirmed by measuring the expansion/contraction of a dense cross-linked PMHS/DVB square sample soaked in the two respective solvents.
Regarding the effects of the different atmosphere treatments on the microstructure, it can be observed that the -H_2 aerogels show some extent of sintering of the particles, clearly visible in the FE-SEM picture for AcH_2 sample, and suggested by a lowering of SSA and pore volume values measured by N_2 physisorption for both AcH_2 and CyH_2. The chemical analysis of the aerogels revealed a free carbon amount close to 40 %wt for all the 4 samples, with 60 %wt of mixed SiOC phase.

3.2.3 Li-ion capacity

To perform the electrochemical tests, the aerogel samples were milled in agate mortar and sieved to <42μm. To measure the lithium charge/discharge capacity, a standard procedure was used to produce the electrodes that were characterized using lithium metal as counter electrode [126], average loads of 2 mg of active material per cm^2 of electrode were calculated. Fifty charge/discharge cycles were performed for every rate tested (1C, 2C, 5C, 10C, 20C), after the whole cycling test the measurements at 1C were repeated to evaluate the aging of the material. The specific capacity vs cycling and charge/discharge rate is summarized in figure 3-38. A charge rate of C corresponds to a specific current of 360 mA/g.
From the results, summarized in table 3-9, it can be clearly seen that the microstructure strongly affects the electrochemical behavior of the SiOC aerogels. The same nominal SiOC composition, with dense microstructure and tested at 1C rate, showed approximately 300 mAh/g [66] while up to doubled capacity are measured for the optimized AcH_2 sample even after the whole cycling test. In the table are also reported the first charge (Q_C) and the first discharge (Q_D) capacities, with the efficiency of the first cycle reported as η.
The low efficiency of the first cycle is thought to be due to the formation of a relatively thick solid electrolyte interphase layer (SEI), that lowers even more the already fairly low first cycle efficiency of SiOC anodes (measured to be 63-67% for this composition [66]). After the first cycle, anyway, the efficiency is greatly increased as can be seen from the stable values reported in figure 3-38. It also appears evident the beneficial effect of the H_2/argon treatment, that was reported to increase the capacity by 150 mAh/g at 1C rate by deactivating the free carbon radicals present in the material [66].
Regarding the role played by the porosity, the small pores present in the cyclohexane aerogels do not increase the reversible capacity, but help to maintain a

very high stability of the anode, showing up to a remarkable 96% of the original 1st discharge capacity after the whole cycling test (consisting of 250 charge discharge at various rate). The bigger pores of the acetone samples on the other side impressively increased the capacity.

At 1C rate the combined effects of high mesopore volume (more than 50 %vol) and lower C radicals concentration (given by the H_2/argon treatment) push the 1st discharge capacity of the AcH_2 sample to more than 900 mAh/g. High values of capacity are maintained even at a rate of 10 to 20C, where the role of mesopores seems to be more important, given the leading values of the AcAr sample that also possess higher pore volume and SSA than AcH_2. The value obtained at 20C for AcAr (306 mAh/g) means that a capacity not far from the theoretical one for graphite (372 mAh/g, the most used anode material) could be reached with just a 2.5 minutes charge.

Sample	Q_C (mAh/g)	Q_D (mAh/g)	η (%)	Q_{10C} (mAh/g)	Q_{20C} (mAh/g)	Q_{1C_rep} (mAh/g)	Q_{1C_rec} (%)
AcAr	1496	763	51	346	306	570	75
AcH_2	1846	919	50	330	261	604	66
CyAr	939	332	35	121	100	307	93
CyH_2	961	495	52	234	165	477	96

Table 3-9 : Summary of the results of lithium uptake experiment for SiOC aerogels

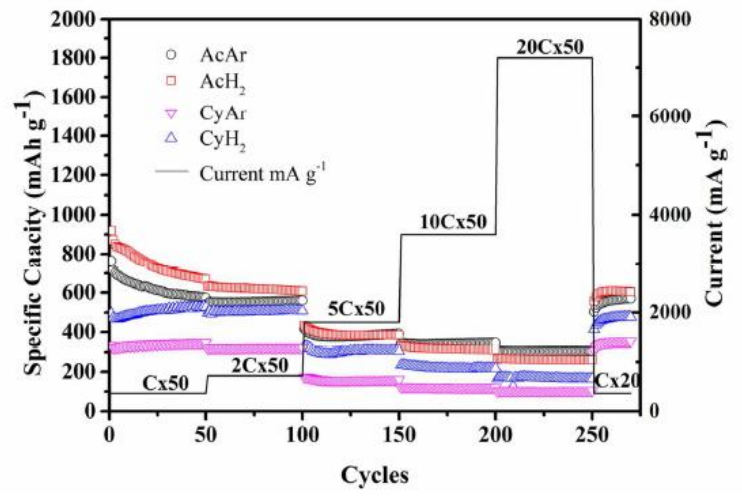

3-38 : Lithium specific capacity vs specific current and cycle number for SiOC aerogels

By applying the PDC aerogel production route to an optimized siloxane composition, SiOC/C aerogels were produced and tested as anodes for lithium ion batteries. The use of different solvents led to very different microstructures in terms of SSA, pore volume and pore size distribution. These differences were explained by the combination of smaller particle size, obtained with cyclohexane solvent, and lower shrinkage during SCD procedure, in the case of acetone. The differences in microstructure ruled the different electrochemical behavior, increasing the stability (cyclohexane series) or the total capacity (acetone series) of the SiOC anode. The pyrolysis in 3% H_2/argon mixture was confirmed to increase the capacity at moderate charge rate.

3.3 Si-C-N system

Part of this section was published in " Zera, E., Perolo, A., Campostrini, R., Li, W., & Sorarù, G. D. (2015). Synthesis and characterization of polymer-derived SiCN aerogel. Journal of the European Ceramic Society, 35(12), 3295-3302." and in " Zera, E., Nickel, W., Kaskel, S., & Sorarù, G. D. (2016). Out-of-furnace oxidation of SiCN polymer-derived ceramic aerogel pyrolized at intermediate temperature (600–800° C). Journal of the European Ceramic Society, 36(3), 423-428."

In polysilazane derived silicon carbonitride, similarly to silicon oxycarbide, the silicon atoms are bonded at the same time to nitrogen and to carbon. The presence of nitrogen substituting oxygen increases the stability of the amorphous network with respect to SiOC and temperature up to 1400°C can be reached without crystallization. Also in this case the presence of mixed bonds grants to the material functional properties like piezoresistivity [60], luminescence [123], [67], lithium intercalation [127] along with mechanical and thermal properties in between silica and silicon carbide [128]. As for SiOC, the properties can be tailored with a control of the chemistry of the ceramic precursor and of the pyrolysis temperature [41].
The proof of concept of the possibility to produce non-oxide ceramic aerogels by the PDC technique was extended also to polysilazane/SiCN system, applying the same conditions used to produce for SMP-10/DVB aerogels to obtain PSZ-20/DVB aerogels. During the study of these aerogels it was also discovered a reaction between the silazane and the supercritical CO_2 and, later on, the reactivity of the ceramic aerogels obtained with a pyrolysis at intermediate temperature towards the atmospheric air. Both these two (unexpected) reactions lead to an uncontrolled enrichment of oxygen in the ceramic material, decreasing the stability at high temperature. In particular, the finding of the high reactivity of the intermediate temperature pyrolyzed ceramic, being confirmed also for SiC aerogels, is thought to

be a general feature of PDCs obtained with a pyrolysis in the range 600-800°C, which are widely used to produce ceramic membranes for gas separation.

3.3.1 Production details

For the investigation of the general features of SiCN aerogels produced by PDC technique, two gels were produced with different amount of solvent, nominally 70 and 90 %vol. In details, the ratio between Si-H and C=C moieties was kept equal to 1, so for every gram of PSZ-20, 0.6 grams of DVB were used. The solvent used was cyclohexane, the weight ratio Pt/PSZ-20 was $6*10^{-5}$ and the cross-linking was performed at 150°C for 20 hours. The aerogels were obtained after SCD procedure and pyrolyzed at different temperature in argon (<1200°C) or in nitrogen (>1200°C).

3.3.2 General features of SiCN aerogels

The silazane aerogels showed a gel yield around 50% and SCD linear shrinkage lower than 10%, similarly to SMP-10/DVB aerogels. The N_2 physisorption isotherms with the corresponding BJH PSD of the two PSZ/DVB aerogels in the polymeric form and after pyrolysis at 1000°C are reported in figure 3-39 and 3-40. In table 3-10 are summarized the values of SSA, density and pore volume relative to the four samples.

	SSA (m^2/g)	N_2 pore volume (cc/g)	Bulk density (g/cc)
90-rt	539	1.53	0.05
70-rt	627	1.36	0.13
90-1000	149	0.64	0.14
70-1000	75	0.25	0.37

Table 3-10: SSA, N_2 pore volume and bulk density of PSZ/DVB and SiCN aerogels

As can be seen, changing the starting amount of solvent allows to change the bulk density of the aerogels. A less expected result, anyway, is that the SSA of the polymeric aerogels is not much different, and even higher for the more dense 70 sample. Additionally, a higher hysteresis for the samples of the 70 series is noticed, which is classically imputed to the presence of ink-bottle shaped pores or, better, to big pores interconnected by smaller pores, all of them being in the meso- range.

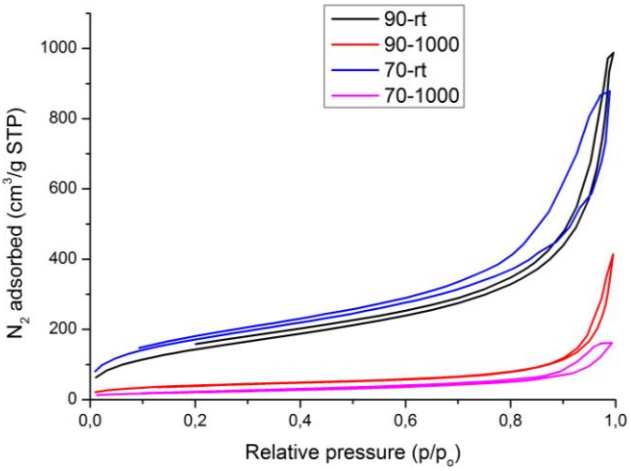

Figure 3-39 : N_2 isotherms measured on PSZ/DVB and SiCN aerogels

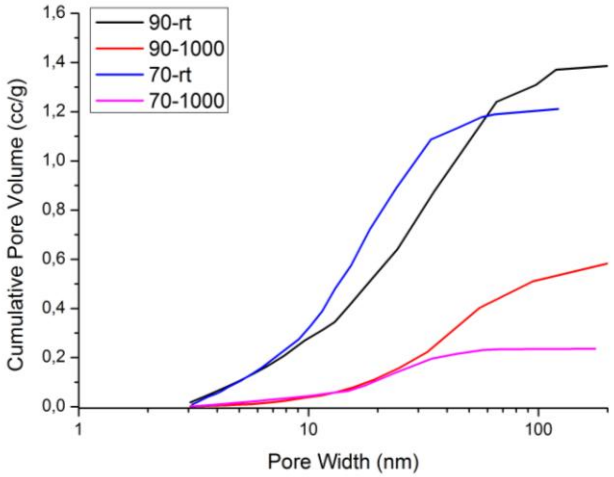

Figure 3-40 : BJH cumulative pore size distribution calculated for on PSZ/DVB and SiCN aerogels

After pyrolysis, a stronger evolution of the microstructure is observed with a much sharper decrease in SSA for the denser aerogel. These results are very similar to those already presented for SMP-10/DVB aerogels produced with 70% and 90 %vol

of solvent (section 3.1.2 and 3.1.3), suggesting that the use of DVB leads to nearly identical results in terms of microstructure.

Concerning the chemistry of the aerogels produced, the FT-IR spectra (figure 3-41) indicate the presence of Si-N (900 cm^{-1}), Si-O (1100-1000 cm^{-1}) and Si-C (830 cm^{-1}) bonds after pyrolysis, with the usual presence of free carbon giving rise to the broad peak centered at 1600 cm^{-1}.

Increasing the temperature of pyrolysis, the aerogel remains amorphous up to 1400°C (in nitrogen atmosphere, to prevent the loss of nitrogen as reported from literature [41]), with large silicon nitride crystals appearing at 1500°C as shown by the XRD pattern (figure 3-42) and FE-SEM image (figure 3-43).

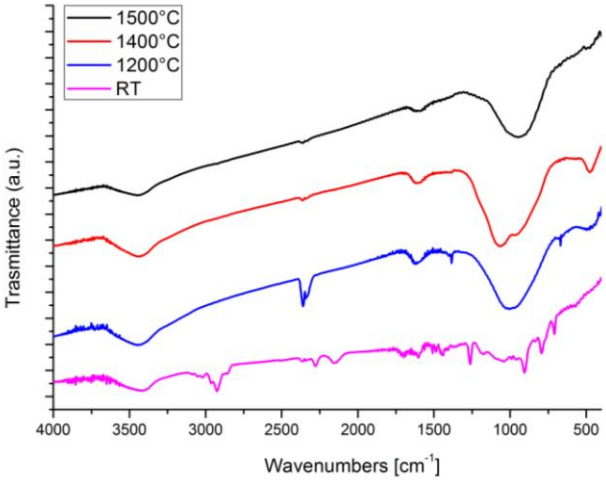

Figure 3-41 : FT-IR spectra of PSZ/DVB aerogel and the relative SiCN aerogels pyrolized at different temperature

These large crystals could probably be formed due to silica presence, that by the carbonitridation reaction (depicted below) leads to Si_3N_4 formation by gaseous intermediate products, allowing the formation of crystals of much larger size compared to those typically obtained (by solid state diffusion) at this temperature. Carbonitridation reaction proceed as:

$$3\ SiO_2 + 6\ C \rightarrow 3\ SiO_{(g)} + 6\ CO_{(g)}$$
$$3\ SiO_{(g)} + 3\ CO_{(g)} + 2\ N_{2\,(g)} \rightarrow Si_3N_4 + 3\ CO_{2\,(g)}.$$

The source of oxygen is (partially) explained by the next subsection of the chapter. Crystalline silicon carbide presence, on the other side, is difficultly ruled out by XRD, due to the overlap of the major peak (2θ ~36°) with Si_3N_4 peaks.

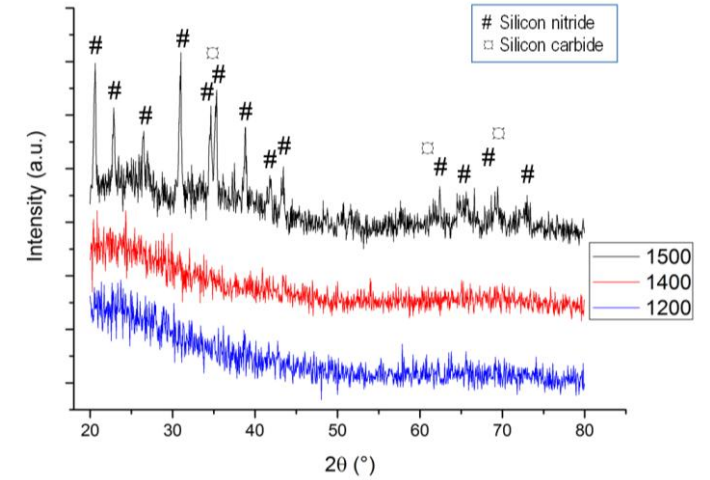

Figure 3-42 : XRD patterns of SiCN aerogels pyrolized at increasing temperature

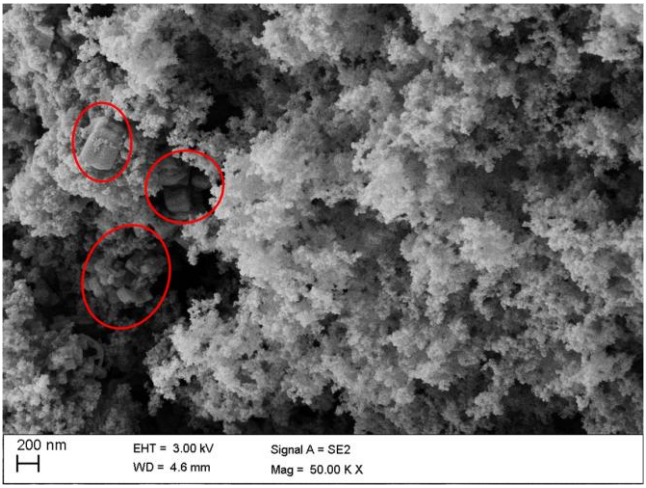

Figure 3-43 : FE-SEM micrographs of SiCN aerogel pyrolized at 1500°C, showing the presence of large crystals

3.3.3 CO_2 reaction with silazane

The first indication of a reaction between the silazane gel and CO_2 is given by the differences in the FTIR spectra collected for the PSZ/DVB aerogel and xerogel, shown in figure 3-44.

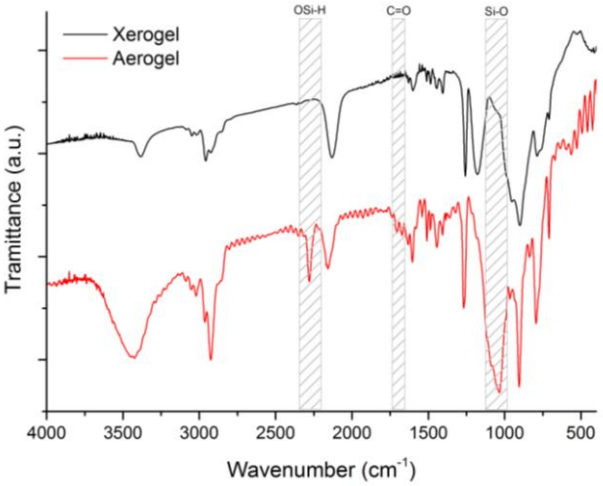

Figure 3-44 : FT-IR spectra of PSZ/DVB aero- and xero- gels

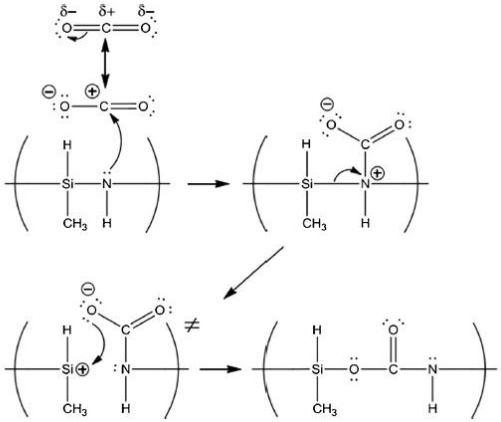

Figure 3-45: Pathway for the insertion of CO_2 in the silazane chains

It is indeed evident the presence of some extra peaks in the spectrum of the SCD material, that were assigned to OSi-H bond (2280 cm^{-1}), C=O (1700 cm^{-1}) and Si-O (1040 cm^{-1}). These bonds could be formed due to the reaction of Si-NH-Si bonds with CO_2, through the reaction pathway proposed in figure 3-45.
By ^{13}C MAS (Magic Angle Spinning) NMR a ratio between CH_3 and C=O groups equal to ~3% was measured and, since all the Si atoms have a methyl groups bonded (figure 2-13), an O/Si ratio of 0.06 can be assumed to be derived from SCD procedure.

3.3.4 Out-of-furnace reaction of SiCN aerogels

The first time a PSZ/DVB aerogel was pyrolized at 800°C (with the aim of studying the increase of SSA related to polymer to ceramic transformation performed at intermediate temperature), it was noticed to glow once exposed to the laboratory air, even though the sample was extracted from the furnace at room temperature. The experiment was reproduced with identical results so a wrong manipulation was excluded and a deeper investigation was dedicated to understand the phenomenon.
The PSZ/DVB aerogels produced with 70 %vol of solvent were pyrolized at increasing temperatures (450, 600, 800 and 1000°C) in argon flow and characterized by means of N_2 physisorption (table 3-11 and figures 3-47, 3-48 and 3-49) and DRIFT spectroscopy (figure 3-46) along with mass loss and shrinkage measurements (table 3-11).
A discrepancy between the mass loss values measured in situ (by thermogravimetry, figure 3-50) and those measured ex situ (reported in table 3-11), weighting a bulk sample before and after the pyrolysis treatment, is evident. Additionally, lower values of loss are measured for samples treated at 600 and 800°C with respect to the aerogel treated at 450°C. This can be explained by a weight gain after the removal of the samples from the furnace, which is thought to be due to a room temperature oxidation of the pyrolized aerogel.

Temperature (°C)	Mass Loss (%)	SSA (m2/g)	Micro pore volume (cc/g)	Linear shrinkage (%)
25	0	634	0,093	0
450	63	725	0,160	25
600	52	367	0,092	25
800	58	240	0,069	30
1000	66	75	0,005	50

Table 3-11: Mass loss, SSA, micropore volume and shrinkage measured on PSZ/DVB aerogel pyrolized at increasing temperature

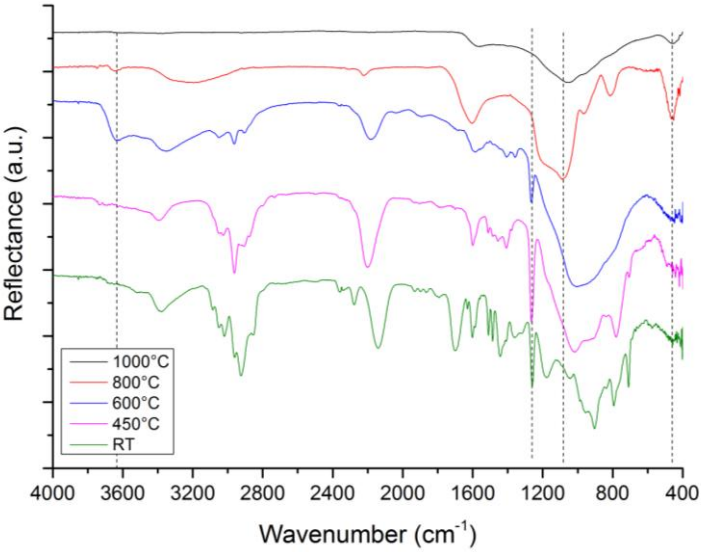

Figure 3-46 : DRIFT spectra of PSZ/DVB aerogel pyrolized at increasing temperature

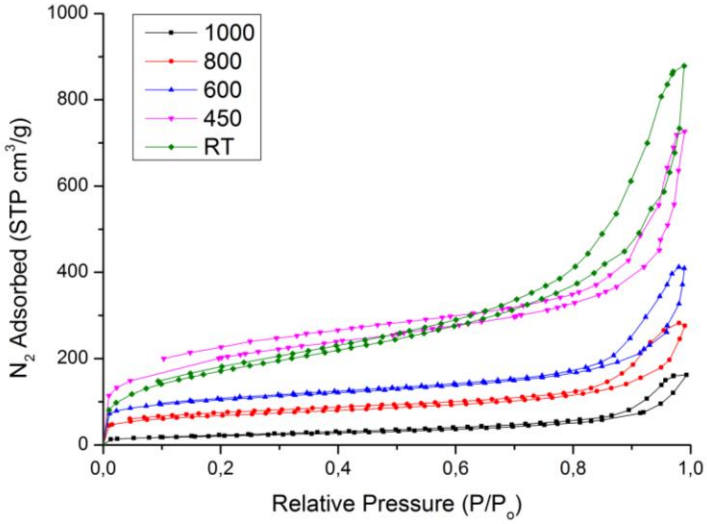

Figure 3-47 N2 physisorption isotherms of PSZ/DVB aerogel pyrolized at increasing temperature

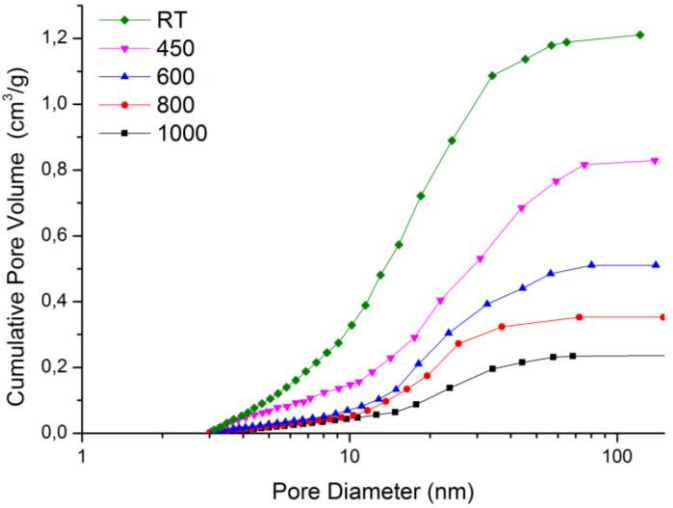

Figure 3-48 : BJH cumulative pore size distribution of PSZ/DVB aerogel pyrolized at increasing temperature

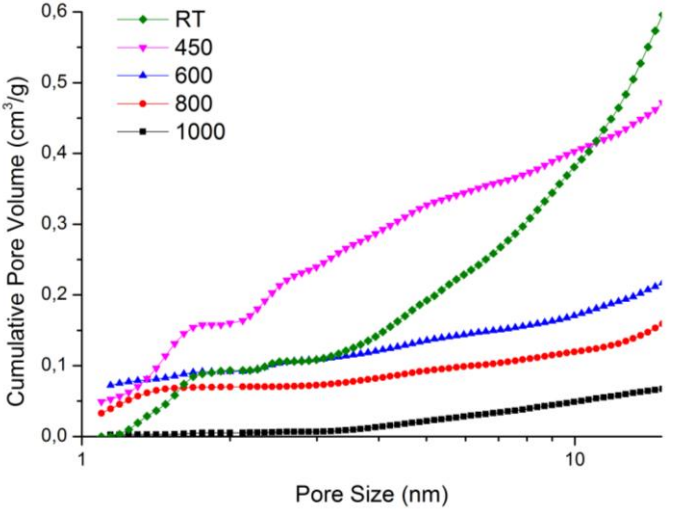

Figure 3-49 : QSDFT cumulative pore size distribution of PSZ/DVB aerogel pyrolized at increasing temperature

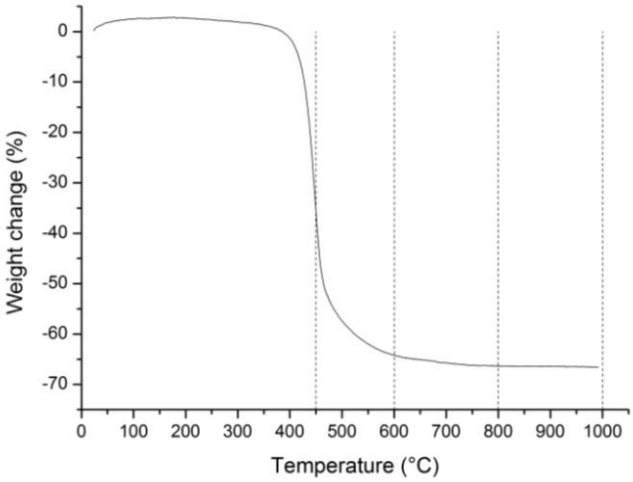

Figure 3-50 : TG curve in argon flow of the PSZ/DVB aerogel

The DRIFT spectra measured (figure 3-46) on the pyrolized aerogels reveal indeed the formation of Si-OH groups (3644 cm^{-1}) in the 600°C treated materials, and of Si-O-Si (1084 and 460 cm^{-1}) in those treated at 800°C. The reactivity of sol-gel derived precursor for silicon oxycarbide pyrolized in this range of temperature was already observed, reported and explained by Singh [129] in 1997. Even if traces of the effects of this reactivity are often reported in the PDC literature, it was never clearly pointed out that this could be the reason of (sometimes high) unexpected oxygen presence in SiC and SiCN obtained from pre-ceramic polymers, even if extra care was taken during manipulation of the polymer and its pyrolysis (glove box use, etc.).
Singh proposed that, in the case of SiOC, the presence of carbon enhances the stability of the SSA of the gels, and additionally observed (in situ) no detectable surface hydroxyl groups at temperature over 800°C. He concluded then that: "It is therefore clear that the Si-OH groups indicated by the spectra of the 800°C -and 900°C- foils must have formed due to a reaction of the surface with moisture during exposure to the ambient" [129].
The reason behind this reactivity (that leads to the pyrophoric behavior observed with aerogels) could be found in the formation of radicals like Si•, $Si-CH_2$•, CH_3•, H• during the cleavage of $Si-CH_3$ and C-H bonds with production of H_2 and CH_4 as already proposed in [130] for siloxanes. Carbon radicals in the ceramic material have been observed with ESR [131] [132] while silicon radicals were never, probably due to their high reactivity towards oxidation of the ceramic product.

The formation of transient microporosity in the pyrolysis of PDC is well known in literature and was confirmed also in this case by N_2 physisorption. The creation of pores is related to the formation of the gaseous decomposition products [77]. The so produced pores are stable up to a certain temperature, until densification takes place (see linear shrinkage data in table 3-11) leading to a closure of the pores with a loss of specific surface, as shown in the evolution of pore size distribution presented in figure 3-48 and 3-49.
To extend the concept of this reactivity at intermediate temperature to other systems, a check was performed pyrolizing an SMP-10/DVB aerogel at 800°C and the same behavior was observed. It is therefore believed that this out-of-furnace oxidation is not restricted to the system studied (PSZ-20/DVB aerogels) but a more general feature of PDC pyrolized in this intermediate temperature range.

3.4 N-doped CDC aerogels

Part of this section was published in " Zera, E., Nickel, W., Hao, G. P., Vanzetti, L., Kaskel, S., & Sorarù, G. D. (2016). Nitrogen doped carbide derived carbon aerogels by chlorine etching of a SiCN aerogel. Journal of Materials Chemistry A, 4(12), 4525-4533."

Aerogels are, by synthesis, hierarchical porous materials with pore size covering the whole meso-range up to macro-range, as already presented by SEM images and by N_2 physisorption. On the other side, the micro-range of the porosity (pores < 2nm) is usually not so well developed and mostly lost upon pyrolysis at higher temperature as seen in the previous section.
A strategy to increase the micropore volume, and the SSA, can be the selective removal of silicon atoms with a high temperature (500-1000°C) Cl_2 treatment. The selective removal of metal atoms from a carbide leaves a highly microporous carbonaceous material, called carbide derived carbon (CDC), which pore size can be controlled changing the etching temperature and the carbide phase [133].
The use of CDCs is widely studied in various energy related applications like: supercapacitors [134], CO_2 sequestration [135], Li-ion batteries [136], hydrogen and methane storage [137]. The CDC route applied to PDC aerogels firstly by Oschatz in 2014 to produce CDC aerogels from SiC [138], obtaining a fully hierarchical porous carbon with very high specific surface and a well developed transport pores system. On the other side, the chlorination of SiCN ceramic was first tried on dense samples by Yeon, obtaining a CDC with micro and meso pores, thanks to the combination of Si-C and Si-N presence [79], no nitrogen was evidenced in the CDC produced.
More recently (and concurrent with the experimental work performed for this section) Ewert etched a mesoporous SiCN (pyrolized at 900°C) with chlorine and reported a

strong decrease of the nitrogen present in the hierarchical N-doped CDC when the etching temperature was increased from 800 to 1000°C [139].
In this section the idea of combining SiCN aerogels and CDC technique to obtain a nitrogen doped CDC aerogel was exploited, and the N-doped CDC aerogels successfully obtained were characterized for CO_2 sequestration and as electrode for aqueous based supercapacitor.

3.4.1 Production of N-doped CDC carbon aerogel

For this study, PSZ/DVB aerogels produced with 70 %vol of cyclohexane were used, using the recipe illustrated in section 3.3.2. The polysilazane/DVB aerogels were cut, put in a quartz boat and placed in a horizontal tubular furnace (Gero RES-E 230/3) equipped with fused quartz tube. The outlet bubbler was filled with NaOH (20g for 200 mL of water) aqueous solution to deactivate unreacted Cl_2 gas. The tube was first flushed with Argon (99.999% Ar, Air Liquide) for 1.5 h at a flow of 150 mL/min. After the purging, the furnace was switched on and heated with a rate of 450 °C/h up to the pyrolysis/chlorination temperature.
To perform the chlorine etching, after one hour holding in Argon flow at the desired temperature (pyrolysis) the inlet gas was changed to a mixture of Cl_2 (99.8% Cl_2, Air Liquide, 80 mL/min) and Ar (70 mL/min), maintaining the same temperature. The etching time varied with the temperature as is reported in table 3-12. Indeed the kinetic of the etching reaction strongly depends on the temperature, so longer times were used for samples etched at low temperature. After the etching, the inlet gas was changed back to pure Ar and the temperature set at 600 °C (with the exception of the 450CDC sample, in which the temperature was maintained constant to avoid further evolution of the material) and kept constant for 1h. Then, the outlet tube was connected to a silicone oil bubbler and pure hydrogen (99.9% H_2, Air Liquide) was connected to the gas inlet. The H_2 flow was maintained for a time depending from the etching time (compatibly with laboratory schedules), and finally the furnace heating was turned off, connecting the inlet gas back to pure to Ar.
The pyrolysis and chlorination in the range 450-1000°C were performed subsequently in the same fused quartz tubular furnace in order to avoid the previously mentioned out-of-furnace oxidation of the aerogels (section 3.3.4). Due to limited maximum temperature of the chlorination furnace, the pyrolysis at 1200°C was performed in a different furnace, the SiCN aerogel in this case was briefly exposed to the atmosphere (at room temperature) before undergoing the same etching process as the 1000CDC sample.

	Pyrolysis (Ar)	Cl_2 Etching	H_2 treatment
450CDC	450 °C -1h	450 °C - 5h	450 °C - 3h
600CDC	600 °C -1h	600 °C - 3h	600 °C - 3h
800CDC	800 °C - 1h	800 °C - 2h	600 °C - 2h
1000CDC	1000 °C - 1h	1000 °C - 1h	600 °C - 1h
1200CDC	1200 °C - 1h	1000 °C - 1h	600 °C - 1h

Table 3-12 Time-temperature for the various stage to produce N-doped CDC aerogel

3.4.2 General features of N-doped CDC carbon aerogel

The DRIFT spectra (figure 3-51) obtained on the chlorinated aerogels reveal the disappearance of all the H related peaks (Si-H, C-H, N-H) and of all those related to Si, with the exception of the 450°C treated sample, which still shows Si-O (1100 and 450 cm^{-1}), Si-N (970 cm^{-1}) and Si-C (810 cm^{-1}) peaks. The samples 600 to 1200 CDC show two broad peaks assigned to C=C bonds (~1600 cm^{-1}) of substituted aromatic structures and to the superimposition of C-O (1250 cm^{-1}) and C-N bonds (~1280 cm^{-1}) [104].

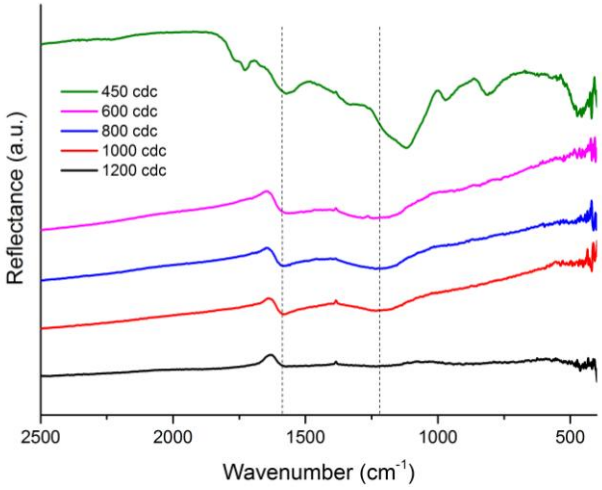

Figure 3-51 : DRIFT spectra of the chlorinated aerogels

The sample produced at 450°C was considered to be non etched and no further efforts were dedicated to its characterization. Additionally, the amount of sample produced at 1200°C was very low and for this reason thermogravimetry measurements were avoided for this sample in order to have enough material for the electrochemical tests.

The FE-SEM pictures presented in figure 3-52 show that the typical aerogel structure is preserved after the chlorine etching, confirming that the transformation from carbide to carbonaceous material is fully conformal [133].

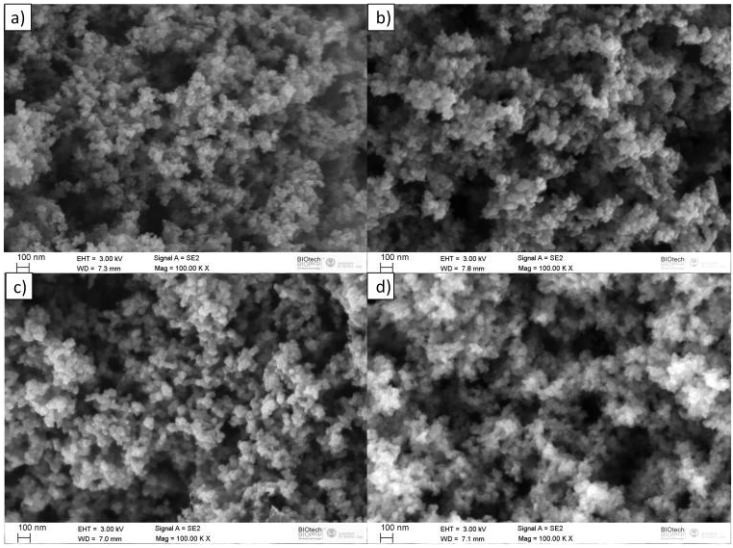

Figure 3-52 : FE-SEM images of 600,800,1000 and 1200CDC aerogels

The TG/DTA measurements in synthetic air flow (figure 3-53, 100 mL/min, 10 °/min) on the 600, 800 and 1000°C produced aerogels show the complete combustion of the CDCs in the range 500-700 °C confirming the successful removal of silicon, which presence would lead to some residue. Interestingly, the mass loss is anticipated for the samples produced at lower temperature, revealing also two separate signals on the DTA trace which ratio changes with the production temperature. This suggests a different reactivity of the CDC produced, probably due to differences in composition (as will be shown with XPS) and in the ordering of the carbon.

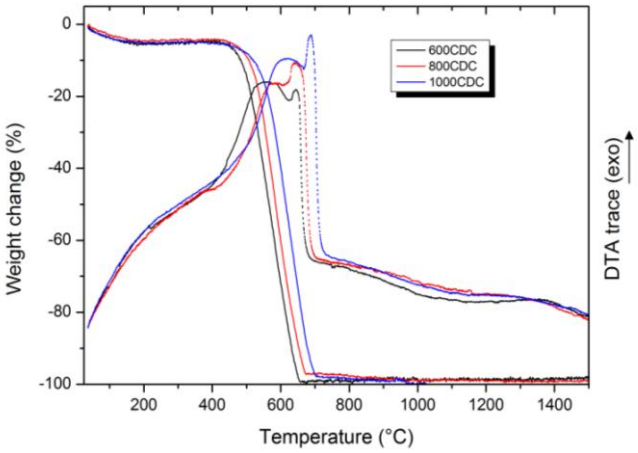

Figure 3-53: TG/DTA curves in flowing synthetic air of CDC aerogels produced at 600, 800 and 1000°C

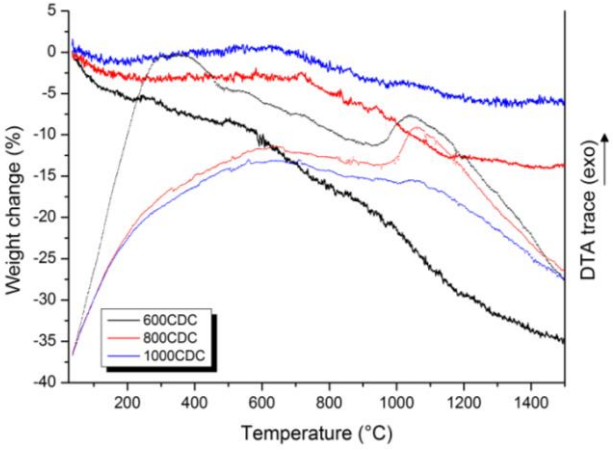

Figure 3-54 : TG/DTA curves in flowing argon of CDC aerogels produced at 600, 800 and 1000°C

The TG/DTA measurements in flowing argon (figure 3-54, 100 mL/min, 10 °/min) also reveal an increasing stability of the N-doped CDC aerogels at increasing synthesis temperature, with a clear weight loss of the 600CDC sample even in completely inert environment.

Additionally, the DTA trace shows an evident exothermic peak around 1050°C for the 600 and 800CDC samples, the same peak can barely distinguished for the 1000CDC aerogel. From literature, the carbide derived carbons produced at low temperature are composed by many different phases, some of which still possess a certain amount of sp^3 carbon [140]. Increasing the temperature above 1000°C, and especially if N is present, strongly lowers the stability of sp^3 carbon [141], leading to the formation of graphitic structures [140]. The exothermic peak could therefore be given by the release of heat related to this sp^3 to sp^2 transition.

XPS spectra (figure 3-55) confirm the presence of nitrogen in the CDC aerogels along with some residual chlorine, which lowers with increasing synthesis temperature, and some oxygen. Traces of residual Si are also detected for the 600CDC and 1000CDC samples. N 1s core spectra (figure 3-56) were recorded and two distinct components can be easily distinguished and assigned to nitrogen bonded to carbon in quaternary (N_q) and pyridinic (N_{py}) sites. The chemical compositions resulting from the survey spectra are reported in table 3-13 with the last column showing the calculated ratio between quaternary and pyridinic N.

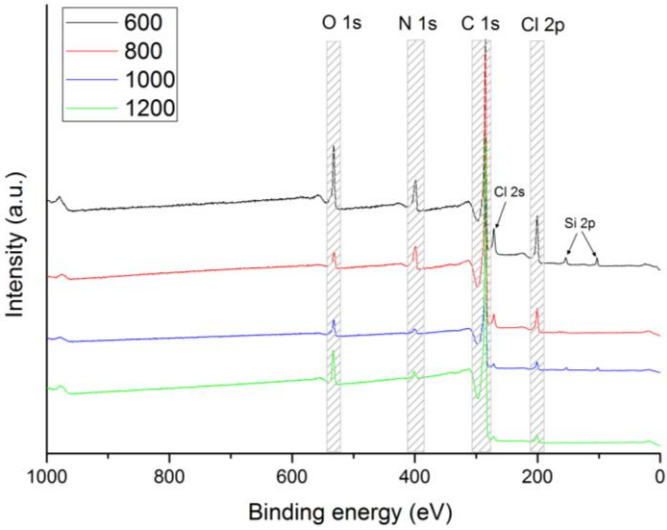

Figure 3-55: XPS survey spectra of the N-CDC aerogels produced

These results clearly reveal a bond rearrangement of N and C upon removal of silicon. Indeed, carbon and nitrogen are not bonded together in low temperature polysilazane derived SiCN [41] so new C-N bonds are formed when the Si "bridges" are removed with chlorine. Additionally, C-N bonds are not stable at high

temperature and nitrogen start be lost at T>800°C, with preferential loss from pyridinic and pyrrolic sites, with mostly quaternary N detectable at high temperature [142] [143]. As a result, a drastic decrease of %at of N is measured by XPS, consistently with Ewert's results [139].

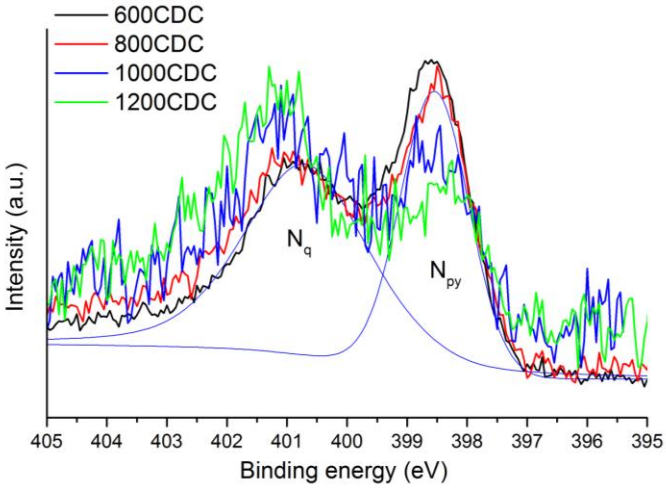

Figure 3-56: N 1s core spectra of the N-CDC aerogels produced

	O (%at)	N (%at)	C (%at)	Cl (%at)	Si (%at)	N_q/N_{py}
600CDC	7.9	9.7	75	5.5	2	1.3
800CDC	2.3	6.7	88.3	2.6	0.1	1.3
1000CDC	3.7	2.5	91.2	1.5	1.2	2.9
1200CDC	3.8	2	93.1	0.9	0.2	4.3

Table 3-13: Summary of XPS chemical composition of the N-CDC aerogels produced

Core spectra also confirms the preferential loss of pyridinic nitrogen. Chlorine is present, in spite of the hydrogen treatment, with a lowering content at increasing etching temperature. This could be ruled out as an effect of high Cl_2/carbide ratio combined with low temperature, that shifts the so called "range III" (which represents the onset of carbon formation from carbide, see [140]) to higher temperature, partially stabilizing the formation of C-Cl moieties. At last, non negligible amounts of

oxygen are also detected but its source, being a kind of ubiquitous element not only in PDC but also in N-doped carbons and CDCs, is still not fully understood.
The removal of silicon creates also a huge amount of micropores, which contributes to increase the SSA well above 1000 m^2/g, as measured with N_2 physisorption and summarized in table 3-14. The N_2 isotherms and the pore size distribution, calculated applying QSDFT to low pressure adsorption isotherms measured with Autosorb machine, are presented in figures 3-57 and 3-58.

	SSA (m^2/g)	µ-PV (cc/g)	m-PV (cc/g)
600CDC	1724	0.48	0.64
800CDC	1468	0.44	0.59
1000CDC	1887	0.54	0.97
1200CDC	1473	0.43	0.61

Table 3-14 : SSA and micro and meso pore volume calculated with N2 physisorption for N-doped CDC aerogels

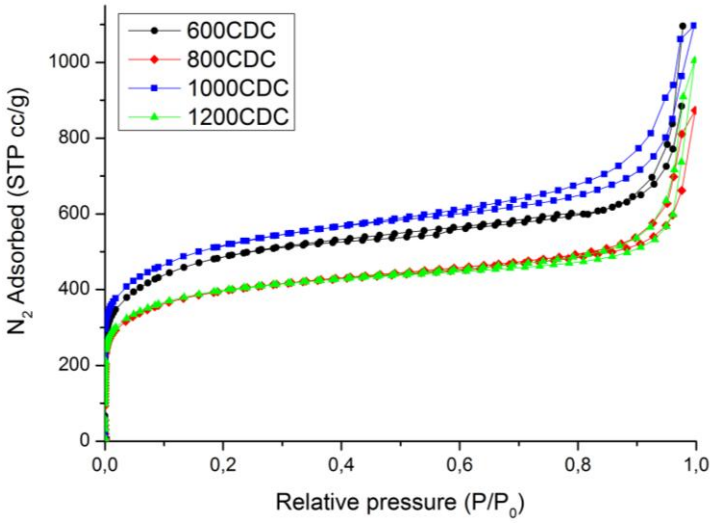

Figure 3-57 : Low pressure nitrogen physisorption isotherms measured with Autosorb

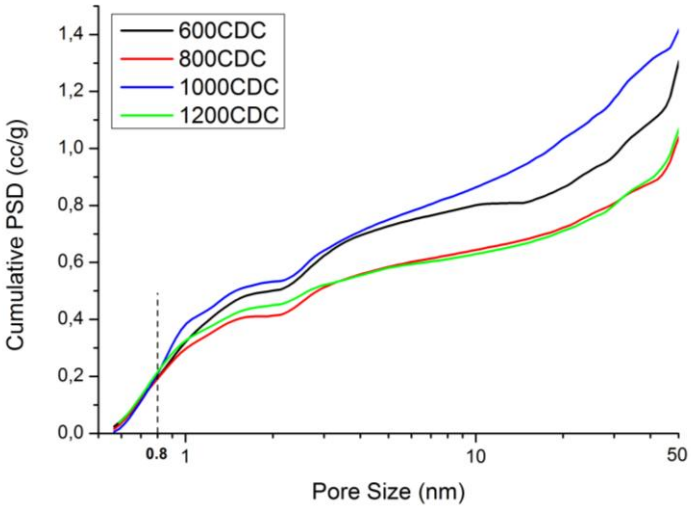

Figure 3-58 : Cumulative pore size distribution obtained applying QSDFT on the low pressure nitrogen isotherms measured on N-doped CDC aerogels

It can be seen that these CDC aerogels can be regarded as truly hierarchically porous materials, possessing meso-macro pores thanks to the aerogel structure, and micropores deriving from the selective removal of silicon through CDC technique.
The trend for pore volume and SSA is not monotonic, and shows two local maxima at 600 and 1000°C. These results can be interpreted as a combination of many effects given by the behavior of the silazane aerogel during pyrolysis and etching. The viscous flow at 800°C close some pores present in the aerogel structure, leading to a reduced pore volume already before the etching and explaining the decrease in SSA and pore volume from 600 to 800°C. At 1000°C the viscosity is increased and this effect is limited [144]. At the same time the increased skeleton density leads to the formation of smaller pores during etching [138] while the evolution of nitrogen increases the total pore volume. This combination of smaller pore size and higher pore volume explains the increase in the SSA value from 800 to 1000°C. At 1200°C Si_3N_4 domains start to be formed, leading to larger pores after etching [79] thus reducing the microporosity and the SSA value. This increase in size of the pores produced by the etching enlarge the mesopores of the aerogel structure, bringing part of them out of the measurable range with nitrogen physisorption technique; explaining the lower pore volume measured for the 1200CDC sample.

3.4.3 CO_2 adsorption and EDLC capacity

As applications for the produced N-doped CDC aerogels, CO_2 sequestration and EDLC electrodes were tested, trying to evaluate the possibly beneficial effects of N presence in the carbon material combined with the hierarchical pore structure. In figure 3-59 are reported the physisorption isotherms measured with CO_2 at 0°C and up to 1 bar (760 torr).

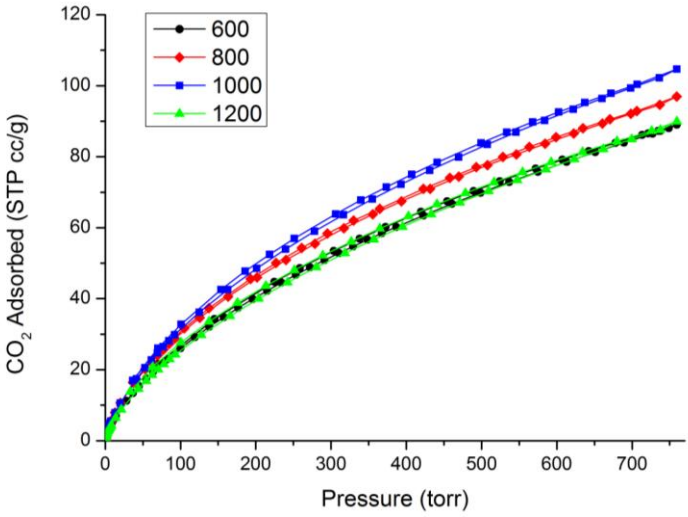

Figure 3-59 : CO_2 adsorption desorption isotherms measured at 0°C

The isotherms reveal a fully reversible pick up of CO_2 along with high values of gas adsorbed per gram of material. In this case anyway, no strong effects of the much higher nitrogen presence in the 600 and 800CDC aerogels is evidenced. Indeed, the best performing material (1000CDC) contains just 2.5% of N compared to 9.5% of the 600CDC sample. The reason for this negligible effect of N could be found, again, with a combination of different contributes.

From literature [145] the ultra-micropores, i.e. pores smaller than 0.8 nm, are thought to be responsible for the major role in adsorption of CO_2 at 0°C and 1 bar. As shown by figure 3-58, all these aerogels possess approximately the same specific volume of ultra-micropore so, in principle, should absorb about the same quantity of CO_2. Basic nitrogen, on the other side, should help the interaction of the walls of the pores with acidic CO_2, leading to a higher pick up of the gas.

Anyway, as shown from XPS, only moderately basic pyridinic groups and nearly neutral quaternary nitrogen groups are present in these N-doped carbons. Additionally, high amount of acidic C-Cl moieties, which can be regarded as detrimental for CO_2 adsorption for the very same reason why basic C-N moieties are considered beneficial, are present in the low temperature obtained CDCs. As a result, similar behaviors are obtained for the four materials, with a slightly higher amount of CO_2 adsorbed from 1000 and 800CDC aerogels that show a good compromise between N and Cl content.

Concerning the EDLC tests, the hierarchical porous structure of N-CDC aerogels helps fast diffusion of the electrolyte ions, increasing the performance of EDLC at high charge-discharge rate. Additionally, nitrogen containing functional groups can initiate some redox reactions with the ions of the electrolyte, giving rise to pseudocapacitance and increasing the overall specific capacitance (C_{spec}). The capacitance-voltage (CV) curves obtained with a scan rate of 10 mV/s and using the produced N-doped CDC aerogels as electrodes are reported in figure 3-60. The curves clearly reveal the pseudocapacitive behavior (bump of C_{spec} at -0.5 and 0.5 V) of the samples produced at 600 and 800 °C as a result of the higher quantity of doping atoms in these two materials.

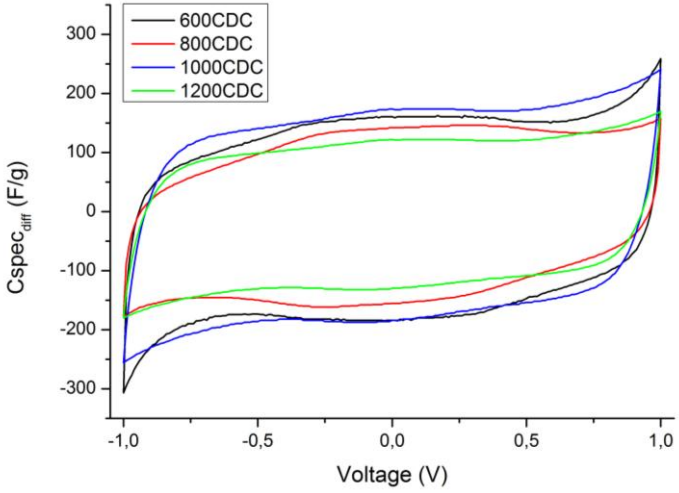

Figure 3-60 : Cyclic voltammetry curves measured on the EDLC produced with the N-doped CDC aerogels as electrodes, 10mV/s scan rate, 1M H_2SO_4 electrolyte

The remarkably high specific C_{spec} for the four materials tested at 10 mV/s are summarized in table 3-15. Since the capacitance value strongly depends from the SSA, the C_{spec} normalized on the area of the active material are also reported. These

normalized values can depend from the pore dimension and from the chemistry of the surface [146]. In our case we noticed a nearly constant value up to 1000°C, with a drop from 8.8 to 7.9 μF/cm^2 between 1000 and 1200°C, probably as an effect of the decrease in small micropore volume in addition to the lower pseudocapacitance noticed.

C_{spec}	600CDC	800CDC	1000CDC	1200CDC
F/g	152	129	164	116
μF/cm^2	8.8	8.8	8.7	7.9

Table 3-15 : Specific capacities evaluated from CV curves at scan rate of 10 mV/s

The 600CDC sample was investigated more in details since it's the first CDC material produced from SiCN at such a low temperature and the one containing the highest quantity of heteroatoms. The CV curves obtained at increasing scan rate are presented in figure 3-61, while the calculated specific capacitance is summarized in table 3-16. It's possible to notice the effect of pseudocapacitance up to a rate of 200 mV/s, while at 1000 mV/s the curve's shape becomes typical of a capacitor with some internal resistance, with the total capacitance decreasing down to 70 F/g. The macro- mesoporous structure of the aerogel helps to maintain the high values even at scan rate as high as 200 mV/s, by providing transport pores that allow easy access of the ions to the active surface.

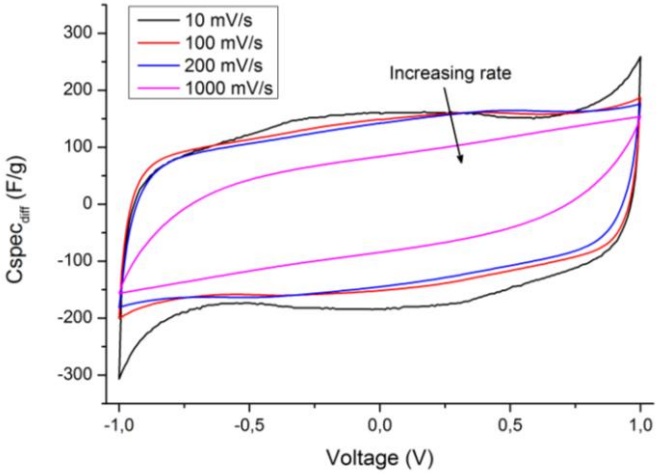

Figure 3-61: CV curves at different scan rates measured on the 600CDC sample

	10 mV/s	100 mV/s	2000 mV/s	1000 mV/s
C_{spec} (F/g)	152	135	127	70

Table 3-16: Specific capacity of 600CDC aerogel at increasing scan rate

The C_{spec} retention with increasing charging/discharging rate was also evaluated by galvanostatic measurement at increasing current density. From the curves obtained, and shown in figure 3-62, it's possible to calculate the C_{spec} at constant discharge current (reported in table 3-17). Also these results indicate a very good capacity retention, with just a moderate ohmic drop at the highest current tested, and high values of specific capacitance, placed among the highest measured for CDCs materials.

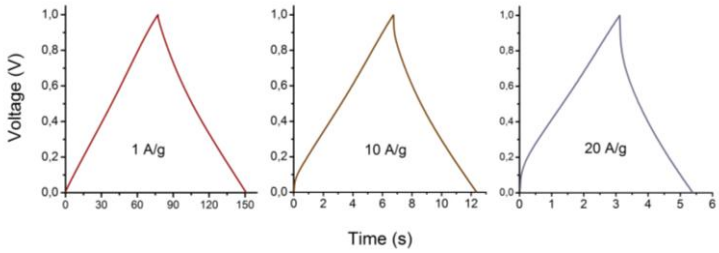

Figure 3-62: Galvanostatic charge/discharge curves measured at increasing specific currents for the 600CDC aerogel

	1 A/g	10 A/g	20 A/g
C_{spec} (F/g)	165	140	123

Table 3-17 : Specific capacities evaluated from galvanostatic curves at increasing specific currents for the 600CDC aerogel

The stability of C_{spec} was evaluated by charging/discharging the EDCL produced with the 600CDC aerogel for 5000 times with a current density of 10 A/g (figure 3-63). The charge/discharge curves of the 1st, 2500th and 5000th cycle are highlighted in the inset of figure 3-63.

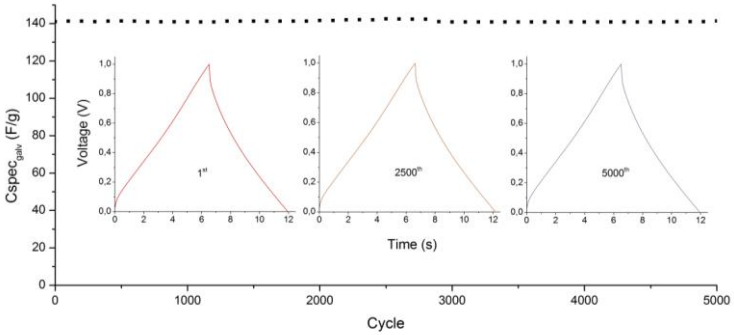

Figure 3-63 : Stability of the 600CDC sample in galvanostatic charge/discharge test at a specific current of 10 A/g.

As shown, no change in the specific capacitance after 5000 cycles at high current density of 10A/g can be appreciated. The excellent cycling stability, which is a fundamental requirement for a candidate material to be used in real capacitors, was actually followed up to 10 000 cycles, with a capacitance retention higher than 99%.

Chapter IV

Conclusions and Future perspectives

Conclusions

The production of aerogels with composition within the Si-C-N-O system was investigated, by using the polymer-derived ceramic technique combined with CO_2 supercritical drying of wet gels. The gels were obtained by cross-linking in highly diluted conditions the ceramic precursors, taking advantage of the hydrosilylation reaction between Si-H and C=C moieties.

The influence of many parameters on the properties of the aerogels were investigated, in order to tune the microstructural and compositional features of the final ceramic materials.

Particular efforts were dedicated to change the amount of carbon in SiC/C aerogels and to understand how to control the density, specific surface area, pore size and thermal stability of the produced ceramics. The use of the tetrafunctional tetravinylsilane as cross-linker replacing the more conventional divinylbenzene allows to produce aerogels with lower carbon amount and higher SSA values, with the drawback of decreased stability of the microstructure at high temperature (2000°C) and increased bulk density. Lowering the amount of DVB on the other side causes higher shrinkage during supercritical drying procedure, which increases the bulk density, and at the same time diminish the content of carbon in the pyrolized aerogels.

Pure SMP-10 gels can be produced and the behavior during supercritical drying procedure is strongly affected by the solvent used for the gelation. Indeed, the use of cyclohexane leads to a nearly complete densification during solvent to CO_2 exchange while the use of tetrahydrofuran allows to limit the shrinkage and preserve the porous structure. The pyrolysis of this pure SMP-10 aerogel at 1500°C in argon creates a porous material with aerogel structure composed by pure SiC.

SiOC/C aerogels were produced with a composition optimized for the use as Li-ion battery anode. The use of two different gelling solvent created very different microstructure dominated by small- (cyclohexane solvent) or big- (acetone solvent) mesopores. The smaller pores revealed beneficial effects by increasing the stability of the capacity after the long cycling test while the microstructure created by the use of acetone led to a great increase in the overall Li-capacity and its preservation even at very high charge discharge rates.

The application of the developed technique to polysilazanes allowed to produce for the first time SiCN aerogels, possessing similar microstructural characteristics to polycarbosilane derived aerogels. These SiCN aerogels were demonstrated to be amorphous up to 1400 °C in nitrogen atmosphere. The research within this composition led also to the recognition of the reactivity of silazanes toward CO_2 and of the PDC pyrolized at intermediate temperature toward atmospheric room temperature oxidation.
Finally, it was demonstrated the possibility to produce nitrogen doped carbide derived carbon aerogels etching at mild temperature amorphous SiCN aerogels. In this case, the microstructure allowed to complete the etching already at temperature as low as 600°C, helping to maintain nitrogen in the final carbonaceous material. These N-doped CDC aerogels possessed a hierarchical microstructure over the whole micro- meso- macro- range of porosity. When used as electrodes in aqueous based electric double layer capacitors they showed remarkable specific capacitance, thanks to the presence of heteroatoms giving rise to pseudocapacitance, which was measured to be stable at high specific current and after long time cycling, as a beneficial effect of the hierarchically porous microstructure.

Future perspectives

The next step for PDC aerogels, apart from further expanding the possible chemical compositions, is to start taking advantage of the peculiar properties possessed and exploiting them for applications that could benefit from them. The possible playground of Si-C-N-O aerogels is very wide, and could cover many energy related specific fields. Pure SiC aerogels possessing high permeability and high thermal conductivity of the skeleton, along with sub-micron pores, are promising catalyst support for endo/exothermic reaction even in very harsh environment. SiC/C on the other side could be used for adsorption of organic and inorganic pollutants, thanks to their high SSA, the high thermal stability allowing the thermal regeneration of the material. SiOC aerogels were tested here as anode for Li-ion batteries, with very good results, but also additional tests to use these materials as electrical and optical sensors are ongoing, that would benefit from the peculiar properties of silicon oxycarbides. In the same way SiCN aerogels could find their way taking advantage of the functional properties introduced by N presence, along with the possibility to produced N-doped CDC aerogels that revealed to possess an intriguing chemical composition combined with the unique microstructure of CDC aerogels.

List of commonly used abbreviation and acronyms

PDC: Polymer Derived Ceramics
SMP-10: Commercial polycarbosilane
PMHS: Commercial polysiloxane
PSZ-20: Commercial polysilazane
SiC: Silicon Carbide
SiOC: Silicon Oxycarbide
SiCN: Silicon Carbonitride
DVB: Divinylbenzene
TVS: Tetravinylsilane
THF: Tetrahydrofuran
RT: Room Temperature
SSA: Specific Surface Area
SCD: Supercritical Drying
CDC: Carbide Derived Carbon
NMR: Nuclear Magnetic Resonance
FT-IR: Fourier Transform Infrared Spectroscopy
DRIFT: Diffuse Reflectance Infrared Fourier Transform Spectroscopy
TG: Thermogravimetry
DTA: Differential Thermal Analysis
FE-SEM: Field Emission (Gun) Scanning Electron Microscope
XRD: X-ray Diffraction
XPS: X.ray Photoelectron Spectroscopy
PSD: Pore Size Distribution
BJH: Barrett-Joyner-Halenda (method for calculating PSD)
QSDFT: Quenched Solid Density Functional Theory (method for calculating PSD)
EDLC: Electric Double Layer Capacitor
$C_{spec:}$: Specific Capacitance

References

[1] «Kistler, S. S. (1931). Coherent Expanded Aerogels and Jellies. Nature, 127, 741.».

[2] «Aegerter, M. A., Leventis, N., & Koebel, M. M. (Eds.). (2011). Aerogels handbook. Springer Science & Business Media.».

[3] «Hector, A. L. (2007). Materials synthesis using oxide free sol–gel systems. Chemical Society Reviews, 36(11), 1745-1753.».

[4] «Pekala, R. W. (1989). Organic aerogels from the polycondensation of resorcinol with formaldehyde. Journal of Materials Science, 24(9), 3221-3227.».

[5] «Pekala, R. W., Alviso, C. T., Kong, F. M., & Hulsey, S. S. (1992). Aerogels derived from multifunctional organic monomers. Journal of Non-Crystalline Solids, 145, 90-98.».

[6] «Gouerec, P., Miousse, D., Tran-Van, F., & Dao, L. H. (1999). Characterization of pyrolized polyacrylonitrile aerogel thin films used in double-layer supercapacitors. Journal of New Materials for Electrochemical Systems, 2, 221-226.».

[7] «Fischer, F., Rigacci, A., Pirard, R., Berthon-Fabry, S., & Achard, P. (2006). Cellulose-based aerogels. Polymer, 47(22), 7636-7645.».

[8] «Aaltonen, O., & Jauhiainen, O. (2009). The preparation of lignocellulosic aerogels from ionic liquid solutions. Carbohydrate Polymers, 75(1), 125-129.».

[9] «García-González, C. A., Alnaief, M., & Smirnova, I. (2011). Polysaccharide-based aerogels—Promising biodegradable carriers for drug delivery systems. Carbohydrate Polymers, 86(4), 1425-1438.».

[10] «Biesmans, G., Randall, D., Francais, E., & Perrut, M. (1998). Polyurethane-based organic aerogels' thermal performance. Journal of Non-Crystalline Solids, 225, 36-40.».

[11] «Daniel, C., Alfano, D., Venditto, V., Cardea, S., Reverchon, E., Larobina, D., ... & Guerra, G. (2005). Aerogels with a microporous crystalline host phase. Advanced materials, 17(12), 1515-1518.».

[12] «An, H., Wang, Y., Wang, X., Zheng, L., Wang, X., Yi, L., ... & Zhang, X. (2010). Polypyrrole/carbon aerogel composite materials for supercapacitor. Journal of Power Sources, 195(19), 6964-6969.».

[13] «Leventis, N., Chandrasekaran, N., Sadekar, A. G., Mulik, S., & Sotiriou-Leventis, C. (2010). The effect of compactness on the carbothermal conversion of interpenetrating metal oxide/resorcinol-formaldehyde

nanoparticle networks to porous metals and carbid».

[14] «Liu, W., Herrmann, A. K., Bigall, N. C., Rodriguez, P., Wen, D., Oezaslan, M., ... & Eychmüller, A. (2015). Noble Metal Aerogels瑕 Synthesis, Characterization, and Application as Electrocatalysts. Accounts of chemical research, 48(2), 154-162.».

[15] «Haranath, D., Rao, A. V., & Wagh, P. B. (1999). Influence of DCCAs on optical transmittance and porosity properties of TMOS silica aerogels. Journal of Porous Materials, 6(1), 55-62.».

[16] «Metzger, T., Léonard, A., Jomaa, W., & Tamon, H. (2011). Understanding and preventing structural changes during drying of gels. Modern Drying Technology, Volume 3: Product Quality and Formulation, 155-229.».

[17] «Hwang, S. W., Jung, H. H., Hyun, S. H., & Ahn, Y. S. (2007). Effective preparation of crack-free silica aerogels via ambient drying. Journal of sol-gel science and technology, 41(2), 139-146.».

[18] «Rolison, D. R., & Dunn, B. (2001). Electrically conductive oxide aerogels: new materials in electrochemistry. Journal of Materials Chemistry, 11(4), 963-980.».

[19] «Leventis, N., Sotiriou-Leventis, C., Zhang, G., & Rawashdeh, A. M. M. (2002). Nanoengineering strong silica aerogels. Nano letters, 2(9), 957-960.».

[20] «Meador, M. A. B., Malow, E. J., Silva, R., Wright, S., Quade, D., Vivod, S. L., ... & Cakmak, M. (2012). Mechanically strong, flexible polyimide aerogels cross-linked with aromatic triamine. ACS applied materials & interfaces, 4(2), 536-544.».

[21] «Hrubesh, L. W., Keene, L. E., & Latorre, V. R. (1993). Dielectric properties of aerogels. Journal of materials research, 8(07), 1736-1741.».

[22] «Pajonk, G. M. (1998). Transparent silica aerogels. Journal of Non-Crystalline Solids, 225, 307-314.».

[23] «Cai, J., Kimura, S., Wada, M., Kuga, S., & Zhang, L. (2008). Cellulose aerogels from aqueous alkali hydroxide–urea solution. ChemSusChem, 1(1-2), 149-154.».

[24] «Hrubesh, L. W. (1998). Aerogel applications. Journal of Non-Crystalline Solids, 225, 335-342.».

[25] «Hüsing, N., & Schubert, U. (1998). Aerogele–luftige Materialien: Chemie, Struktur und Eigenschaften. Angewandte Chemie, 110(1-2), 22-47.».

[26] «Fricke, J., & Emmerling, A. (1998). Aerogels—recent progress in production techniques and novel applications. Journal of Sol-Gel Science and Technology, 13(1-3), 299-303.».

[27] «Moreno-Castilla, C., & Maldonado-Hódar, F. J. (2005). Carbon aerogels for catalysis applications: An overview. Carbon, 43(3), 455-465.».

[28] «http://www.cabotcorp.com/,» [Online].

[29] «http://www.aerogel.com/,» [Online].

[30] «http://www.orosapparel.com/,» [Online].

[31] «http://www.aerogeltechnologies.com/,» [Online].

[32] «http://www.michalous.com/,» [Online].

[33] «Chantrell, P. G., & Popper, P. (1965). Inorganic polymers and ceramics. Special Ceramics, 67.».

[34] «W. Verbeek, ''Production of Shaped Articles of Homogeneous Mixtures of Silicon Carbide and Nitride''; Ger. Offen., 2218960 (Bayer AG), November 8, U.S. Patent No. 3853567, 1973.».

[35] «Yajima, S., Hayashi, J., Omori, M., & Okamura, K. (1976). Development of a silicon carbide fibre with high tensile strength.».

[36] «Colombo, P., Mera, G., Riedel, R., & Sorarù, G. D. (2010). Polymer-derived ceramics: 40 years of research and innovation in advanced ceramics. Journal of the American Ceramic Society, 93(7), 1805-1837.».

[37] «Colombo, P. (Ed.). (2010). Polymer derived ceramics: from nano-structure to applications. DEStech Publications, Inc.».

[38] «Mera, G., Gallei, M., Bernard, S., & Ionescu, E. (2015). Ceramic Nanocomposites from Tailor-Made Preceramic Polymers. Nanomaterials, 5(2), 468-540.».

[39] «Bernard, S., & Miele, P. (2014). Polymer-derived boron nitride: a review on the chemistry, shaping and ceramic conversion of borazine derivatives. Materials, 7(11), 7436-7459.».

[40] «Laine, R. M., & Babonneau, F. (1993). Preceramic polymer routes to silicon carbide. Chemistry of materials, 5(3), 260-279.».

[41] «Kroke, E., Li, Y. L., Konetschny, C., Lecomte, E., Fasel, C., & Riedel, R. (2000). Silazane derived ceramics and related materials. Materials Science and Engineering: R: Reports, 26(4), 97-199.».

[42] «Jansen, M., Jäschke, B., & Jäschke, T. (2002). Amorphous multinary ceramics in the Si-BNC system. In High Performance Non-Oxide Ceramics I (pp. 137-191). Springer Berlin Heidelberg.».

[43] «Riedel, R., Mera, G., Hauser, R., & Klonczynski, A. (2006). Silicon-based polymer-derived ceramics: synthesis properties and applications-Journal of the Ceramic Society of Japan, 114(1330), 425-444.».

[44] «Schulz, M. (2009). Polymer derived ceramics in MEMS/NEMS–a review on production processes and application. Advances in applied ceramics, 108(8), 454-460.».

[45] «Zaheer, M., Schmalz, T., Motz, G., & Kempe, R. (2012). Polymer derived non-oxide ceramics modified with late transition metals. Chemical Society Reviews, 41(15), 5102-5116.».

[46] «Ionescu, E., Kleebe, H. J., & Riedel, R. (2012). Silicon-containing polymer-derived ceramic nanocomposites (PDC-NCs): preparative approaches and properties. Chemical Society Reviews, 41(15), 5032-5052.».

[47] «Bernardo, E., Fiocco, L., Parcianello, G., Storti, E., & Colombo, P. (2014). Advanced ceramics from preceramic polymers modified at the nano-scale: A review. Materials, 7(3), 1927-1956.».

[48] «Wynne, K. J., & Rice, R. W. (1984). Ceramics via polymer pyrolysisdagger. Annual Review of Materials Science, 14(1), 297-334.».

[49] «Colombo, P., Paulson, T. E., & Pantano, C. G. (1994). Atmosphere effects in the processing of silicon carbide and silicon oxycarbide thin films and coatings. Journal of Sol-Gel Science and Technology, 2(1-3), 601-604.».

[50] «Yu, S. H., Riman, R. E., Danforth, S. C., & Leung, R. Y. (1995). Pyrolysis of Titanium-Metal-Filled Poly (siloxane) Preceramic Polymers: Effect of Atmosphere on Pyrolysis Product Chemistry. Journal of the American Ceramic Society, 78(7), 1818-1824.».

[51] «Greil, P. (1995). Active-Filler-Controlled Pyrolysis of Preceramic Polymers. Journal of the American Ceramic Society, 78(4), 835-848.».

[52] «Greil, P., & Seibold, M. (1992). Modelling of dimensional changes during polymer-ceramic conversion for bulk component fabrication. Journal of materials science, 27(4), 1053-1060.».

[53] «Riedel, R., Kienzle, A., Dressler, W., Ruwisch, L., Bill, J., & Aldinger, F. (1996). A silicoboron carbonitride ceramic stable to 2,000 C. Nature, 382(6594), 796-798.».

[54] «Papendorf, B., Nonnenmacher, K., Ionescu, E., Kleebe, H. J., & Riedel, R. (2011). Strong Influence of Polymer Architecture on the Microstructural Evolution of Hafnium-Alkoxide-Modified Silazanes upon Ceramization. Small, 7(7), 970-978.».

[55] «Cai, T., Qiu, W. F., Liu, D., Han, W. J., Ye, L., Zhao, A. J., & Zhao, T. (2013). Synthesis of soluble poly-yne polymers containing zirconium and silicon and corresponding conversion to nanosized ZrC/SiC composite ceramics. Dalton Transactions, 42(12), 42».

[56] «An, L., Wang, Y., Bharadwaj, L., Zhang, L., Fan, Y., Jiang, D., ... & Chow, L. C. (2004). Silicoaluminum carbonitride with anomalously high resistance to oxidation and hot corrosion. Advanced Engineering Materials, 6(5), 337-340.».

[57] «Pantano, C. G., Singh, A. K., & Zhang, H. (1999). Silicon oxycarbide glasses. Journal of Sol-Gel Science and Technology, 14(1), 7-25.».

[58] «Li, Q., Yin, X., Duan, W., Kong, L., Hao, B., & Ye, F. (2013). Electrical, dielectric and microwave-absorption properties of polymer derived SiC ceramics in X band. Journal of Alloys and Compounds, 565, 66-72.».

[59] «Iwamoto, Y., Völger, W., Kroke, E., Riedel, R., Saitou, T., & Matsunaga, K. (2001). Crystallization behavior of amorphous silicon carbonitride ceramics derived from organometallic precursors. Journal of the American Ceramic Society, 84(10), 2170-2178.».

[60] «Zhang, L., Wang, Y., Wei, Y., Xu, W., Fang, D., Zhai, L., ... & An, L. (2008). A silicon carbonitride ceramic with anomalously high piezoresistivity. Journal of the American Ceramic Society, 91(4), 1346-1349.».

[61] «Ryu, H. Y., Wang, Q., & Raj, R. (2010). Ultrahigh-Temperature Semiconductors Made from Polymer-Derived Ceramics. Journal of the American Ceramic Society, 93(6), 1668-1676.».

[62] «Ramakrishnan, P. A., Wang, Y. T., Balzar, D., An, L., Haluschka, C., Riedel, R., & Hermann, A. M. (2001). Silicoboron–carbonitride ceramics: A class of high-temperature, dopable electronic materials. Applied Physics Letters, 78(20), 3076-3078.».

[63] «Saha, A., Shah, S. R., Raj, R., & Russek, S. E. (2003). Polymer-derived SiCN composites with magnetic properties. Journal of materials research, 18(11), 2549-2551.».

[64] «Noborisaka, M., Kodama, H., Nagashima, S., Shirakura, A., Horiuchi, T., & Suzuki, T. (2012). Synthesis of transparent and hard SiOC (− H) thin films on polycarbonate substrates by PECVD method. Surface and Coatings Technology, 206(8), 2581-2584.».

[65] «Narisawa, M., Watase, S., Matsukawa, K., Dohmaru, T., & Okamura, K. (2012). White Si–O–C (–H) particles with photoluminescence synthesized by decarbonization reaction on polymer precursor in a hydrogen atmosphere. Bulletin of the Chemical Society of Japan».

[66] «Pradeep V.S. (2013). Study of Silicon Oxycarbide (SiOC) as Anode Materials for Li-ion. PhD dissertation».

[67] «Karakuscu A. (2010) Synthesis and Characterization of Luminescent Nanostructured SiOC Thin Films. PhD dissertation».

[68] «Cromme, P., Scheffler, M., & Greil, P. (2002). Ceramic tapes from preceramic polymers. Advanced Engineering Materials, 4(11), 873-877.».

[69] «Colombo, P., Paulson, T. E., & Pantano, C. G. (1997). Synthesis of silicon carbide thin films with polycarbosilane (PCS). Journal of the American Ceramic Society, 80(9), 2333-2340.».

[70] «Goerke, O., Feike, E., Heine, T., Trampert, A., & Schubert, H. (2004). Ceramic coatings processed by spraying of siloxane precursors (polymer-spraying). Journal of the European Ceramic Society, 24(7), 2141-2147.».

[71] «Hanemann, T., Ade, M., Börner, M., Motz, G., Schulz, M., & Hausselt, J. (2002). Microstructuring of preceramic polymers. Advanced Engineering Materials, 4(11), 869-873.».

[72] «Schiroky, G. H., Miller, D. A., Aghajanian, M. K., & Fareed, A. S. (1996, November). Fabrication of CMCs and MMCs using novel processes. In Key Engineering Materials (Vol. 127, pp. 141-152). Trans Tech Publications.».

[73] «Bakumov, V., Schwarz, M., & Kroke, E. (2009). Emulsion processing of polymer-derived porous Si/C/(O) ceramic bodies. Journal of the European Ceramic Society, 29(13), 2857-2865.».

[74] «Riedel, R., Passing, G., Schönfelder, H., & Brook, R. J. (1992). Synthesis of dense silicon-based ceramics at low temperatures. Nature, 355(6362), 714-717.».

[75] «Vakıfahmetoğlu Ç. (2009) Fabrication and characterization of porous ceramics with hierarchical porosity. PhD dissertation».

[76] «Colombo, P., Sglavo, V., Pippel, E., & Woltersdorf, J. (1998). Joining of reaction-bonded silicon carbide using a preceramic polymer. Journal of Materials Science, 33(9), 2405-2412.».

[77] «Maddocks, A. R., Cassidy, D. J., Jones, A. S., & Harris, A. T. (2009). Synthesis of nanoporous silicon carbide via the preceramic polymer route. Materials Chemistry and Physics, 113(2), 861-867.».

[78] «Biasetto, L., Pena-Alonso, R., Soraru, G. D., & Colombo, P. (2008). Etching of SiOC ceramic foams. Advances in Applied Ceramics, 107(2), 106-110.».

[79] «Yeon, S. H., Reddington, P., Gogotsi, Y., Fischer, J. E., Vakifahmetoglu, C., & Colombo, P. (2010). Carbide-derived-carbons with hierarchical porosity from a preceramic polymer. Carbon, 48(1), 201-210.».

[80] «Clauß, B. (2008). Fibers for ceramic matrix composites. Ceramic Matrix Composites: Fiber Reinforced Ceramics and their Applications, 1-20.».

[81] «Karakuscu, A., Ponzoni, A., Comini, E., Sberveglieri, G., & Vakifahmetoglu, C. (2014). SiC Foams Decorated with SnO2 Nanostructures for Room

Temperature Gas Sensing. International Journal of Applied Ceramic Technology, 11(5), 851-857.».

[82] «Frind, R., Oschatz, M., & Kaskel, S. (2011). Polymerization of polycarbosilanes in high internal phase emulsions for the synthesis of macroporous silicon carbide catalysts (polyHIPE-SiC). Journal of Materials Chemistry, 21(32), 11936-11940.».

[83] «Vakifahmetoglu, C., Presser, V., Yeon, S. H., Colombo, P., & Gogotsi, Y. (2011). Enhanced hydrogen and methane gas storage of silicon oxycarbide derived carbon. Microporous and Mesoporous Materials, 144(1), 105-112.».

[84] «Wilson, A. M., Zank, G., Eguchi, K., Xing, W., & Dahn, J. R. (1997). Pyrolysed silicon-containing polymers as high capacity anodes for lithium-ion batteries. Journal of power sources, 68(2), 195-200.».

[85] «Hirayama, M., Caseri, W. R., & Suter, U. W. (2001). U.S. Patent No. 6,316,057. Washington, DC: U.S. Patent and Trademark Office.».

[86] «http://www.starfiresystems.com/aerospace.html».

[87] «Geissinger, A., Oberle, J., Teschner, W., Boeder, H., & Heussner, K. H. (1999). U.S. Patent No. 5,961,888. Washington, DC: U.S. Patent and Trademark Office.».

[88] «Valle, M., Ferrari, S., Orlandi, M., Turani, S., & Pagani, M. (2009). Use of polysiloxane resins in friction materials. Advances in Applied Ceramics, 108(8), 461-467.».

[89] «Soraru, G. D., Dalcanale, F., Campostrini, R., Gaston, A., Blum, Y., Carturan, S., & Aravind, P. R. (2012). Novel polysiloxane and polycarbosilane aerogels via hydrosilylation of preceramic polymers. Journal of Materials Chemistry, 22(16), 7676-7680.».

[90] «Interrante, L. V., Moraes, K., Liu, Q., Lu, N., Puerta, A., & Sneddon, L. G. (2002). Silicon-based ceramics from polymer precursors. Pure and applied chemistry, 74(11), 2111-2117.,» [Online].

[91] «Mei, M., He, X. B., Qu, X. H., Hu, H. F., & Zhang, Y. D. (2013, October). Characterizations of liquid polycabosilane (LPCS) used as SiC matrix precursor for CLVD process. In Advanced Materials Research (Vol. 750, pp. 195-199).».

[92] «Whitmarsh, C. K., & Interrante, L. V. (1992). U.S. Patent No. 5,153,295. Washington, DC: U.S. Patent and Trademark Office.».

[93] «Kaur, S., Riedel, R., & Ionescu, E. (2014). Pressureless fabrication of dense monolithic SiC ceramics from a polycarbosilane. Journal of the European Ceramic Society, 34(15), 3571-3578.».

[94] «KiON Speciality Polymers. Technical Bulletin TB2.».

[95] «Dando, N. R., Perrotta, A. J., Strohmann, C., Stewart, R. M., & Seyferth, D. (1993). Methylhydridopolysilazane and its pyrolytic conversion to silicon nitride-silicon carbide (Si3N4/SiC) ceramics. Chemistry of materials, 5(11), 1624-1630.».

[96] «Nghiem, Q. D., Nguyen, C. T., & Kim, D. P. (2008). Controlled/living radical polymerization of vinylcyclicsilazane by RAFT process and their block copolymers. Journal of Polymer Science Part A: Polymer Chemistry, 46(13), 4594-4601.».

[97] «Gérardin, C., Taulelle, F., & Bahloul, D. (1997). Pyrolysis chemistry of polysilazane precursors to silicon carbonitride. Journal of Materials Chemistry, 7(1), 117-126.».

[98] «Wang, H., & Fischman, G. (1994). Kinetic studies of the reactions between silicon nitride and carbon. Journal of Thermal Analysis and Calorimetry, 41(1), 135-146.».

[99] «Herrmann, M., Schuber, C., Rendtel, A., & Hübner, H. (1998). Silicon nitride/silicon carbide nanocomposite materials: I, fabrication and mechanical properties at room temperature. Journal of the American Ceramic Society, 81(5), 1095-1108.».

[100] «Bahloul, D., Pereira, M., & Gerardin, C. (1997). Pyrolysis chemistry of polysilazane precursors to siliconcarbonitride. J. Mater. Chem., 7(1), 109-116.».

[101] «Lu, S., Melo, M. M., Zhao, J., Pearce, E. M., & Kwei, T. K. (1995). Organic-inorganic polymeric hybrids involving novel poly (hydroxymethylsiloxane). Macromolecules, 28(14), 4908-4913.».

[102] «Blum, Y. D., U.S. Patent 5,319,121 (June 7, 1994).».

[103] «Blum, Y. D., MacQueen, D. B., & Kleebe, H. J. (2005). Synthesis and characterization of carbon-enriched silicon oxycarbides. Journal of the European Ceramic Society, 25(2), 143-149.».

[104] Socrates, G. (2004). Infrared and Raman characteristic group frequencies: tables and charts. John Wiley & Sons..

[105] «Davidson, G. (1971). The vibrational spectrum of tetravinylsilane. Spectrochimica Acta Part A: Molecular Spectroscopy, 27(7), 1161-1169.».

[106] «Speier, J. L., Zimmerman, R., & Webster, J. (1956). The addition of silicon hydrides to olefinic double bonds. Part I. The use of phenylsilane, diphenylsilane, phenylmethylsilane, amylsilane and tribromosilane. Journal of the American Chemical Society, 78».

[107] «Speier, J. L., Webster, J. A., & Barnes, G. H. (1957). The addition of silicon hydrides to olefinic double bonds. Part II. The use of group VIII metal catalysts. Journal of the American Chemical Society, 79(4), 974-979.».

[108] «Saam, J. C., & Speier, J. L. (1958). The addition of silicon hydrides to olefinic double bonds. Part III. The addition to non-terminal olefins in the presence of chloroplatinic acid. Journal of the American Chemical Society, 80(15), 4104-4106.».

[109] «Lewis, L. N., Stein, J., Gao, Y., Colborn, R. E., & Hutchins, G. (1997). Platinum catalysts used in the silicones industry. Platinum Metals Review, 41(2), 66-75.».

[110] «Nakajima, Y., & Shimada, S. (2015). Hydrosilylation reaction of olefins: recent advances and perspectives. RSC Advances, 5(26), 20603-20616.».

[111] «http://saf.chem.ox.ac.uk/operating-principles-3.aspx».

[112] «Sing, K. S. (1985). Reporting physisorption data for gas/solid systems with special reference to the determination of surface area and porosity (Recommendations 1984). Pure and applied chemistry, 57(4), 603-619.».

[113] «Salameh C.M. (2014). Synthèse de matériaux nitrures fonctionnels à base de bore ou d'aluminium pour des applications en énergie (production et stockage de l'hydrogène). PhD dissertation».

[114] «Hanzawa, Y., Hatori, H., Yoshizawa, N., & Yamada, Y. (2002). Structural changes in carbon aerogels with high temperature treatment. Carbon, 40(4), 575-581,» [Online].

[115] «Perez-Cantu, L., Liebner, F., & Smirnova, I. (2014). Preparation of aerogels from wheat straw lignin by cross-linking with oligo (alkylene glycol)-α, ω-diglycidyl ethers. Microporous and Mesoporous Materials, 195, 303-310.».

[116] «Grishechko, L. I., Amaral-Labat, G., Szczurek, A., Fierro, V., Kuznetsov, B. N., Pizzi, A., & Celzard, A. (2013). New tannin–lignin aerogels. Industrial Crops and Products, 41, 347-355.».

[117] «Wang, S. Y., & Wu, N. L. (1998). Tin oxide gel shrinkage during CO 2 supercritical drying. Journal of non-crystalline solids, 224(3), 259-266.».

[118] «Ye, L., Ji, Z. H., Han, W. J., Hu, J. D., & Zhao, T. (2010). Synthesis and characterization of silica/carbon composite aerogels. Journal of the American Ceramic Society, 93(4), 1156-1163.».

[119] «Amaral-Labat, G., Szczurek, A., Fierro, V., Masson, E., Pizzi, A., & Celzard, A. (2012). Impact of depressurizing rate on the porosity of aerogels. Microporous and Mesoporous Materials, 152, 240-245.».

[120] «Sanz-Moral, L. M., Rueda, M., Mato, R., & Martín, Á. (2014). View cell

investigation of silica aerogels during supercritical drying: Analysis of size variation and mass transfer mechanisms. The Journal of Supercritical Fluids, 92, 24-30.».

[121] «Riedel, R., Toma, L., Janssen, E., Nuffer, J., Melz, T., & Hanselka, H. (2010). Piezoresistive effect in SiOC ceramics for integrated pressure sensors. Journal of the American Ceramic Society, 93(4), 920-924.».

[122] «Karakuscu, A., Ponzoni, A., Aravind, P. R., Sberveglieri, G., & Soraru, G. D. (2013). Gas sensing behavior of mesoporous SiOC glasses. Journal of the American Ceramic Society, 96(8), 2366-2369.».

[123] «Menapace, I., Mera, G., Riedel, R., Erdem, E., Eichel, R. A., Pauletti, A., & Appleby, G. A. (2008). Luminescence of heat-treated silicon-based polymers: promising materials for LED applications. Journal of Materials Science, 43(17), 5790-5796.».

[124] «Zhuo, R., Colombo, P., Pantano, C., & Vogler, E. A. (2005). Silicon oxycarbide glasses for blood-contact applications. Acta Biomaterialia, 1(5), 583-589.».

[125] «Sorarù, G. D., Modena, S., Guadagnino, E., Colombo, P., Egan, J., & Pantano, C. (2002). Chemical durability of silicon oxycarbide glasses. Journal of the American Ceramic Society, 85(6), 1529-1536.».

[126] «Pradeep, V. S., Ayana, D. G., Graczyk-Zajac, M., Soraru, G. D., & Riedel, R. (2015). High Rate Capability of SiOC Ceramic Aerogels with Tailored Porosity as Anode Materials for Li-ion Batteries. Electrochimica Acta, 157, 41-45.».

[127] «Kolb, R., Fasel, C., Liebau-Kunzmann, V., & Riedel, R. (2006). SiCN/C-ceramic composite as anode material for lithium ion batteries. Journal of the European Ceramic Society, 26(16), 3903-3908.».

[128] «Shah, S. R., & Raj, R. (2002). Mechanical properties of a fully dense polymer derived ceramic made by a novel pressure casting process. Acta Materialia, 50(16), 4093-4103.».

[129] «Singh, A. K., & Pantano, C. G. (1997). Surface chemistry and structure of silicon oxycarbide gels and glasses. Journal of Sol-Gel Science and Technology, 8(1-3), 371-376.».

[130] «Bahloul-Hourlier, D., Latournerie, J., & Dempsey, P. (2005). Reaction pathways during the thermal conversion of polysiloxane precursors into oxycarbide ceramics. Journal of the European Ceramic Society, 25(7), 979-985.».

[131] «Soraru, G. D., Babonneau, F., & Mackenzie, J. D. (1990). Structural evolutions from polycarbosilane to SiC ceramic. Journal of Materials Science,

25(9), 3886-3893.».

[132] «Trassl, S., Motz, G., Rössler, E., & Ziegler, G. (2002). Characterization of the Free-Carbon Phase in Precursor-Derived Si-C-N Ceramics: I, Spectroscopic Methods. Journal of the American Ceramic Society, 85(1), 239-244.».

[133] «Gogotsi, Y., Nikitin, A., Ye, H., Zhou, W., Fischer, J. E., Yi, B., ... & Barsoum, M. W. (2003). Nanoporous carbide-derived carbon with tunable pore size. Nature materials, 2(9), 591-594.».

[134] «Chmiola, J., Largeot, C., Taberna, P. L., Simon, P., & Gogotsi, Y. (2010). Monolithic carbide-derived carbon films for micro-supercapacitors. Science, 328(5977), 480-483.».

[135] «Presser, V., McDonough, J., Yeon, S. H., & Gogotsi, Y. (2011). Effect of pore size on carbon dioxide sorption by carbide derived carbon. Energy & Environmental Science, 4(8), 3059-3066.».

[136] «Lee, J. T., Zhao, Y., Thieme, S., Kim, H., Oschatz, M., Borchardt, L., ... & Yushin, G. (2013). Sulfur-Infiltrated Micro-and Mesoporous Silicon Carbide-Derived Carbon Cathode for High-Performance Lithium Sulfur Batteries. Advanced Materials, 25(33), 4573-».

[137] «Yeon, S. H., Knoke, I., Gogotsi, Y., & Fischer, J. E. (2010). Enhanced volumetric hydrogen and methane storage capacity of monolithic carbide-derived carbon. Microporous and Mesoporous Materials, 131(1), 423-428.».

[138] «Oschatz, M., Nickel, W., Thommes, M., Cychosz, K. A., Leistner, M., Adam, M., ... & Kaskel, S. (2014). Evolution of porosity in carbide-derived carbon aerogels. Journal of Materials Chemistry A, 2(43), 18472-18479.».

[139] «Ewert, J. K., Weingarth, D., Denner, C., Friedrich, M., Zeiger, M., Schreiber, A., ... & Kempe, R. (2015). Enhanced capacitance of nitrogen-doped hierarchically porous carbide-derived carbon in matched ionic liquids. Journal of Materials Chemistry A, 3(37».

[140] «Presser, V., Heon, M., & Gogotsi, Y. (2011). Carbide-Derived Carbons–From Porous Networks to Nanotubes and Graphene. Advanced Functional Materials, 21(5), 810-833.».

[141] «Robertson, J. (2002). Diamond-like amorphous carbon. Materials Science and Engineering: R: Reports, 37(4), 129-281.».

[142] «Zhang, S., Tsuzuki, S., Ueno, K., Dokko, K., & Watanabe, M. (2015). Upper limit of nitrogen content in carbon materials. Angewandte Chemie International Edition, 54(4), 1302-1306.».

[143] «Fujisawa, K., Tojo, T., Muramatsu, H., Elías, A. L., Vega-Díaz, S. M., Tristán-López, F., ... & Terrones, M. (2011). Enhanced electrical conductivities of N-

doped carbon nanotubes by controlled heat treatment. Nanoscale, 3(10), 4359-4364.».

[144] «Sánchez-Jiménez, P. E., Downs, J. A., & Raj, R. (2010). Transient Viscous Flow During the Evolution of a Ceramic (Silicon Carbonitride) from a Polymer (Polysilazane). Journal of the American Ceramic Society, 93(9), 2567-2570.».

[145] «Zhang, Z., Zhou, J., Xing, W., Xue, Q., Yan, Z., Zhuo, S., & Qiao, S. Z. (2013). Critical role of small micropores in high CO 2 uptake. Physical Chemistry Chemical Physics, 15(7), 2523-2529.».

[146] «Simon, P., & Gogotsi, Y. (2008). Materials for electrochemical capacitors. Nature materials, 7(11), 845-854.».

Scientific production

" Zera, E., Campostrini, R., Aravind, P. R., Blum, Y., & Sorarù, G. D. (2014). Novel SiC/C aerogels through pyrolysis of polycarbosilane precursors. Advanced Engineering Materials, 16(6), 814-819."

" Nguyen, V.L., Zera, E., Perolo, A., Campostrini, R., Li, W., & Sorarù, G. D. (2015). Synthesis and characterization of polymer-derived SiCN aerogel. Journal of the European Ceramic Society, 35(12), 3295-3302."

" Zera, E., Nickel, W., Kaskel, S., & Sorarù, G. D. (2016). Out-of-furnace oxidation of SiCN polymer-derived ceramic aerogel pyrolized at intermediate temperature (600–800° C). Journal of the European Ceramic Society, 36(3), 423-428."

" Zera, E., Nickel, W., Hao, G. P., Vanzetti, L., Kaskel, S., & Sorarù, G. D. (2016). Nitrogen doped carbide derived carbon aerogels by chlorine etching of a SiCN aerogel. Journal of Materials Chemistry A, 4(12), 4525-4533."

" Ghafarinazari, A., Zera, E., Lion, A., Scarpa, M., Sorarù, G. D., Mariotto, G., & Daldosso, N. (2016). Isoconversional kinetics of thermal oxidation of mesoporous silicon. Thermochimica Acta, 623, 65-71."

" Assefa, D., Zera, E., Campostrini, R., Soraru, G. D., & Vakifahmetoglu, C. (2016). Polymer-derived SiOC aerogel with hierarchical porosity through HF etching. Ceramics International. In press."

" Sasikumar, P. V., Zera, E., Graczyk-Zajac, M., Riedel, R., & Sorarù, G.D., (2016) Structural Design of Polymer Derived SiOC Ceramic Aerogels for High-rate Li-ion Storage Applications. Journal of the American Ceramic Society, Manuscript accepted for publication"

" Sorarù, G.D., Zera, E., Campostrini, R., Aerogels from preceramic polymers. Handbook of Sol-Gel Science and, Technology, 2nd edition. Eds.: L. Klein, A. Jitianu and M. Aparicio, Spinger (2016) Book chapter accepted for publication"

" Sorarù, G.D., Campostrini, R., Ejigu, A.A., Zera, E. & Jana, P. (2016) Processing and characterization of polymer derived SiOC foam with hierarchical porosity by HF etching. Revised version submitted to the Journal of the Ceramic Society of Japan"

Participation to Congresses, Schools and Workshops

E. Zera, R. Campostrini, G. D. Sorarù, "SiC/C Aerogels through Preceramic Polymer Pyrolysis Route", (Oral presentation), International Conference "Materials Science and Engineering" (MSE 2014), Darmstadt, Germany September 23 – 25, 2014.

E. Zera, P. Jana, G. D. Sorarù, "Silicon Carbide, Silicon Oxycarbide and Silicon Carbonitride Foams", the 11th Pacific Rim Conference of the Ceramic Societies, August 30th – September 4th, 2015, Jeju, Korea

Acknowledgements

I wish to express my sincere thanks to Gian Domenico Sorarù, who accepted me as a PhD student and guided me through these years of doctorate school. I really appreciated the freedom I was granted and the honest relationship that was built time after time; I couldn't have found a better advisor.
I want to thank the University of Trento for the grants that supported my studies along with travels for conferences and periods abroad.
Then, I'm in debt also with professors Dirè, Ceccato, Lutterotti, Motta, Sglavo, Kaskel and technicians Vanzetti, Bortolotti, Ischia, Moschini and Callone for helping me to characterize my materials.
(Very) Warm thanks to Michele, Artan, Van Lam, Pradeep, Benjamin, Evgeny, John, Andrea, Giulia, Filippo, Dawit, Winfried, Guang-Ping, Lars, Felix, Bob, Prasanta, Chrystelle, Susana, Matteo (D.P. and F.), Mattia, Vincenzo, Daniele, Alberto, Hamid and Ali, together with always present Livio, Alexia and (prof.) Renzo; with whom I spent great time in lab, at the coffee machine, at lunch and sometimes also out from the academic walls.
Thanks to all the bachelor and master students that I had the privilege to introduce into the field of experimental research, - 'I learned a lot while teaching you how to move the first steps in lab.'
And to all the friends out there, - 'you helped me to keep well balanced study/work and personal life, and you are way too many to be mentioned here, just be aware this work is (partially) the reason why sometimes I was so busy, worried or tired.'
One big "thank you!" to mamma e papà for... well, there's no need to say why, I simply owe you too much.

Sara, you withstood me writing three thesis, I promise you this is the last one! (along with unconditional Love, of course.....)